Low-Cost, Passive UHF RFID Tag Antenna-Based Sensors for Pervasive Sensing Applications

by

Rahul Bhattacharyya

Submitted to the Department of Civil and Environmental Engineering
in partial fulfillment of the requirements for the degree of

Doctor of Philosophy in The Field of Civil and Environmental Systems

at the

MASSACHUSETTS INSTITUTE OF TECHNOLOGY

June 2012

Signature of the Author... .....
Department of Civil and Environmental Engineering
May 04, 2012

Certified by.....
Sanjay E. Sarma
Professor of Mechanical Engineering
Thesis Supervisor

Certified by.....
Andrew J. Whittle
Professor of Civil and Environmental Engineering
Thesis Reader

Certified by.....
George A. Kocur
Senior Lecturer in Civil and Environmental Engineering
Thesis Reader

Accepted by.....
Heidi M. Nepf
Chair, Departmental Committee for Graduate Students

Low-Cost, Passive UHF RFID Tag Antenna-Based Sensors for Pervasive Sensing Applications

by

Rahul Bhattacharyya

Submitted to the Department of Civil and Environmental Engineering
on May 04, 2012, in partial fulfillment of the
requirements for the degree of
Doctor of Philosophy in The Field of Civil and Environmental Systems

Abstract

In the future, large-scale sensor deployment would enable many areas such as infrastructure condition monitoring and supply chain management. However, many of today's wireless sensor technologies are still too expensive to meet this need. Radio Frequency IDentification (RFID) offers good potential for the development of pervasive sensors: RFID tags have a proven track record of large-scale, highly integrated deployment for object identification in the retail and consumer goods industry. Furthermore, the last decade has seen much progress in making RFID a reliable, standardized wireless communication medium with the ability to mass produce low-cost RFID tags.

My thesis introduces the concept of *RFID Tag Antenna-Based Sensing (RFID TABS)*. In this approach, a change in the sensed parameter of interest induces a controlled change in the geometry or boundary conditions of an RFID tag's antenna. The resultant change in the tag's response signal can then be detected by an RFID reader. My approach builds upon current developments in RFID technology. For instance, the manufacturing techniques for the mass production of low-cost RFID tags can be used for pervasive tag-sensor development. My thesis examines TABS in a two-pronged approach:

First, I demonstrate how three fundamental tag and reader signal properties can be used for sensing and propose three classes of TABS:

- *Amplitude Modifying (AM) TABS* use RFID reader transmitted power and tag response power for sensing. I illustrate proof of concept using a displacement sensor. I demonstrate that both these power metrics can be used to reliably measure structural displacement to a precision of 2.5 mm using commercial RFID tags.

- *Frequency Modifying (FM) TABS* relate changes in the sensed parameter to a shift in the tag's *optimal operating frequency* — the carrier frequency for which the tag is best tuned to respond to the reader. I demonstrate proof of

concept using a temperature threshold sensor — the crossing of a design temperature threshold results in a shift in the sensor's optimal operating frequency. I demonstrate that the sensor works reliably over a 3 m read range and in different environmental conditions.

- *Phase Modifying (PM) TABS* use tag backscatter phase for sensing. I provide a brief summary of the factors influencing RF phase and outline the design for a PM TABS fluid level sensor that uses RFID tag response phase to detect the presence or absence of fluid in a beverage glass. I highlight the challenges in the practical implementation of this approach by demonstrating the sensitivity of RFID tag phase to three extraneous factors.

Second, I introduce the concept of *Non-Electric Memory* to record short timescale threshold crossovers in the sensed parameter that may occur when the tag-sensor is unpowered. When information about, rather than the exact time of, the threshold occurrence is sufficient, non-electric memory provides a solution. I demonstrate how non-electric memory can be integrated into sensor design at minimal added cost. In the proof of concept of a temperature threshold sensor, I design a thermally actuated shape memory polymer switch to permanently change the electrical properties of an RFID tag when the temperature threshold is crossed. I demonstrate that the design works reliably over a read range of 3 m and is independent of the material on which the sensor is deployed.

In summary, this thesis demonstrates how an RFID tag can be adapted for low-cost, pervasive sensing. Sensor prototypes illustrate proof of concept in three application areas. Extensions to two other applications are also discussed.

Thesis Supervisor: Sanjay E. Sarma
Title: Professor of Mechanical Engineering

Thesis Reader: Andrew J. Whittle
Title: Professor of Civil and Environmental Engineering

Thesis Reader: George A. Kocur
Title: Senior Lecturer in Civil and Environmental Engineering

Acknowledgments

I'd like to dedicate this thesis to my family who put up with six long years of my absence. My mother, Varsha, who taught me how to stay true to my goals and who has always been my strongest voice of support. My father, Palak, who has always been the guiding role model in my life and who inspired me to be an engineer. My grandparents, Prabhakar and Nalini, whose unfaltering confidence in me re-motivates me everytime I feel self doubt. My brother, Pinaky, whose pragmatism tinged with witticism has helped me navigate several of life's crucial decisions. You all have and continue to bring out the best in me.

I am very grateful to my advisor, Prof. Sanjay Sarma, for believing in me, for providing me with great advice and the freedom and flexibility to pursue my ideas. Christian Floerkemeier, who played a key role in helping me along on my PhD journey. My thesis committee members, Prof. Andrew Whittle and Dr. George Kocur, for providing me with valuable feedback for improving the quality of my thesis. I have learned a lot from all of you. My lab-mates, Isaac Ehrenberg, Sumeet Kumar and Ajay Deshpande, with whom I have had many stimulating discussions. Sriram Krishnan, who tirelessly helped me edit several iterations of my thesis draft and who serves as an excellent sounding board for all my ideas. I will also fondly remember the interesting conversations I have had with Alex Ilic, Austin Oehlerking, Radu Gogoana, Sam Wieland, Dylan Erb, Segio Herrero, Stephen Ho, Ed Schuster and all my lab-mates. Sincere thanks are due to Patricia Glidden, Kris Kipp, Cintia Castro, Jeanette Marchocki and all the administrative staff who helped me along the way.

I will have fond memories at MIT because of the life-long friendships that I have forged here: Amanda Redlich, Eric Heubel, Dave Shirokoff, Mike Matejek, Will Leight, Amanda Zangari, Patricia Engel, Sian Kleindienst, Miguel and Joana Pardal, Shreerang Chhatre, Ted Golfinopoulos, Emily Xi, Arghavan Safavi-Naini, Matt Branham, Jennifer Park and Camille Kemble. I couldn't have asked for a truer set of friends.

Contents

List of Figures

List of Tables

Chapter 1

Beyond IDentification - RFID Tags as Sensors

There are many applications that would benefit from the widespread deployment of wireless sensors. For example, civil concrete infrastructure is prone to local effects like cracking and spalling. Instrumenting such structures with a large scale deployment of strain and crack sensors would enable maintenance engineers to accurately detect and localize damage zones which would otherwise compromise structural integrity. Similarly, tagging each and every perishable goods item passing through the cold chain with temperature or contaminant detection sensors would allow for quality assurance checks before being sold to the end consumer. The widespread deployment of wireless sensors in agriculture would allow for the timely detection of forest fire conditions or propagation of plant disease. The common underlying theme of many of these applications is that the sensor response requirement can be very simplistic or coarse. For example, information on whether or not a threshold level of strain in a beam or bacterial concentration in an environment exceeds a threshold would suffice. What matters is that the scale at which these coarse sensors are deployed be pervasive and highly integrated with the process being monitored so high visibility and maximum benefit can be obtained.

There are a host of wireless sensing technologies available today — each offering a tradeoff between affordability and sophistication. The more sophisticated a sensor is

in terms of read range, the ability to store data, on-board computational capabilities, precision and accuracy, the more expensive it gets. This limits the scale at which it can be deployed. Unfortunately, many of the sensors available today are still too expensive for a truly pervasive and highly integrated scale of deployment that we seek. I explore the opportunity of using RFID tag-based sensors as a possible solution to this problem.

Radio Frequency Identification (RFID) has gained traction as an effective wireless technology for object identification. RFID tags serve as a digital proxy for an object to which they are physically attached. The electronic identifier of an RFID tag can be used, for example, to track the movement of an object through a transportation network. Similarly, RFID enabled identity cards can be used to grant or restrict access to a specific location or resource. RFID technology thus enables the networking of physical objects and resources and enables the vision of having an *Internet of Things* [1]. To facilitate the mapping of every physical object into the digital world, EPC Global, the standards body driving RFID standardization and adoption, has introduced a numbering convention whereby each RFID tag has a globally distinct identifier, called the *Electronic Product Code (EPC)* [2].

Besides globally unique identification, RFID technology offers several additional advantages over competitive object identification technologies, like the bar code, in terms of superior read range, line-of-sight-free operations and ease of supply chain process automation [3] [4]. Research in the past decade has addressed most of the barriers to RFID adoption such as lowering transponder cost [5] [6], standardizing communication protocols [7] and implementing security measures [8]. As a result of which, RFID has seen pervasive deployment for object identification in the consumer goods and apparel industry. We are thus presented with a robust and standardized wireless communication platform with the ability to mass produce low-cost RFID tags — a good medium for pervasive sensing applications.

My thesis introduces the concept of *RFID Tag Antenna-Based Sensing (TABS)* where changes in a sensed parameter of interest are related to a change in the geometry or boundary conditions of the RFID tag's antenna. This in turn manifests itself as

a change in the tag signal response which can be detected by a reader. The TABS concept makes no modification to the RFID tag's single integrated microchip and so a TABS sensor is little more than a specialized RFID tag. The TABS approach thus benefits from current research advancements in RFID technology while seamlessly extending it for wireless sensing applications.

I begin this chapter, by providing a brief summary of the UHF RFID wireless communication framework and use this to outline my contributions. I then highlight the advantages and shortcomings of my sensing approach relative to active, semi-passive and passive sensing technologies. Finally, I introduce three specific application areas for which sensor prototypes are developed in this thesis.

1.1 Reader-Tag Communication Framework

I summarize the UHF RFID communication framework in this section, highlighting only those aspects of reader-tag and tag-reader communication and power transfer that are necessary to understand the thesis contributions outlined in Section 1.2. A more detailed review can be found in a review by Dobkin [9].

Fig 1-1 illustrates an UHF RFID system comprising of an RFID reader and a passive tag. The reader performs the following two functions:

- The reader sends out a continuous power wave, P_{reader}, which impinges on the RFID tag. This power is used by the RFID tag to carry out its operations.

- The reader next encodes query commands to the tag by amplitude modulation of this continuous transmitted power wave.

The RFID tag scavenges power from the reader-transmitted continuous power wave. It then responds to the reader query, and conveys its EPC identifier, by modulating its backscatter response.

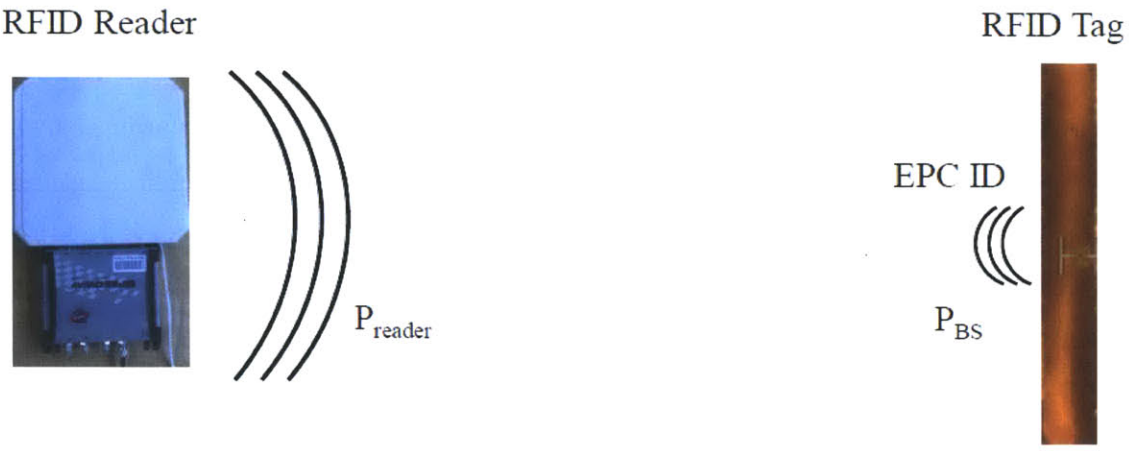

Figure 1-1: RFID system depicting reader and tag communication

1.2 The Tag Antenna-Based Sensing (TABS) Approach

Using the communication framework proposed in Section 1.1, I outline my contributions to tag antenna-based sensing along the following two dimensions:

1.2.1 Tag and Reader Signal Parameters for Sensing

While analyzing a tag reply for EPC data, RFID readers also log three fundamental signal properties — tag backscatter power, reader carrier frequency and RFID tag phase angle response. Furthermore, the power at which the reader antenna transmits can also be set between an upper and lower bound to control the read range, or zone of influence, of the reader.

I examine how the three RFID tag signal properties and RFID reader transmitted power can be exploited for sensing by using them to encode changes in a physical parameter of interest. I demonstrate how this can be achieved by having a change in the physical parameter induce a controlled change in the electrical properties of the RFID tag's antenna. I propose three classes of TABS:

- I propose a class of **Amplitude Modifying (AM) TABS** where the following signal properties are used for sensing:

- **Reader Threshold Transmitted Power**: Changes in a physical parameter of interest manifest themselves as an increase or decrease in the minimum (threshold) transmitted power that needs to be supplied by the reader in order to just power up the RFID tag and cause it to respond to interrogation. ΔP_{reader} in Fig 1-2(a) illustrates the concept.
- **RFID Tag Backscatter Power**: Changes in a physical parameter of interest manifest themselves as a controlled increase or decrease in tag backscatter signal power as illustrated by ΔP_{BS} in Fig 1-2(b).

In Chapter 2, I develop the relevant theoretical background for AM TABS and then illustrate proof of concept via the design of an RFID displacement sensor.

- I propose a class of **Frequency Modifying (FM) TABS** which relate a change in the physical parameter of interest to a change in the *optimal operating frequency band* of the tag-sensor. For a fixed reader-tag separation, the optimal operating frequency band can be defined as the band of frequencies in which the RFID tag sensor requires least reader transmitted power to respond to reader interrogation. Alternatively, we can think of this as the frequency band at which the tag is best tuned to respond to the reader. Fig 1-2(c) illustrates the concept. In Chapter 4, I discuss the design of a narrow band frequency selective antenna that can be used to implement this sensing approach. Two illustrative prototypes in fluid level sensing and temperature threshold sensing are considered to demonstrate proof of concept.

- In Chapter 5, I discuss a class of **Phase Modifying** (PM) TABS that use RFID tag phase as a proxy for the physical parameter of interest. Fig 1-2(d) illustrates the concept of a PM TABS sensor. I outline the design of a PM TABS fluid level sensor that uses backscatter phase to detect whether or not a beverage glass is full of water. Via numerical simulation and preliminary experimental results, I demonstrate the practical challenges of implementing PM TABS due to phase sensitivity to three extraneous factors. I then propose

three open questions that better quantify the effect of these extraneous factors on RF phase and help determine the scope of PM TABS.

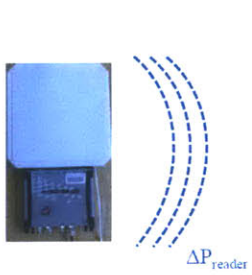

(a) AM TABS: Reader transmitted power for sensing

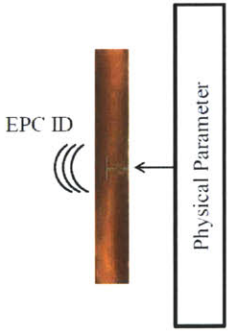

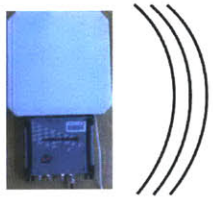

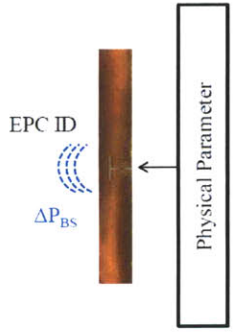

(b) AM TABS: Tag backscattered power for sensing

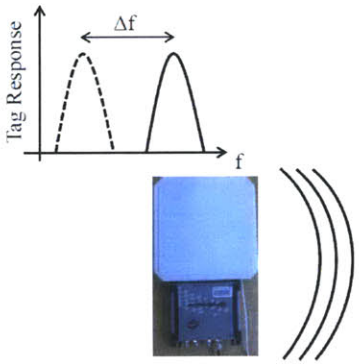

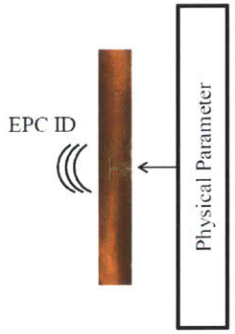

(c) FM TABS: Tag optimal operating frequency for sensing

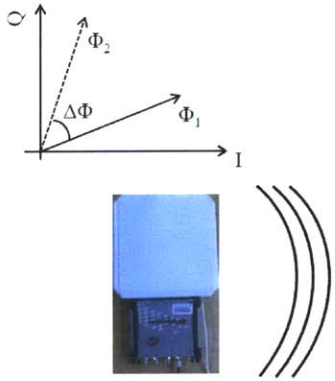

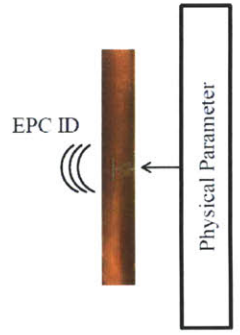

(d) PM TABS: Tag RF phase angle for sensing

Figure 1-2: Reader and tag signal parameter-based transduction methods

1.2.2 Threshold Crossover Detection vs. Instantaneous State Reporting

Passive sensors, like TABS, report the state of the physical parameter of interest at the time of reader interrogation. Recording a time history of data or triggering alarms would require additional memory and on-board power sources and this entails a higher degree of sensor sophistication and increased sensor cost. This detracts from the theme of low-cost, pervasive sensing.

Fig 1-3(a) illustrates the performance of a TABS sensor which is used to monitor a physical parameter that undergoes small, moderate and critically large perturbations over time before reverting back to small perturbations. All these changes can be recorded, as long as the reader is continually within range of the TABS device. However, any changes occurring at the time the reader is unpowered will be missed.

On the other hand, there may be cases where critical threshold crossovers such as impulse exposure to excessive humidity or temperature, must be recorded even when the sensor is unpowered by a reader. Chapter 3 proposes the concept of **low-cost, non-electric memory** whereby the crossing of a threshold of interest triggers a permanent change in the structure or boundary condition of the RFID tag's antenna. Moreover, I demonstrate how this can be achieved without significantly increasing the cost of the sensor. This change is triggered even when the TABS device is unpowered and can be detected every subsequent time the sensor is interrogated. Fig 1-3(b) illustrates the concept of non-electric memory where the crossing of a critical threshold in the physical parameter permanently changes the RFID tag antenna properties.

1.3 Comparison to Related Work

Different wireless sensing technologies can be best compared by a trade off between the number of features offered and affordability. In this section, I compare and contrast the popular wireless sensing technologies, including the TABS approach, according to this tradeoff.

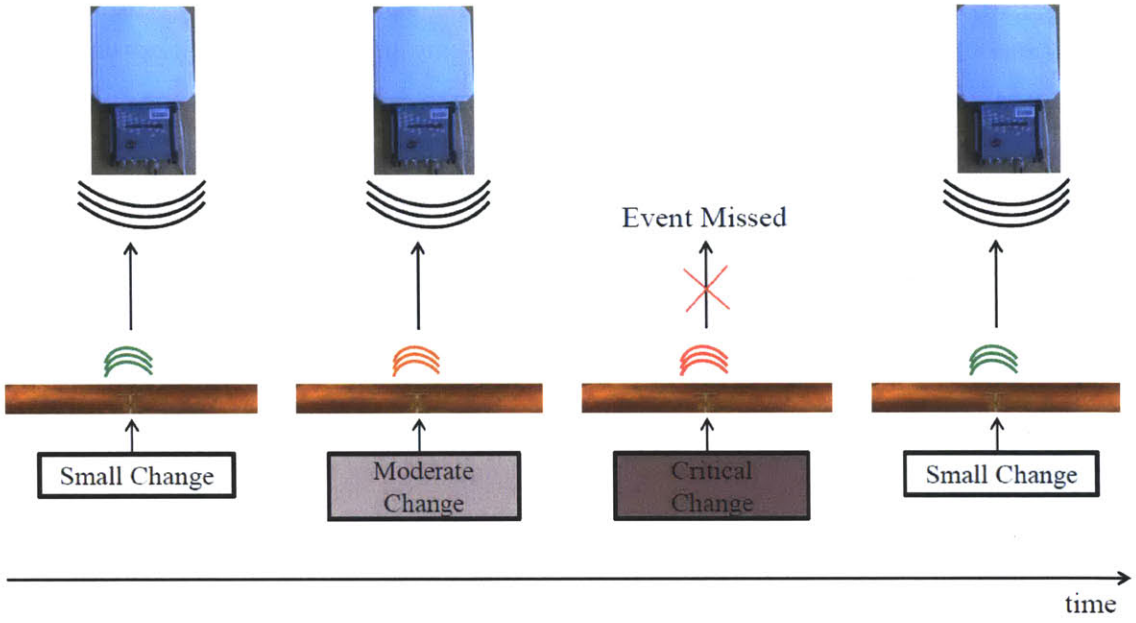

(a) Sensor reports the state of the physical parameter at the time of reader interrogation

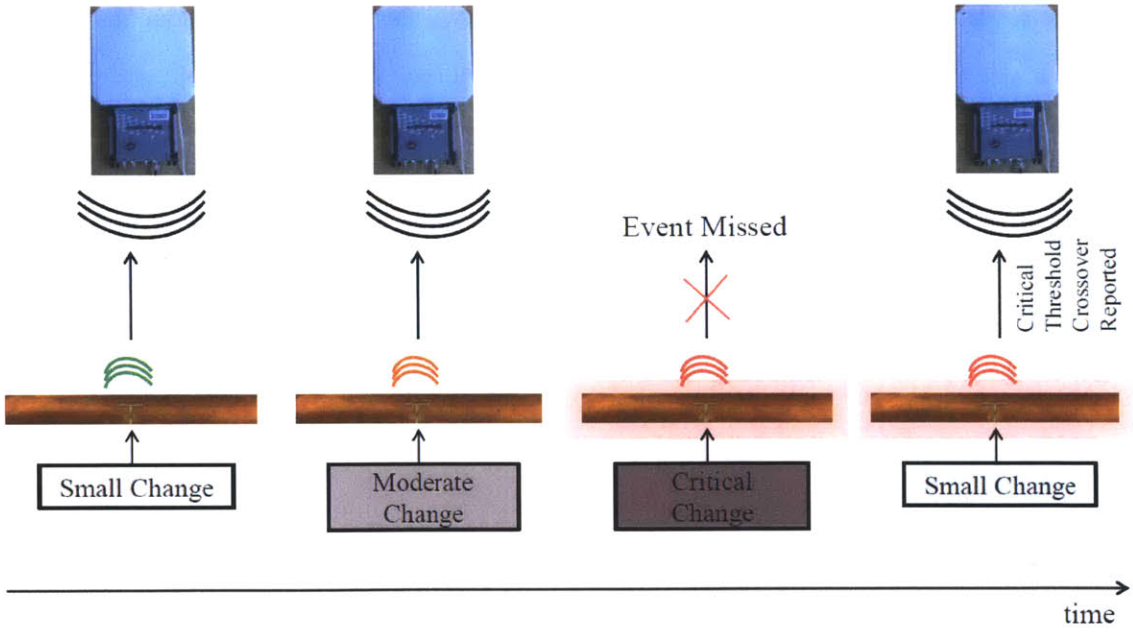

(b) Non electric memory records threshold crossovers by permanently changing tag antenna properties

Figure 1-3: TABS-based state inference methods

1.3.1 Conventional Wireless Sensing

Most wireless sensing technology focuses on the transmission of sensed data which can be achieved with varying degrees of sophistication. One possible approach is to design the wireless sensing device for high precision and accuracy using good quality electronics. The performance can also be enhanced with optional components like on-board memory to store a time history of data, a battery to power the on-board electronics and boost communication range and microcontrollers for programming flexibility. A classic current example is the Sun SPOT wireless sensor node [10]. These features increase the cost of the sensor node which directly impacts the scope and scale of sensor deployment.

Another approach would be to use microelectronic components which are less power intensive and perhaps replace the on-board battery with a front end for power scavenging. A typical example is the Intel WISP platform [11]. This reduces sensor cost but also reduces the read range and on-board computational capabilities of the sensor. In this section, I classify the popular wireless sensing approaches according to the trade-off between sensor cost and degree of sophistication. While doing so, I attempt to identify application spaces ideally suited for each type of sensing philosophy.

Active Wireless Sensors

Active wireless sensors typically consist of a MEMS device or some transduction component that converts changes in the sensed parameter to an electrical response, an on-board battery source, memory for data storage, a microcontroller for processing and wireless communication infrastructure such as an antenna. Fig 1-4(a) illustrates the typical structure of an active wireless sensor node. These sensors have several advantages such as communication range in the hundreds of meters or more in radius, the ability to store time history of data samples, good sampling accuracy and precision. Furthermore with appropriate programming, event-based alarm triggering and monitoring may also be implemented [12]. As a result of which, these sensors have

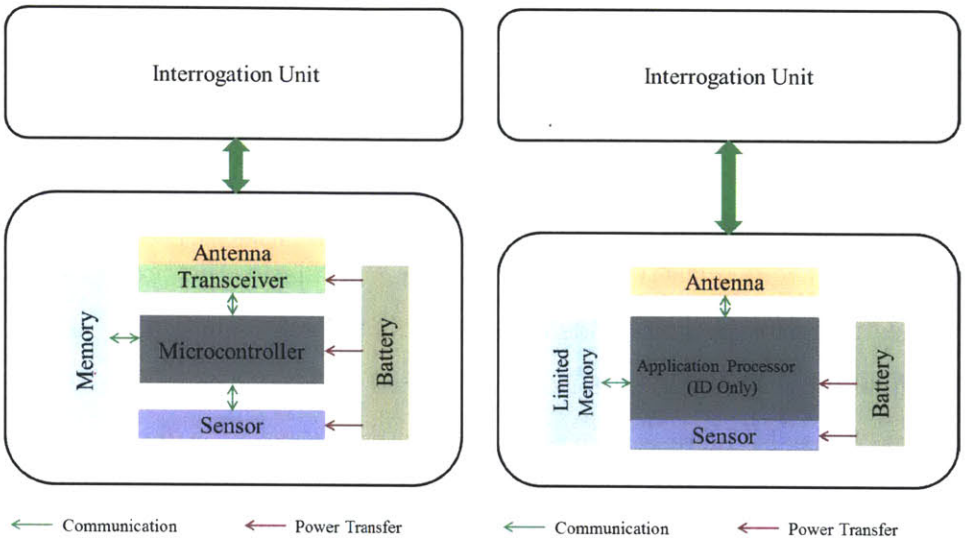

(a) Typical active wireless sensor node

(b) Typical semi-passive wireless sensor node

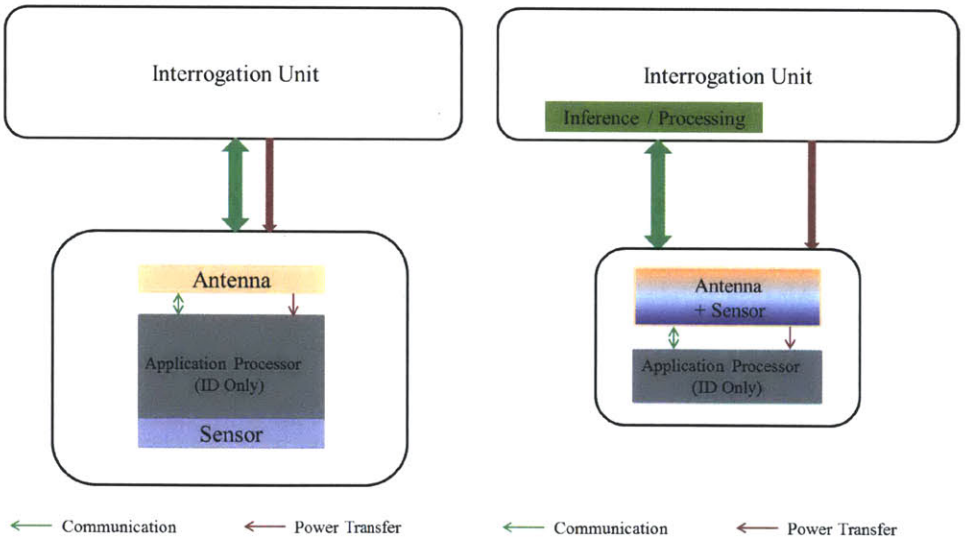

(c) Typical passive wireless sensor node

(d) Tag antenna-based sensing

Figure 1-4: Types of wireless sensors

found application in a wide variety of fields from infrastructure asset management [13] to food quality assurance and agriculture [14]. Puccinelli and Haenggi [15] present an excellent overview of some of the popular active wireless sensing technologies and outline a broad selection of application areas.

However, these sensors have their share of shortcomings that could hinder the scope of application. As outlined in [13] and [14], battery power management and sensor network topology are critical to control the sensor's operational life. Periodic replacement of batteries may be cumbersome or impractical in instances such as environmental and infrastructure monitoring. Similarly, the presence of several discrete electronic components adds to the cost of the sensor node [15] and this may be prohibitively expensive in situations which call for pervasive or large-scale sensor deployment. This also increases the size and weight of the sensor unit which might be undesirable in certain applications. Reducing sensor component costs while minimizing impact on performance and devising innovative techniques for optimizing battery management has become an important area of research [16], [17].

In terms of scope, active wireless sensors are useful in applications which warrant a dedicated monitoring device where the cost of deployment can be justified. For example, an active wireless sensor is ideal for real-time temperature monitoring in the transportation of transplant organs. The high cost reduces the scale of spatial deployment but these sensors could still be used in those environments where sensor node mobility can be used to adequately address the spatial coverage problem [18].

Semi-Passive Wireless Sensors

Active wireless sensors may be prohibitively expensive in situations which call for large-scale sensor deployment where the budget for monitoring is limited and/or coverage via sensor mobility is not an option. In these situations, semi-passive sensing presents a good compromise between sensor functionality, read range and cost.

A typical semi-passive sensor (c.f Fig 1-4(b)) consists of an electrical transduction component for the sensed parameter of interest, an antenna for communication, a light-weight application processor, limited battery source as well as a limited amount

of memory to store data points. The sensor relies on an external power source (typically the interrogation unit) for communication, but uses battery power for the on-board electronics. There has been much development work in semi-passive RFID based temperature sensing for deployment in the cold chain. Early work by Jedermann and Lang [19] compared the performance of three popular types of semi-passive RFID based temperature sensors in terms of cost, accuracy, capacity for data storage and service life. Since then, efforts have been made to reduce sensor form factor and improve battery life expectancy [20].

Semi-passive sensors, having fewer and cheaper discrete electronic components, are typically an order of magnitude cheaper than their active counterparts and so can be deployed at a much larger scale allowing for much tighter process integration. They thus offer temperature, humidity and other information at a much larger scale in cold chain shipping processes. However, these types of sensors employ power efficient electronics as well as a limited on-board power source and so the read range, on board memory as well as the extent to which these sensors can be customized via programming is limited. Furthermore, it is still not economically viable to tag each and every logistical unit in the cold chain using these devices which is the ideal scale of deployment.

Passive Wireless Sensors

In an effort to lower sensor cost further, there has been research into developing and designing passive wireless sensors. Unlike semi-passive or active wireless sensors which make use of an on board battery, passive devices rely completely on power scavenging both for operating the on-board sensor as well as for communication.

One possible approach is to make use of mechanical-electrical transduction techniques such as ambient vibrations and piezoelectric effects to power sensor operations [21] [22]. More commonly, however, the wireless sensor makes use of power supplied by the interrogation unit. Fig 1-4(c) outlines the typical structure of a passive wireless sensing device.

Sensors based on Surface Acoustic Wave (SAW) technology are a well known pas-

sive sensing option used commercially today. For instance, Scholl *et.al* [23] describe how SAW technology can be adapted to design humidity, temperature and torque sensors by relating these parameters to a change in the signal response phase of the SAW device. Similarly, Intel's WISP platform is a passive RFID front end to sensor electronics and has been successfully applied to sense temperature over a broad range of 70°C [11] as well as to sense contact [24].

Passive sensing devices consist of electronics that can reliably function on scavenged power. These are typically limited in functionality and are low cost as well as an order of magnitude cheaper than their semi-passive counterparts. This means that for the same monitoring budget an even greater scale of deployment can be achieved with these sensors. At the same time passive sensing devices suffer from a short read range of a few meters at best. Scenarios which involve the deployment of these sensors also need to factor in an appropriate data extraction strategy. One popular way of achieving this is through mobile agents called as *data mules* that periodically come within interrogation range of the sensor [25]. For example, the SAW temperature sensors deployed on electrical equipment in [23] are read by an interrogation unit suspended close at hand. Furthermore, the on-board electronics are designed to be power efficient so enhanced features such as capacity for memory storage and programmability are absent. This makes recording impulse events such as the crossing of a temperature threshold a challenge in those scenarios where continuous reader monitoring is not possible.

1.3.2 Tag Antenna-Based Sensing

While passive sensors present a good compromise between affordability and functionality, the assembly of custom discrete, low power electronics adds a cost overhead to the sensor manufacturing process — especially when interfacing these with the RFID tag's IC. The TABS paradigm proposed in this thesis, makes no modification to the RFID tag's single integrated IC. Rather, changes in the physical parameter of interest are mapped to changes in the structure or boundary conditions of an RFID tag's antenna. This manifests itself as a controlled change in the electrical properties

of the tag's antenna and thus the signal response of the tag. Signal processing and inference operations are abstracted to the reader side, making the TABS sensor little more than a specialized RFID tag. This allows the TABS technique to directly leverage and benefit from concurrent advancements in RFID research while seamlessly extending it for wireless sensing applications. For instance, TABS sensors are subject to the same improvements in low-cost RFID tag mass production techniques. Fig 1-4(d) illustrates the structure of a TABS sensor.

The general idea of using an antenna as a sensor has become an area of some interest in the recent years. I presented the concept of AM TABS via the design of a displacement sensor [26]. Similar amplitude modification ideas were explored by Siden *et.al*, in the design of a moisture and relative humidity sensor [27] and by Marrocco *et.al*, who showed how changes in the dielectric properties of a medium can be correlated to changes in performance of an RFID tag [28].

I proposed the concept of non-electric memory for recording critically high impulse events that may occur even when the tag-sensor is unpowered. I demonstrated proof of concept via the design of a TABS temperature threshold sensor, which could be used to detect whether or not a critical temperature threshold was ever exceeded [29]. I subsequently improved this design by making use of a shape memory polymer-based thermally actuated switch which emphasized the potential of smart materials engineering in sensor design [30]. In very similar work, Marrocco *et.al* make use of shape memory alloys to design RFID temperature threshold switches [31]. Since then, researchers have utilized chemically responsive HF RFID antennas for detecting and discriminating between mixtures of different volatile organic compounds [32].

I next proposed the concept of FM TABS whereby a change in some physical parameter of interest is correlated to a controlled shift in the frequency band at which the RFID tag is most receptive to reader interrogation. The American UHF RFID spectrum of 902-928 MHz is ideally suited for this type of sensing as the 26 MHz bandwidth is wide enough to accommodate frequency shifts that can be detected using commercial RFID readers. In Chapter 4, I demonstrate proof of concept via the design of an FM TABS temperature threshold [33] and fluid level sensor.

Besides directly leveraging the well established infrastructure for mass manufacturing of low-cost, robust RFID tags, there are other advantages of using TABS. TABS use the standardized Gen 2 Protocol for tag-reader communication and thus data can be seamlessly transferred between multiple business partners as is typical in supply chain operations. Furthermore, since TABS can be interrogated using off the shelf RFID reader equipment, RFID enabled business entities can integrate sensing functionality in their operations at zero additional setup cost.

While TABS allows for the development of robust, low-cost tag-sensors for pervasive sensing, they have certain shortcomings. Like other passive sensors, TABS have a limited read range of a few meters and would require an efficient data extraction strategy as well. Furthermore, the manipulation of a tag's geometry or boundary conditions by a sensed parameter is often initiated via mechanical methods — such as the actuation of a metal plate relative to an RFID tag. This leads to coarser estimates of the physical parameter of interest than those obtained obtained from a corresponding digital silicon counterpart.

However these sensors can be deployed at a much larger scale since they leverage the RFID tag manufacturing infrastructure for the low-cost, mass production of tag sensors. Furthermore, a simple coarse response such as detecting the presence or approximate magnitude of the physical parameter might in fact be sufficient. For example, simple pervasive strain alarm sensors that indicate whether or not the strain in a concrete bridge deck exceeds design specifications would be invaluable in health monitoring of civil infrastructure. TABS devices could also be used in tandem with active sensors for hybrid sampling schemes that optimally gather information about the state of a system [34].

In the next section, I discuss three application scenarios that lend themselves well to the TABS approach. Prototype development in these three areas is considered in this thesis. I conclude this section with Fig 1-5 that summarizes the tradeoffs between the different paradigms of sensing discussed in this chapter.

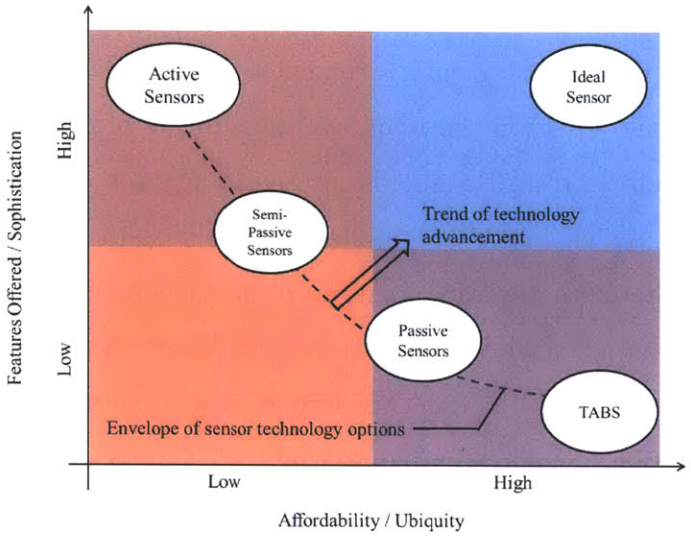

Figure 1-5: Tradeoffs in wireless sensing

1.4 Application Domains Considered for Prototype Development

In this thesis, I examine sensor development in three representative areas that would benefit from the TABS approach to pervasive sensing:

- *Infrastructure Asset Management*: Civil infrastructure like bridges and buildings are typically made of inhomogeneous construction materials like concrete which are prone to local effects such as cracking and hence, offer a prime environment for pervasive sensor deployment. Structural health monitoring would greatly benefit from strain threshold alarm sensors which change state on being exposed to critical strain levels or displacement sensors that monitor excessive sagging in beams or buckling in columns. Periodic inspection can be achieved by instrumenting reader units on passing highway maintenance trucks or any other service vehicle that passes over (or close to) the structure at regular intervals. Structural conditions remain fairly static over time and thus this frequency of monitoring should be sufficient. In Chapter 2, I introduce the design of a displacement sensor for application in this area.

- *Cold Chain*: TABS are well suited for cold chain monitoring, since many supply chains have already have been instrumented with RFID monitoring infrastructure. One could envision the item level monitoring of parameters such as the crossing of temperature thresholds, presence or absence of botulism or other kinds of food toxins at discrete points in the cold chain using TABS based sensors. This allows for the early removal of detrimental food items and has the potential to assign chain of custody responsibility. In Chapter 3 and Chapter 4, I discuss several alternative designs of a temperature threshold sensor with application in cold chain monitoring.

- *Energy*: TABS are well suited for applications in the energy sector. For example, the problem of clathrate [35] build up in the oil and natural gas industry could be addressed by designing a TABS based blockage detector for pervasive deployment in oil pipelines. Another common problem of detecting the fluid level of electrolyte in backup generator batteries could be addressed using a TABS based fluid sensor. In Chapter 4 and Chapter 5, I examine two possible approaches for the design of a fluid level sensor.

Chapter 2

Amplitude Modifying (AM) TABS

UHF RFID tags work on the principle of radiative power transfer between the reader and tag antennas. Tag performance, in terms of read range, centers around the reader-tag power budget links. The *Forward Link*, focuses on the transmission of power from the reader antenna to the RFID tag's IC, while the *Reverse Link* focuses on the reception of tag backscatter power at the reader antenna [9] [36]. From a power measurement perspective, there are two parameters on the reader side that can be regulated or measured: the power supplied by the reader's transmitted antenna and the differential backscatter power received from an RFID tag.

These power metrics have been examined for several diverse applications in the literature. For instance, backscatter power has been used to provide location estimates of an RFID tag ([37], [38]). Similarly the impact of metals and water on RFID tag backscatter power and reader transmitted power, and thus read range, have been studied by Deavours *et.al* [39]. In this chapter, I demonstrate how both these power parameters can be used for sensing applications.

2.1 AM TABS 1: Using Reader Threshold Transmitted Power for Sensing

In this section, I discuss the term *Reader Threshold Transmitted (TX) Power*, its relationship with the forward link power budget and how it can be used for sensing. I provide only a summary of relevant background terminology — a detailed review of power transmission, to and from an RFID tag, may be found in several references ([9], [40]).

Fig 2-1(a) illustrates a typical RFID reader-tag system. Note that the RFID tag has been represented by the equivalent circuit model depicting the antenna impedance and the chip impedance for the condition where the RFID tag is scavenging power from the reader. I define P_t to be the power transmitted by the reader antenna and $G_{reader}(\theta, \phi)$ to be the directional gain of the reader antenna in the direction of the tag. The reader-tag separation distance is denoted by d. At this distance, the power density impinging on the tag is calculated as per the Friis Transmission equation [9] for free space applications and is given as

$$P(d) = \frac{P_t G_{reader}(\theta, \phi)}{4\pi d^2}. \tag{2.1}$$

Assuming the RFID tag has a directional gain of $G_{tag}(\theta, \phi)$ and the wavelength of the reader carrier signal is λ, the tag's effective area can be computed as [9]

$$A_e = \frac{G_{tag}(\theta, \phi)\lambda^2}{4\pi}. \tag{2.2}$$

Therefore, the total power impinging on the RFID tag's antenna computed from Eq 2.1 and Eq 2.2 can be written as

$$P_{tag|antenna} = \frac{P_t G_{reader} G_{tag} \lambda^2 p_L}{(4\pi d)^2} \tag{2.3}$$

The expressions for $G_{tag}(\theta, \phi)$ and $G_{reader}(\theta, \phi)$ are condensed to G_{tag} and G_{reader} from this point on for the sake of brevity. Eq 2.3 also includes a polarization mismatch

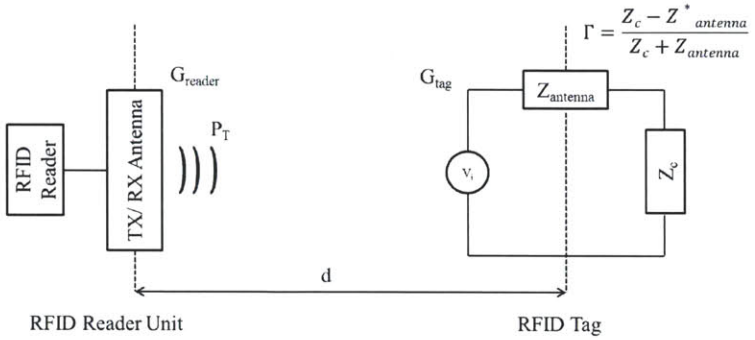

$$P_{threshold} = \frac{P_{sens}}{G_{reader} G_{tag} \left(\frac{\lambda}{4\Pi d}\right)^2 (1 - |\Gamma|^2)}$$

(a) Reader threshold transmitted power

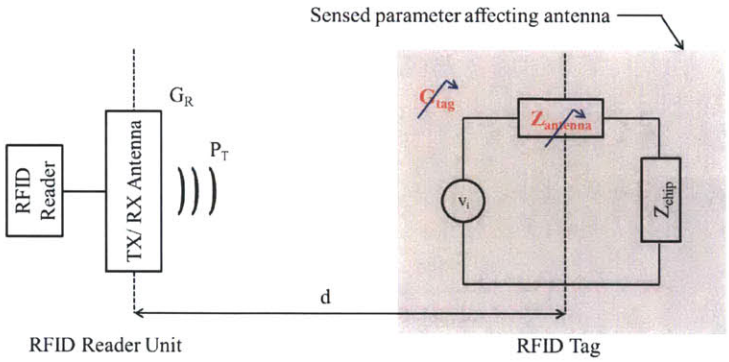

$$P_{threshold}(\Delta) = \frac{P_{sens}}{G_{reader} G_{tag}(\Delta) \left(\frac{\lambda}{4\Pi d}\right)^2 (1 - |\Gamma(\Delta)|^2)}$$

(b) Threshold power-based sensing

Figure 2-1: AM TABS 1: Using reader threshold transmitted power for sensing

loss factor p_L that depends upon the tag and reader electric field polarizations and is a function of the orientation of the reader antenna relative to a tag antenna. Since it is not critical to our analysis, I will assume $p_L = 1$ for simplicity. Of the power impinging on the tag antenna, a part of it is scattered from or dissipated in the tag antenna and the other part is transferred to power up the tag integrated circuit (IC). The fraction of power transferred from the antenna to the chip depends on how 'well matched' the tag IC is to the antenna impedance and this is measured by a parameter known as the power wave reflection coefficient Γ [41]

$$\Gamma = \frac{Z_c - Z^*_{antenna}}{Z_c + Z_{antenna}}. \tag{2.4}$$

Here Z_c and $Z_{antenna}$ are the chip and antenna impedances respectively and $Z^*_{antenna}$ is the complex conjugate of $Z_{antenna}$. The power absorbed by the chip can then be computed as [42]

$$\begin{aligned} P_{chip} &= P_{tag|antenna}(1 - |\Gamma|^2) \\ &= \frac{P_t G_{reader} G_{tag} \lambda^2 (1 - |\Gamma|^2)}{(4\pi d)^2}. \end{aligned} \tag{2.5}$$

Rearranging Eq 2.5 we get

$$P_t = \frac{P_{chip}}{G_{reader} G_{tag} (\frac{\lambda}{4\pi d})^2 (1 - |\Gamma|^2)}. \tag{2.6}$$

I define the chip sensitivity, $P_{sens} = min(P_{chip})$, as the minimum power needed to activate the tag's IC. $P_{threshold}$ can thus be defined as the minimum reader transmitted power that needs to be supplied so that the tag just receives P_{sens}:

$$P_{threshold} = \frac{P_{sens}}{G_{reader} G_{tag} (\frac{\lambda}{4\pi d})^2 (1 - |\Gamma|^2)}. \tag{2.7}$$

A sensing strategy can be devised by having changes in a parameter of interest induce changes in the geometry or boundary conditions of an RFID tag. Thus manifests itself in a change in $Z_{antenna}$ and G_{tag} as shown in Fig 2-1(b). $Z_{antenna}$ and G_{tag}

now become functions of changes (Δ) in the parameter of interest. Thus $P_{threshold}$ itself becomes a non-linear function of changes in the parameter of interest as outlined below.

$$P_{threshold}(\Delta) = \frac{P_{sens}}{G_{reader}G_{tag}(\Delta)(\frac{\lambda}{4\pi d})^2(1-|\Gamma(\Delta)|^2)}. \tag{2.8}$$

I investigate the applicability of threshold transmitted power for sensing via the design of an RFID displacement sensor. The sensor design and sample results are outlined in Section 2.3.

2.2 AM TABS 2: Using Tag Backscatter Power for Sensing

In this section, I discuss the concept of *RFID Tag Backscatter Power*, its relationship with the reverse link power budget, and the application to sensing. I introduce the concept by providing a summary of the relevant background terminology - the reader is referred to ([9], [40], [43]) for details.

Fig 2-2(a) illustrates an RFID reader-tag system where the tag has been represented by the equivalent circuit model for the state where the RFID tag is backscattering ID information back to the reader. The tag IC has two impedance states denoted by Z_{c1} and Z_{c2} as shown in the figure. By rapidly switching between states 1 and 2, the tag modulates a backscatter response and communicates with the reader. There are several modulation schemes like amplitude, phase and hybrid modulation that have been investigated [44], however discussing these is beyond the scope of this thesis. For the purposes of this chapter, I focus on the amplitude modulated backscatter response where one state, say Z_{c1}, is typically well matched to $Z_{antenna}$ while the other, Z_{c2} is poorly matched typically being a short or open circuit condition. This is represented by two power wave reflection coefficients for the two load conditions:

$$\Gamma_i = \frac{Z_{ci} - Z^*_{antenna}}{Z_{ci} + Z_{antenna}}. \tag{2.9}$$

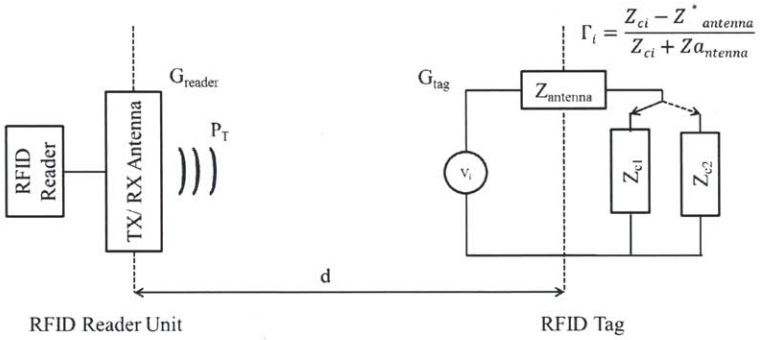

$$P_{bs|reader} = P_T\left(\frac{G_{reader} G_{tag} \lambda^2}{(4\Pi d)^2}\right)^2 (|\Gamma_1 - \Gamma_2|^2)$$

(a) Differential backscatter power

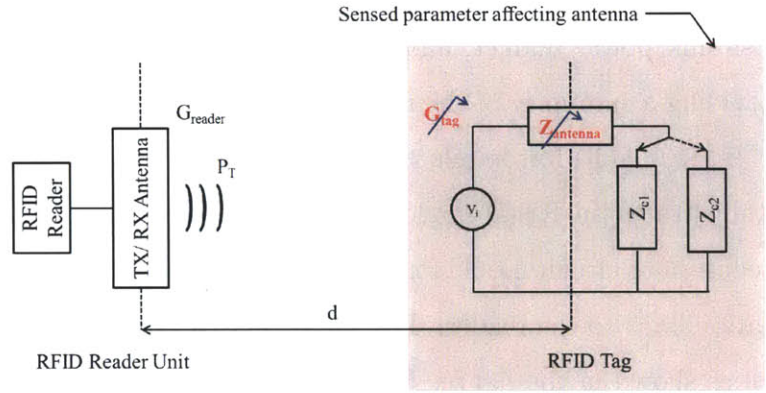

$$P_{bs|reader}(\Delta) = P_T\left(\frac{G_{reader} G_{tag}(\Delta) \lambda^2}{(4\Pi d)2}\right)^2 (|\Gamma_1(\Delta) - \Gamma_2(\Delta)|^2)$$

(b) Backscatter power-based sensing

Figure 2-2: AM TABS 2: Using tag differential backscatter power for sensing

Here the index $i = 1, 2$. It is easy to see that $|Z_{c1}| \approx 0$ and $|Z_{c2}| \approx 1$. Considering the tag circuit, the power impinging on the RFID tag induces a voltage V_0 which is manifested in current I_i flowing through the tag circuit. The magnitude and phase of I_i depends on the chip impedance state Z_{ci}.

$$I_i = \frac{V_0}{Z_{antenna} + Z_{ci}} \tag{2.10}$$

The differential backscatter power reflected from the RFID tag's antenna towards the reader antenna is a manifestation of the tag flipping between two impedance states and is given by [43]:

$$P_{BS|tag} = \frac{1}{2}|I_1 - I_2|^2 G_{tag}. \tag{2.11}$$

Here $P_{BS|tag}$ is the backscatter power radiating from the tag's antenna. Now using Eq 2.10 and Eq 2.9, we can rewrite I_i

$$I_i = \frac{V_0(1 - \Gamma_i)}{Z_{antenna} + Z^*_{antenna}}. \tag{2.12}$$

I express $Z_{antenna} = R_a + j * X_a$ where R_a is the sum of the radiating resistance and ohmic resistance of the tag antenna and X_a is the reactance of the tag's antenna, we can rewrite Eq 2.12 as

$$I_i = \frac{V_0(1 - \Gamma_i)}{2R_a}. \tag{2.13}$$

Using Eq 2.13 in Eq 2.11 we obtain the expression for $P_{BS|tag}$ [43] to be:

$$P_{BS|tag} = \frac{{V_0}^2}{8R_a}|\Gamma_1 - \Gamma_2|^2 G_{tag}. \tag{2.14}$$

The term $\frac{{V_0}^2}{8R_a}$ corresponds to the power available to the RFID tag and, for free space conditions, is captured by Eq 2.3. Thus Eq 2.14 can be rewritten as

$$P_{BS|tag} = \frac{P_t G_{reader} G_{tag} \lambda^2}{(4\pi d)^2}|\Gamma_1 - \Gamma_2|^2 G_{tag}. \tag{2.15}$$

Note that in Eq 2.15, I have dropped the (θ, ϕ) notations for G_{reader} and G_{tag} and have assumed that $p_L = 1$. Factoring in path losses on the way back to the reader and the directional gain of the reader itself, we can make an estimate of the differential backscatter power detected at the reader, under free space condition assumptions, to be:

$$\begin{aligned} P_{BS|reader} &= \frac{P_t G_{reader} G_{tag} \lambda^2}{(4\pi d)^2} |\Gamma_1 - \Gamma_2|^2 * \frac{G_{tag}}{4\pi d^2} * \frac{G_{reader} \lambda^2}{4\pi} \\ &= P_t (\frac{G_{reader} G_{tag} \lambda^2}{(4\pi d)^2})^2 |\Gamma_1 - \Gamma_2|^2. \end{aligned} \tag{2.16}$$

As discussed in Section 2.1, a tag antenna based sensing strategy involves a change in the tag geometry or boundary conditions brought about by a change in the sensed parameter. This causes a change in $Z_{antenna}$ and G_{tag} as shown in Fig 2-2(b). Γ_1 and G_{tag} thus become functions of changes (Δ) in the parameter of interest. Thus $P_{BS|reader}$ itself becomes a non-linear function of changes in the parameter of interest as outlined below

$$P_{BS|reader}(\Delta) = P_t (\frac{G_{reader} G_{tag}(\Delta) \lambda^2}{(4\pi d)^2})^2 |\Gamma_1(\Delta) - \Gamma_2(\Delta)|^2. \tag{2.17}$$

2.3 Case Study: AM TABS Displacement Sensing

It is a known fact that RFID tag performance degrades in close proximity to metals and water. Prior research has tried to quantify this [39] and propose solutions in terms of innovative antenna design [45] [46] or via the use of appropriate background dielectric structures [47]. I adopt a different approach of utilizing this inherent disadvantage for sensing applications. I design a displacement sensor by mapping displacements to a change in the relative position between an RFID tag and a metal plate and quantify how the position of the metal plate influences tag performance [26].

2.3.1 Description of the Experimental Setup used for Displacement Sensing

Fig 2-3(a) illustrates the experimental setup used for displacement sensing. A simply supported beam is subjected to a variable load at its midpoint. A metal plate is attached to the midpoint of the beam directly under the applied load. An RFID tag is placed at a reference distance R=65 mm from the metal plate. By increasing the load, the midspan displacement Δ of the beam is progressively increased from 0 mm to 50 mm in steps of 2.5 mm as outlined in Fig 2-3(b). The chosen range of 50 mm is typical of displacements in civil infrastructure as outlined by Hou *et.al* [48]. In this section, I discuss the specifics of the experimental setup with regards the reader and tag equipment used, and the positioning of the reader-tag system.

- For the purposes of this experiment, I use the Impinj Banjo [49] RFID tag which has a form factor of 80 X 80 mm and which is printed with conductive silver ink. The RFID tag IC used is the Impinj Monza [50] which is fully Gen 2 compliant.

- To demonstrate proof of concept, I use the Voyantic Tag Measurement Equipment [51] for high precision threshold and backscatter measurements from the RFID tag. Comparative measurements from commercial off-the-shelf RFID equipment are then made to examine applicability of this sensing methodology in the field.

- The reader-tag separation was set at 1000 mm for the experiment and ensuring line of sight between the reader and tag antennas. The experiments were conducted in an open room without any special anechoic provisions [52] to simulate real conditions. However, recognizing that power amplitude measurements are prone to multipath effects, I repeat each power measurement experiment at least five times for every test in order to get an estimate of the variation in the data.

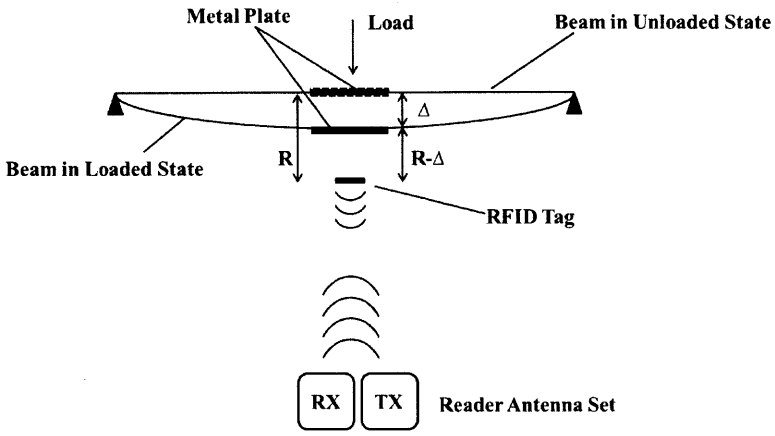

(a) Deflection of beam midpoint under load

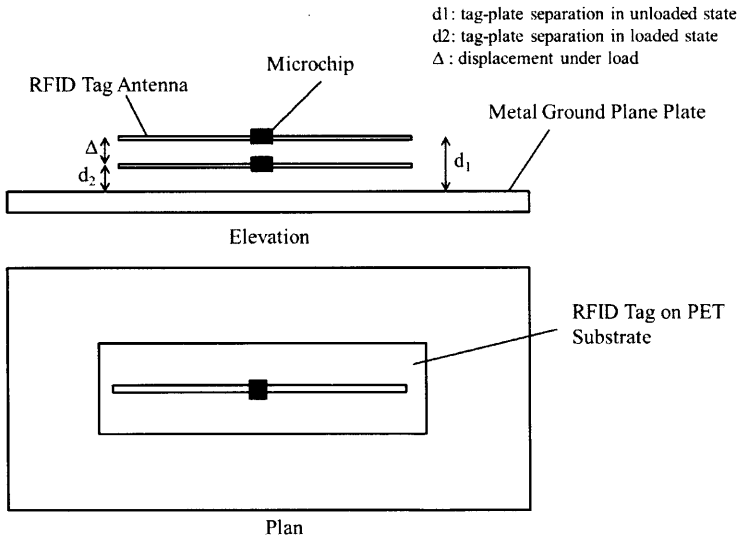

(b) Movement of plate relative to tag

Figure 2-3: Experimental setup to measure displacement: displacements are mapped to a change in relative position between the RFID tag and a metal plate and the effect on RFID tag performance is measured

2.3.2 Determining Proof of Concept: Results with Precision Tag Power Measurement Equipment

I test the sensor hypothesis using the precision tag power measurement capabilities of the Voyantic Lite Equipment [51]. Fig 2-4(a) illustrates the plot of reader threshold transmitted power as a function of displacement. As we can see from the figure, the curve follows a monotonically increasing trend. This trend is logically sound — as the metal plate comes closer to the tag, it increasingly detunes $Z_{antenna}$ relative to Z_{c1} making $|\Gamma|$ in Eq 2.5 smaller. Thus for a given reader-tag separation, the reader needs to supply more transmitted power in order to just power up the RFID tag. It is encouraging to note that over the dynamic range of 15 mm (27.5 mm to 42.5 mm in Fig 2-4(a)) there is a one-one correspondence between threshold transmitted power and displacement. The standard error bars correspond to five measurement repetitions. We see that the sensor has a precision of about 2.5 mm.

Fig 2-4(b) illustrates the plot of reader detected backscatter power as a function of displacement. Note that in the experiment, the reader transmitted power is fixed at 36 dBm Equivalent Isotropically Radiated Power (EIRP). As we can see from the figure, this is a monotonically decreasing curve for beam displacements of 27.5 mm to 45 mm. This trend is logically sound as well — as the metal plate comes closer to the tag, Γ_1 reduces and thus $|\Gamma_1 - \Gamma_2|$ in Eq 2.16 reduces as well. The backscatter power received at the reader for a given reader-tag separation and fixed reader transmitted power thus decreases. This result is encouraging as well since it demonstrates that displacements can be successfully and unambiguously mapped to tag backscatter power over a dynamic range of 17.5 mm (27.5 mm to 45 mm in Fig 2-4(b)) and to a resolution of 2.5 mm using an ordinary off-the-shelf RFID tag.

The reader may question why the backscatter measurements corresponding to a beam displacement of 0–15 mm do not conform to the decreasing trend observed in Fig 2-4(b), and I examine this further in Section 2.4.3.

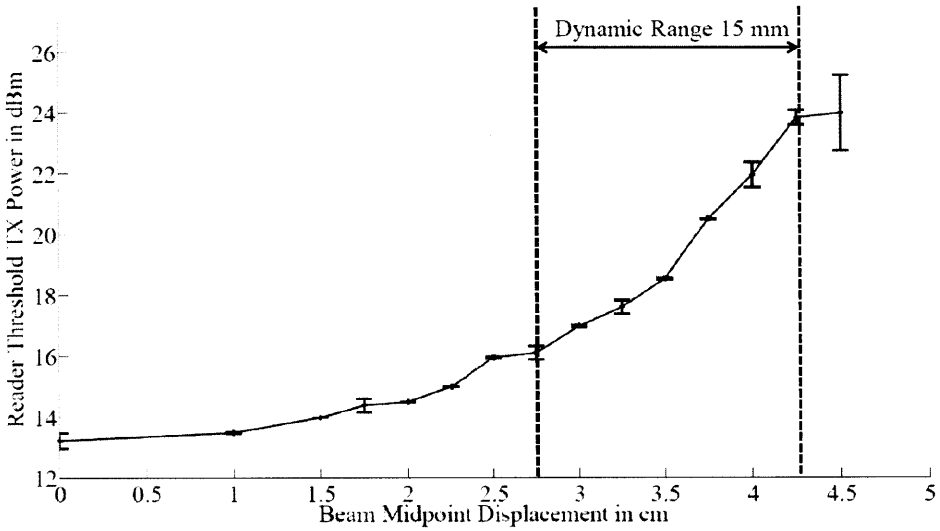

(a) Threshold power vs. displacement

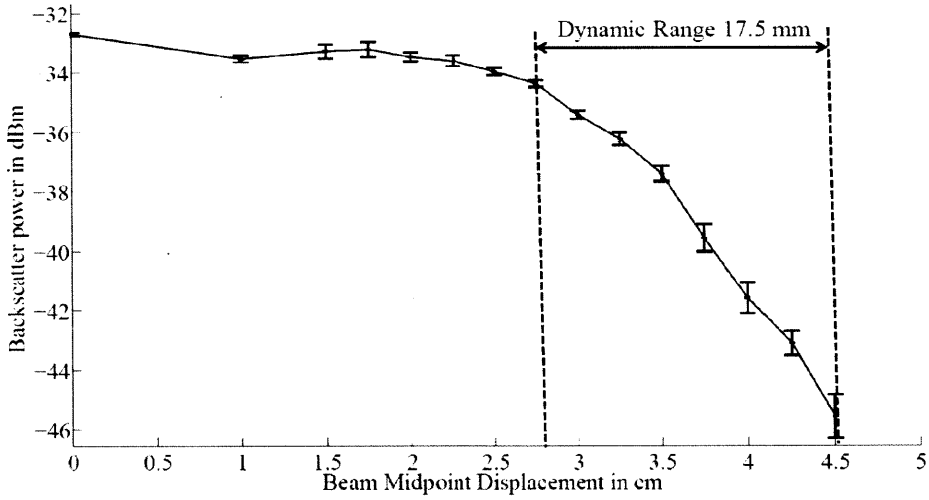

(b) Backscatter power vs. displacement

Figure 2-4: Proof of concept: Displacement measurements with precision tag power measurement equipment; average values are plotted and the error bars correspond to the standard deviation over 5 repetitions; the Impinj Banjo RFID tag was used and the reader-tag separation was set to 1 m

2.3.3 Determining Universal Applicability: Results with Commercial RFID Reader Equipment

The Voyantic Lite equipment is designed for precision tag measurements and has several features such as sophisticated on board signal processing electronics and the ability to fix reader operating frequency. Equipment of this type is designed for research purposes and cannot easily be used in practice because it violates the FCC's frequency hopping regulation [9]. Furthermore, price of the equipment may be prohibitive for some applications. It is therefore important to assess the displacement sensor performance using a commercially available UHF RFID reader such as the Impinj Speedway [53].

Fig 2-5(a) and Fig 2-5(b) illustrate the variation of displacement with threshold and backscatter power respectively. The standard error bars in these graphs were computed over 40 measurements. When using the Impinj RFID reader, as we can see, the trends of the curves remain the same as in Fig 2-4; however, the measurements are subject to much greater uncertainty and the performance curves are not as smooth. This is because, unlike the Voyantic Lite equipment,the Impinj equipment is designed for maximizing tag throughput and not precision power measurements. Thus the on board electronics are less precise. Furthermore, the Impinj reader implements FCC mandated frequency hopping [9] and changes reader operating frequency every 400 ms. Changes in operating frequency cause subtle changes in Z_c,$Z_{antenna}$ and thus Γ_1 and Γ_2. This adds to the measurement uncertainty.

Fig 2-6 illustrates variation of tag backscatter power signal with reader operating frequency when the Impinj tag is placed at a distance of 1 m from the reader and illuminated with 36 dBm EIRP of transmitted power. Approximately 40 data points are taken at each frequency to determine variation. As we can see from the figure, not only is there a variability of about 1.5 dBm at a specific frequency but the mean backscatter power varies by up to 1.5 dBm across frequencies in the 902-928 MHz band. The combination of less precise electronics and frequency hopping contributes to additional measurement error and reduces the dynamic range and resolution of

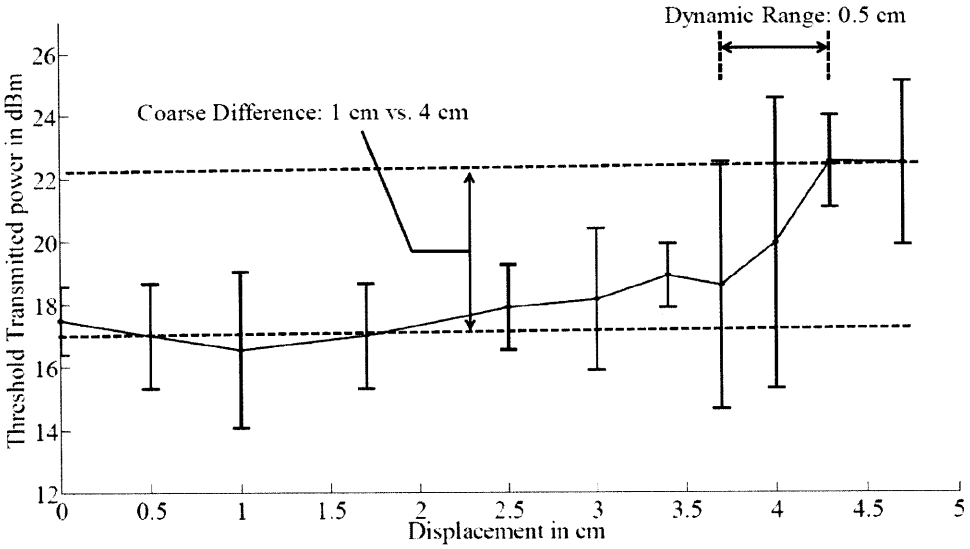

(a) Threshold power vs. displacement

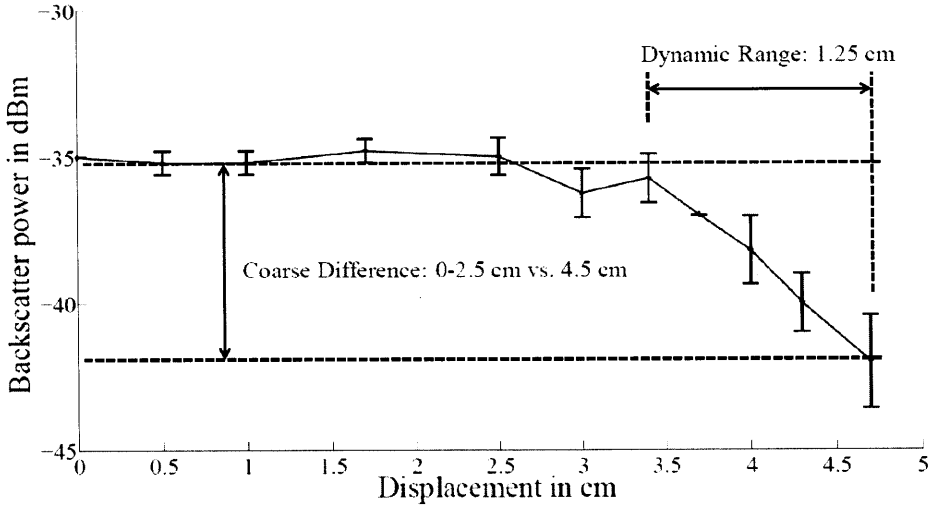

(b) Backscatter power vs. displacement

Figure 2-5: Determining applicability: Displacement measurements using off-the-shelf RFID reader equipment such as the Impinj Speedway; average values over 40 measurements are plotted and the standard error bars are reported; the Impinj Banjo RFID tag is used and the tag-reader separation is set to 1 m

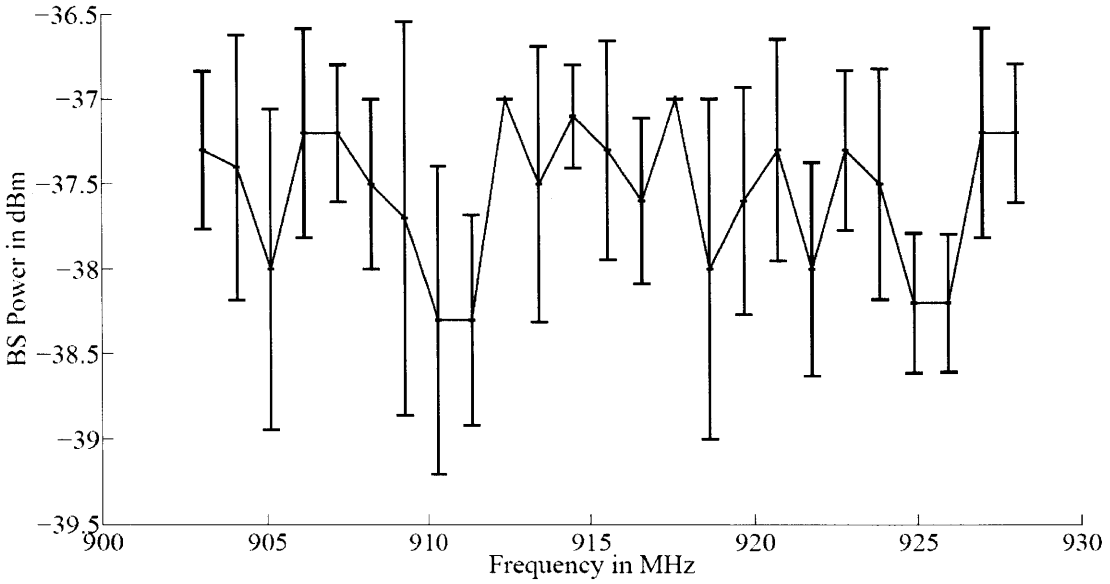

Figure 2-6: Variation of backscatter power with frequency when using the Impinj Speedway equipment: 40 data points were taken per channel and the average values with standard error bars were reported; tag-reader separation was set to 1 m and the reader was transmitting at 36 dBm EIRP

measurement.

From Fig 2-5(a), we observe that the dynamic range of the sensor is 0.5 cm (corresponding to plate displacements of 3.75 to 4.25 cm) when using threshold transmitted power as a sensing metric. Similarly, if we use backscatter power as a sensing metric, we observe from Fig 2-5(b) that the dynamic range of the sensor is about 1.25 cm (corresponding to plate displacements of 3.5 to 4.75 cm). Despite the reduced dynamic range and sensor resolution, we can envision using commercial RFID equipment to assess coarse differences in beam displacement such as differentiating between 0-1 and 4 cm of displacement. In Section 2.4.3, I comment more on the dynamic range of measurements.

2.4 Comparison of AM TABS 1 and AM TABS 2

The performance of AM TABS 1 and 2 can be compared through two performance metrics that influence their area of application and scope of deployment:

2.4.1 Performance Metric 1: Speed of Interrogation

Establishing the threshold transmitted power is a time consuming process and typically involves starting the experiment at the minimum reader transmitted power, looking for the tag-sensor, and then gradually stepping up the power in increments until the tag is detected or the FCC maximum value of 36 dBm EIRP [9] is reached.

For example, if the reader has N discrete power settings, determining the threshold power is an O(N) process in the naive case and a O(log N) process using a binary search technique [54]. Assuming that we pause for t seconds at each power setting to look for the RFID tag and establish that it reliably responds, the threshold sweep requires O(t*log N) seconds when using a binary search technique.

On the other hand, measurements using backscatter power do not require the determination of a threshold and thus can be conducted at a fixed power setting, say 36 dBm EIRP. Therefore determining state with backscatter power typically takes t seconds to complete.

Thus for situations calling for rapid state inferences, such as temperature monitoring of goods passing by a dock door reader in the supply chain, backscatter power-based AM TABS find greater appeal.

2.4.2 Performance Metric 2: Measurement Precision

To understand sensor precision, we must examine the sources of variability in tag power measurement. Uncertainty in power measurements can be attributed to multipath effects as well as the power and frequency dependence of the RFID tag IC impedance.

Effect of Multipath on Sensor Precision

The first source of uncertainty, multipath effects, are a function of environment and are known to influence power measurements. To demonstrate this, I examine the effect of moving a metallic reflector in close proximity of the experimental setup as seen in Fig 2-7(a). For a tag-reader separation d of 1 m, the distance x is set so that

the path difference p is λ and 0.5 λ. These correspond to constructive and destructive interference and are together known as propagation channel fading [9]. The variation of backscatter power as a function of transmitted power is measured for a beam displacement, Δ=4.25 cm. We observe that the backscatter power reflected by the tag is consistently more for the constructive interference case. Thus the position of sources of reflection certainly does influence the power measurements from the RFID tag. It is important to note that threshold transmitted power based measurements suffer from single channel fading (reader-tag propagation) while backscatter power measurements are prone to double channel fading (reader-tag-reader propagation). Thus the effect of channel fading is more significant for backscatter power-based AM TABS.

Effect of Chip Impedance on Sensor Precision

The second source of variability is the RFID tag IC's impedance. It is known that Z_c is a function of both input power and frequency [55]. Frequency hopping mandated in US UHF RFID operations [9] would change the instant value of Z_c and thus Γ in Eq 2.7 as well as Γ_1 in Eq 2.16. This adds to the measurement uncertainty in the case of both AM TABS 1 and 2, when using a commercial RFID reader such as the Impinj Speedway. We may note that tag power measurement tools such as the Voyantic Lite allows us to fix the reader operating frequency, removing this source of uncertainty. This would explain the smaller error bars associated with measurements taken with the Voyantic Lite equipment.

In the case of the threshold-based AM TABS, the input power supplied to the chip is equal to P_{sens} which is a constant value for a given IC. Thus Z_c at P_{sens} is a constant quantity. In the backscatter-based AM TABS, the input power reaching the IC is variable and depends on reader-tag separation, the transmitted power supplied by the reader antenna and multipath effects. Thus Z_c varies with input power in the case of backscatter-based AM TABS — an additional source of uncertainty. We would thus expect measurements based on threshold AM TABS to have better precision - a fact that is corroborated by looking at the error bars on Fig 2-4(a) relative to Fig 2-

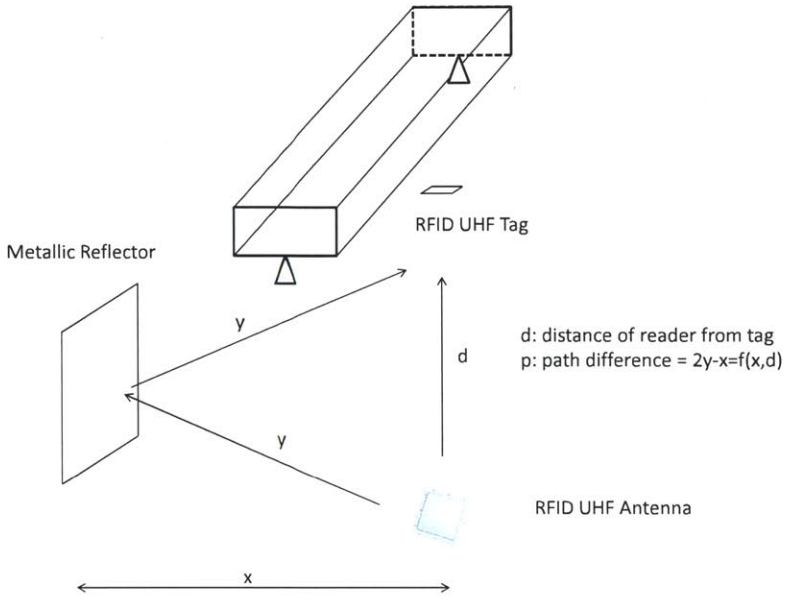

(a) Experimental setup to determine multipath effect of reflectors in the vicinity of the displacement sensor setup

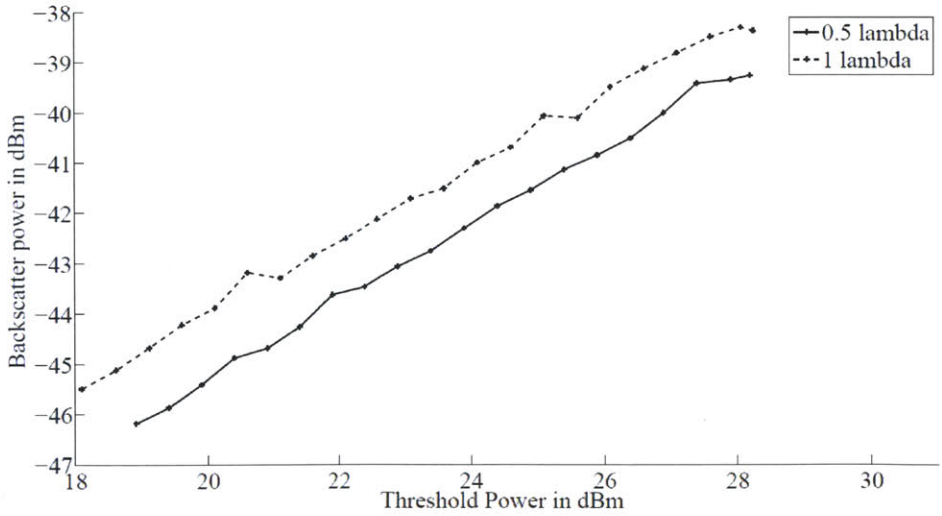

(b) Effect of multipath on backscatter power for the displacement sensor setup

Figure 2-7: Determining the effect of multipath due to the presence of metallic reflectors in proximity to the displacement sensor setup; measurements correspond to a reader carrier frequency of 915 MHz; experiments are conducted using precision tag power measuring equipment

4(b). Thus in situations requiring better precision threshold-based AM TABS have better appeal.

2.4.3 Comments on the Dynamic Range of the AM TABS Displacement Sensor

Section 2.4.2 provided a summary of the sources of measurement uncertainty for the AM TABS displacement sensor. I use this background to comment further on the dynamic range of the sensor.

Dynamic Range using the Voyantic Lite Equipment

Multipath effects cause varying amount of input power to reach the chip which causes variations in Z_c. This might explain why the backscatter measurements corresponding to a beam displacement of 0—15 mm do not conform to the curve's decreasing trend as observed in Fig 2-4(b). It is possible that the changes to Z_c for small beam displacements of 0—15 mm may be more sensitive to random multipath effects than the metal plate's position. Once the metal plate is close, corresponding to a beam displacement of 25 mm and greater, the detuning effect of the plate dominates. This is why the monotonically decreasing trend in Fig 2-4(b) appears only for larger beam displacements of 25—45 mm

Dynamic Range using the Impinj Equipment

A similar explanation can be extended to the results with the Impinj equipment. Here in addition to the fluctuations in Z_c due to multipath, frequency hopping adds additional variability to the value of Z_c. From Fig 2-5(a) we see that the average threshold transmitted power seems to at first decrease till Δ=10 mm and then gradually increase. The region of significance is between 37.5—42.5 mm when the metal plate is very close to the RFID tag where the detuning effect of the metal plate overrides these uncertainties. Similarly, looking at Fig 2-5(b), we see that there are fluctuations in the curve's trend, with an anomalous dip at Δ=30 mm. Once again, the region of

significance is between 35—47.5 mm when the metal plate is very close to the RFID tag.

This theory can be easily verified by repeating the experiment in another environment where the multipath conditions would be different. However, I do not examine this any further in this thesis and leave it as a open question for future work.

2.5 Related Work in AM TABS

Besides displacement sensing, amplitude modification has been applied for sensing other modalities as well. For instance, Siden *et.al* investigate the application of tag backscatter and reader threshold transmitted power for moisture and relative humidity sensing [27]. They conclude that both metrics can be reliably applied to detect both relative humidity levels over 70% and to detect increases in ambient water content due to leaks. Recognizing the need for read-range independence, the authors also make use of a reference tag in their experiments. We note that in this case as well the sensing strategy was implemented using commercially available RFID tags.

Marrocco *et.al*, discuss how differences in dielectric permittivity can be related to backscatter response signatures of either multiple RFID tags clustered on the material to be monitored or to the response of a multi port RFID tag placed on the material to be monitored [28]. The authors provide a theoretical background and then validate their approach by testing how effectively they can sense the height of sugar in a carton via simulation and experimentation. The authors eliminate not only the dependence on read range, but also the variability associated with different tag-reader orientations.

In similar work, I use backscatter measurements at multiple antennas to detect the level of fluid in a beverage glass in a crowded restaurant-like setting [56]. While multipath interference prevented me from successfully identifying fluid level, I was able to use the technique to detect binary level events - such as the presence or absence of fluid near an RFID tag - with a reasonable degree of success.

Chapter 3

Non-Electric Memory Methods for Threshold Crossover Detection

Passive sensors like TABS draw power from an external RF field for communication and operation which means that sensor data can be gathered only when the TABS device is within the interrogation field of an RFID reader. Unfortunately, short duration impulse events such as the crossing of a critical temperature threshold in cold chains, or the violation of design strain levels in a bridge deck under passing traffic, may occur when the tag-sensor is unpowered. Recording threshold crossovers is not possible with unpowered passive tag sensors. One way of addressing this problem is to add on-board memory with an additional power supply to record these impulse events. However, this adds to the cost of the sensor and reduces the scope for pervasive sensor deployment.

There is a need for alternative methods of recording threshold crossovers that occur even when the tag is unpowered without significantly adding to the cost of the sensor. In this chapter, I propose the *concept of low-cost, non-electric memory* as a possible solution. Threshold crossovers are recorded by effecting a permanent change in the RFID tag's geometry or in the boundary conditions of the RFID tag. For instance an antenna geometry change could be effected by having a part of the antenna tear off whenever a threshold is exceeded. Similarly, a boundary condition change could be implemented by having the background dielectric of the RFID tag

abruptly change whenever a threshold is exceeded. This manifests itself in a change in backscatter or threshold transmitted power which can be detected, the next time the sensor is interrogated.

I demonstrate how a temperature threshold sensor can be constructed by making use of the fact that RFID tag performance degrades in proximity to metals [9]. The sensor design has undergone two evolutions. The first design illustrates proof of concept, but suffers from several performance limitations. The second version overcomes several of these limitations. The remainder of this chapter discusses these two design approaches.

3.1 TABS-Based Temperature Threshold Sensing using Fluid Phase Changes

Cold chain operations are a prime application area that would benefit from pervasive sensing. Temperatures within a cold room are known to fluctuate up to $\pm 3°C$ of the design ambient temperature [57]. These fluctuations are known to have an adverse effect on food quality [58] and with an estimated 30% perishables being damaged or destroyed in transit [59], there is a dire need for better visibility in supply chain operations. Simulations have shown that sensor deployment can not only offset food wastage costs, but also reduce carbon costs in supply chain management brought about by the transportation and storage of spoiled food [60]. Ideally, we seek item level tagging of products passing through the supply chain and TABS based temperature sensors present a viable solution [29].

3.1.1 Non-Electric Memory: Recording Temperature Threshold Crossovers with Unpowered Tags

Figure 3-1(a) illustrates the design concept of non-electric memory. The sensor consists of two Alien Squiggle UHF RFID tags [61] attached to a plastic jacket. The dimensions of the plastic envelope are outlined in Table 3.1 (c.f Fig 3-1(a) and Fig 3-2

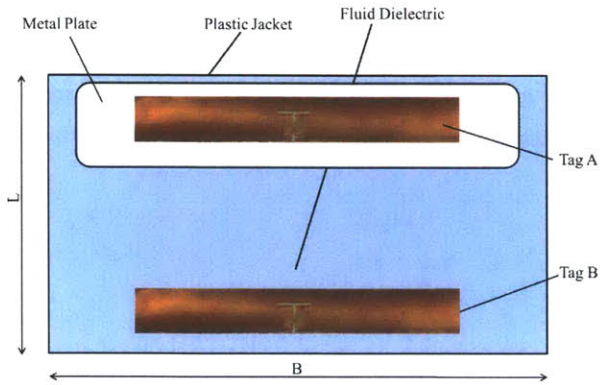

(a) Design of a temperature threshold sensor that makes use of a change in fluid phase and actuation of a metal plate to record the exceeding of a temperature threshold

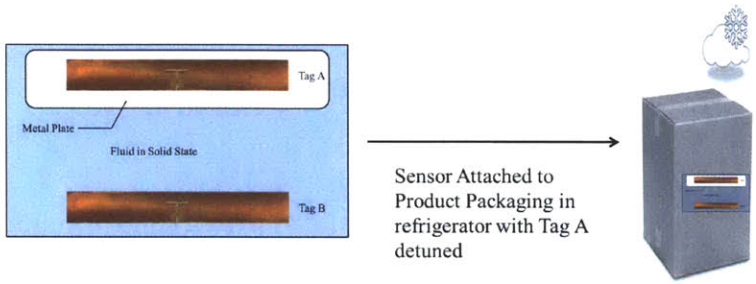

(b) Initialization step: Freezing the metal plate behind the upper RFID tag and placing it on the goods to be monitored

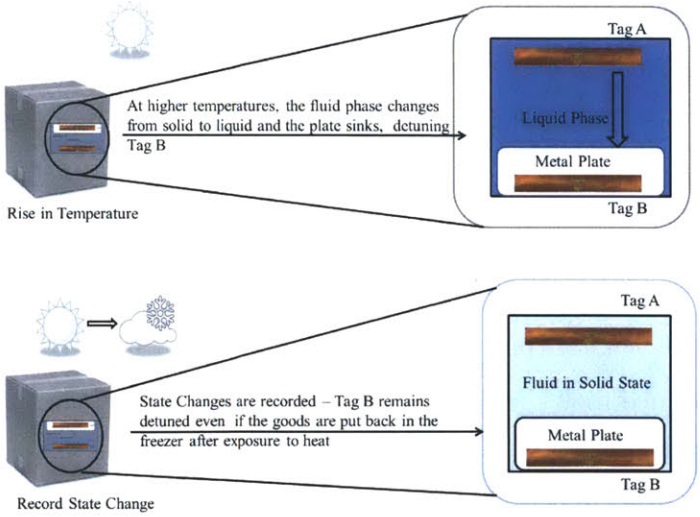

(c) Working concept: The change in fluid phase and the actuation of the metal plate records a critical state change

Figure 3-1: Concept of low-cost, non-electric memory: Using temperature induced fluid-phase changes in the boundary conditions of an RFID tag to record temperature threshold crossovers

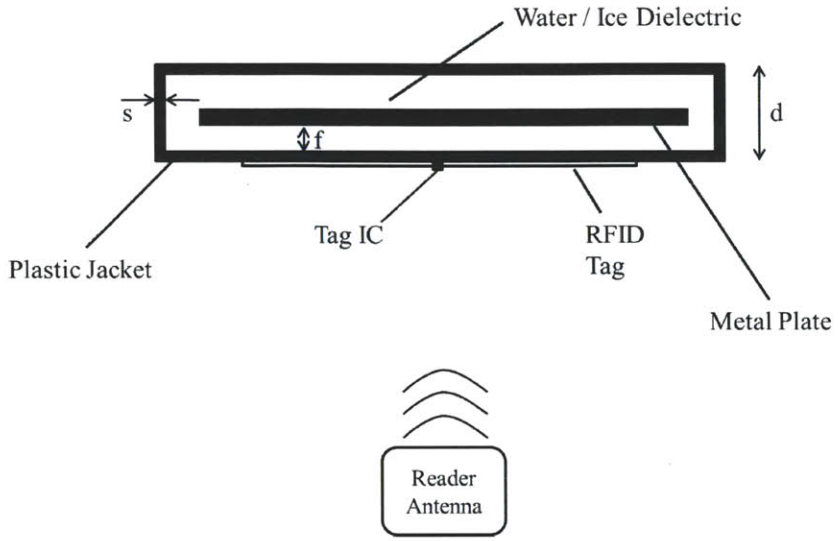

Figure 3-2: Fluid-phase temperature threshold sensor in section emphasizing the separation, f, between the metal plate and the RFID tags

for dimensions). The inside of the envelope is filled with a control volume of water. In this case study, the temperature threshold is set to 0^oC - the freezing point of water. A metal plate, free to move within the plastic jacket can either take a position behind Tag A or Tag B as shown in the figure.

The sensor is initialized by freezing the metal plate in an aqueous solution behind Tag A. The sensor is then deployed on the product to be monitored in the refrigerator as shown in Fig 3-1(b). If the temperature in the freezer unit remains at or below freezing during transit, the ice remains frozen with the metal plate behind tag A. Tag A being more severely detuned by the metal plate would respond with a weaker backscatter signal than tag B. However, if the sensor is exposed to a higher temperature, the ice melts and the plate descends to a position behind tag B now detuning tag B relative to tag A as seen in Fig 3-1(c). Thus by detecting a swap in relative backscatter signal strength, from a weaker tag A response to a stronger tag A response (relative to tag B), it is possible to infer that the temperature threshold was exceeded the next time the sensor is interrogated with an RFID reader. The added advantage of using relativistic measurements is that the sensor performance is independent of reader-tag separation. Even if the items are placed back in the

Table 3.1: Dimensions of the temperature threshold sensor prototype that makes use of a change in fluid phase to record temperature threshold crossovers

Dimension	Value (mm)
Jacket Length (L)	160
Jacket Breadth (B)	100
Jacket Depth (d)	6
Jacket Material Thickness (s)	1.3

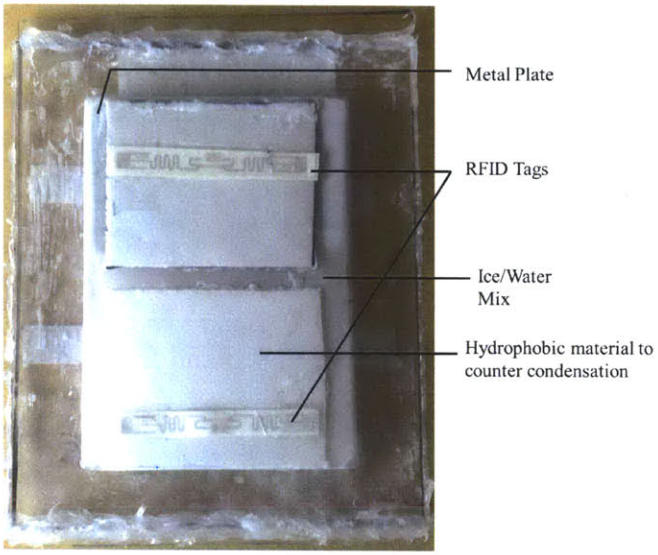

Figure 3-3: Sensor prototype that makes use of a fluid phase change and actuation of a metal plate to record state information

refrigerator, the metal plate remains behind tag B thus preserving state information. Fig 3-3 illustrates the temperature sensor prototype.

3.1.2 Discussion of the Performance of the Fluid-Phase Temperature Threshold Sensor

The sensor was initialized by freezing the metal plate in solution behind Tag A as shown in Fig 3-1(b). I test the sensor prototype at a sensor-reader separation of half a meter and at a reader transmitted power of 36 dBm EIRP. The Impinj Speedway UHF RFID reader was used for the experiments [53].

As seen from Fig 3-4, the test is begun by taking the sensor out of the refrigerator and placing it at an ambient temperature of 18^0C at t=0 seconds. As time passes,

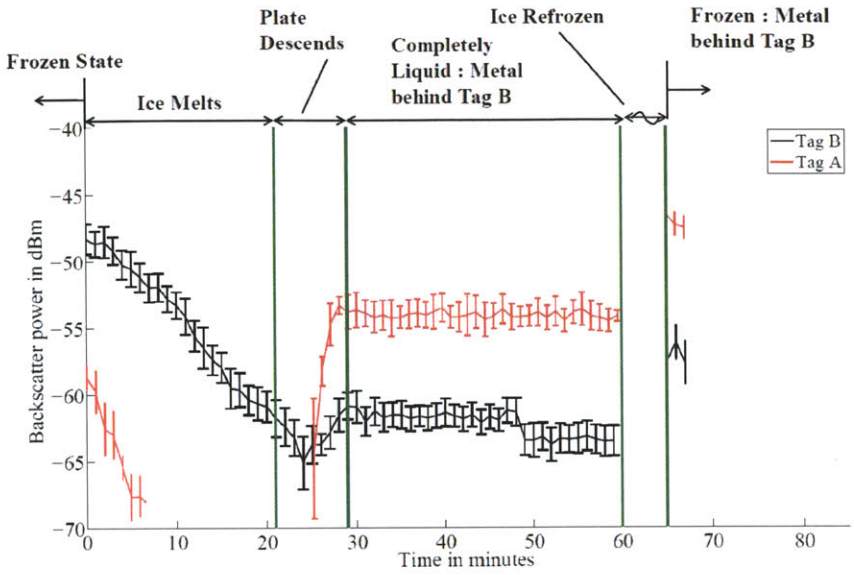

Figure 3-4: Backscatter response of both RFID tags when the fluid-phase temperature sensor is placed at an external temperature of 18°C and for a reader-sensor separation of 0.5 m

the ice starts to melt and the background dielectric for both tags involves increasing amount of water. Water molecules tend to orient themselves so as to cancel out incoming electric fields and thus water detunes the tag antenna more severely than ice. Thus between 0 and 20 minutes, the performance of both tags starts reducing as seen in the figure. Between 10 and 20 mins we see that there is no observed response from tag A.

It is observed that the ice completely melts and the plate descends to detune tag B at about 21 minutes. Thus after 21 minutes, tag B gives a worse performance than tag A. We observe that the sensor performs as per the design specifications with tag A initially performing worse than tag B and then better once the fluid phase changes state and the metal plate actuates. Furthermore, the fluid phase, plastic jacket and metal plate are inexpensive and this serves to demonstrate that non-electric memory can be implemented without significantly adding to sensor cost.

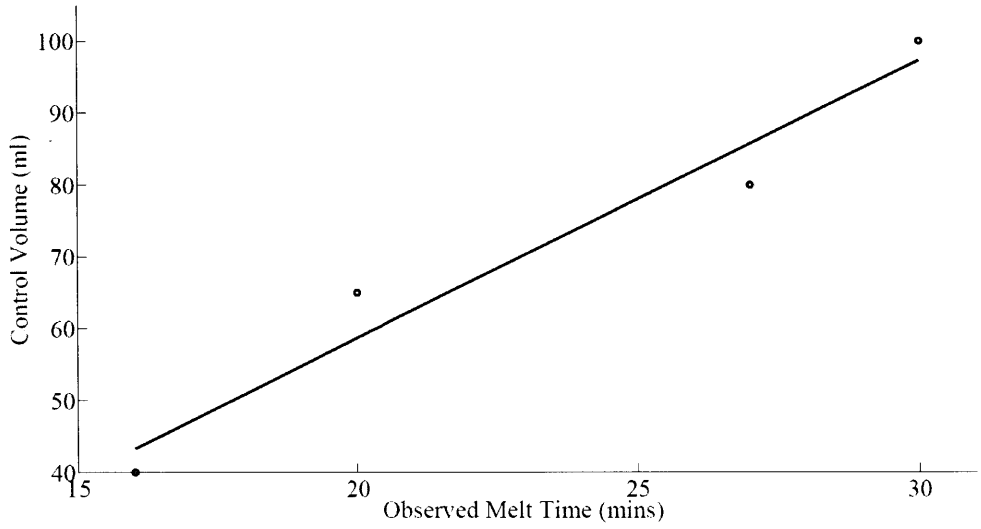

Figure 3-5: Controlling metal plate actuation time via water control volume for the fluid-phase temperature threshold sensor

Effect of the Control Volume of Water in the Plastic Jacket

The sensor is designed so that the ice completely melts and the plate starts to descend after an arbitrarily chosen 20 minutes. This time, defined as the *tolerance interval* of the sensor, is the amount of time the sensor can be placed at a specified temperature above the design threshold without triggering a state change. Designing a tolerance interval is important because it is conceivable that the sensor will be subjected to acceptable high temperature impulses such as when the goods are being removed from a freight truck and being moved to a warehouse's distribution center. The precise determination of the threshold interval is a conduction heat transfer design problem and factors into account the plastic jacket dimensions and control volume of water. In this thesis, I do not investigate this any further. Instead, for the purposes of this case study, I empirically determine the dependence of the tolerance interval on the control volume of water (c.f Fig 3-5).

Idiosyncrasies of the Fluid-Phase Temperature Threshold Sensor Design

The following interesting observations are particular to this sensor design:

- After 23 minutes tag A is no longer detuned by the metal, but its performance

is worse than that of tag B at t=0, since the background dielectric for tag A is water, which detunes the tag antenna more severely, rather than ice. To verify this, I refreeze the sensor with the metal plate behind tag B. As seen from Fig. 3-4, the response of tag A then improves to levels comparable with tag B at t=0.

- It is important to examine why tag B gives a perceivable response after t=23 while tag A does not give a response between t=10 and t=20 since the dielectric conditions behind both tags are virtually identical in these time frames. My explanation is the following: the metal plate is initially frozen flush behind the plastic jacket so as to minimize the thickness of the ice layer (dimension f in Fig. 3-2) between the plastic jacket and the metal plate, which I refer to as f_{min}. When the ice is melting, the relatively thin layer of water of thickness f_{min} and the metal plate together detune the tag antenna up to the point where the tag IC fails to power up and this results in no response from tag A in the t=10 to t=20 window. Under the influence of gravity, the plate descends to detune tag B, however does so in such a way that the dimension f is no longer f_{min}. The increased separation brought about by the descent of the metal plate reduces the severity of the tag antenna detuning up to the point where the RFID tag IC is able to power up. This is why tag B is detected for t$\geq$23 mins.

3.1.3 Limitations of the Current Design

While this sensor design successfully illustrates proof of concept, there are a number of design challenges that need to be overcome:

- The read range of this sensor is short — restricted to 0.5 m. If the test is conducted for a read range of more than 0.5 m, tag B is never detected once the metal plate actuates. Fig 3-6 is an illustrative representation which demonstrates sensor performance at a read distance of 1 m. As we see from the figure, the loss of tag B as a reference makes it difficult to perform relativistic backscatter power measurements for both sensor states. The loss of a reference makes

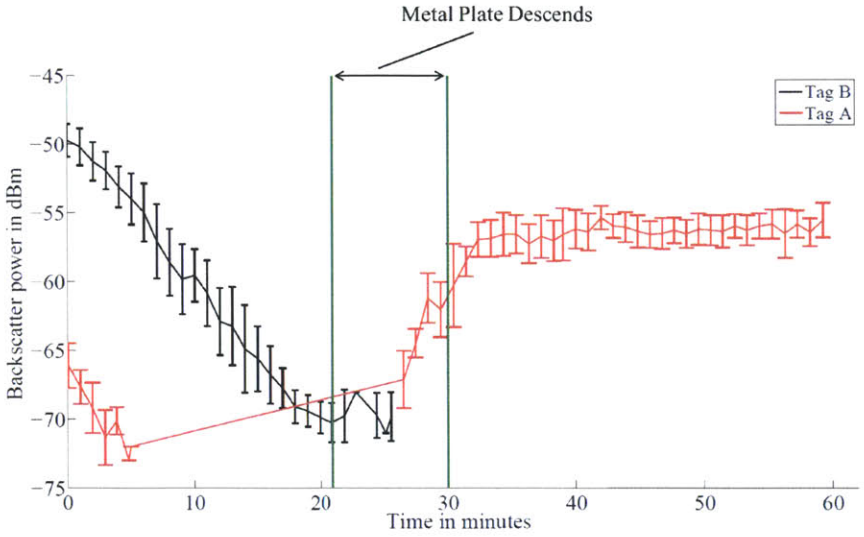

Figure 3-6: Fluid-phase temperature threshold sensor performance for 1 m reader-sensor separation

state measurements read range dependent.

- The material of deployment significantly affects sensor performance as observed in Fig 3-7. As we can see from the figure, the performance of tag A and B varies significantly depending upon whether the sensor is deployed on a cardboard box or a metal surface. Given that the supply chain consists of several different types of materials that need to be tagged, designing sensor performance to be agnostic of material of deployment is important.

- Security is another issue that needs to be addressed. For instance, a one-way mechanical valve that prevents the metal plate from being reset, either accidentally or deliberately, needs to incorporated into the sensor design.

- This also means that the sensor can only be placed on the sides of the packaging since the metal plate needs to actuate under the influence of gravity.

- Threshold temperatures less than 0°C can be designed by mixing water with a suitable impurity like salt or alcohol, however the problem of selecting a suitable, non toxic medium for temperatures above 0°C needs to be considered.

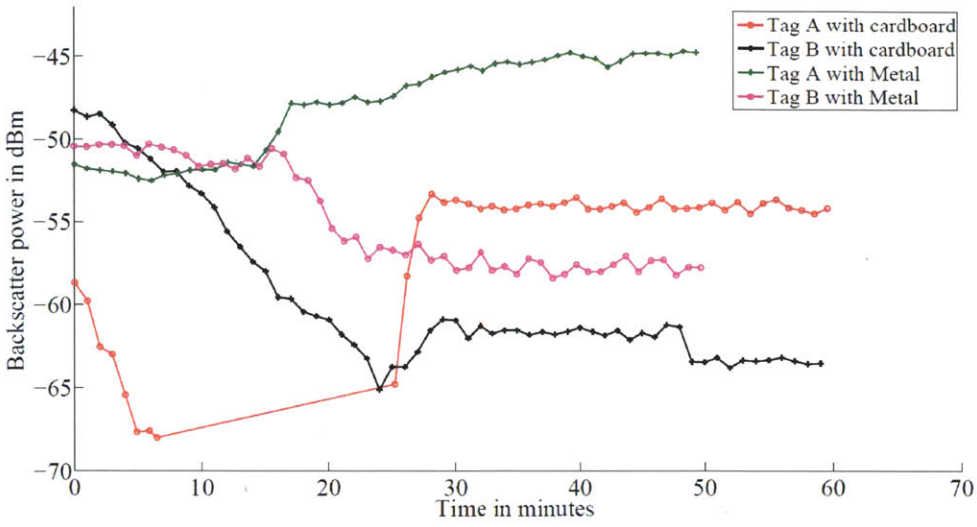

Figure 3-7: Fluid-phase temperature threshold sensor performance when deployed on different materials

- Another interesting problem is surface condensation. Water vapour in the air tends to condense on the surface of the RFID tag antenna, due to the presence of the underlying ice layer, and introduces an additional arbitrary source of detuning.

- Finally, the initialization step of freezing the metal plate in solution flush behind tag A is a cumbersome one.

In the next section, I propose the design of a solid state version of the threshold sensor that improves on several of the disadvantages of this design.

3.2 Temperature Threshold Sensing using Shape Memory Polymer (SMP) Actuation

The fluid-phase temperature threshold sensor, outlined in Section 3.1, demonstrated proof of concept, but suffered from several limitations. In order to improve the sensor design, I consider the potential of using temperature-responsive shape memory polymers (SMP) for non-electric memory [30]. This section provides a brief introduction

to shape memory polymers and their relevant chemical and mechanical properties. The sensor design is next discussed and proof of concept of a temperature threshold sensor that makes use of SMP's to record temperature crossovers is demonstrated. Finally, I examine the advantages of this design approach and demonstrate that it solves many of the shortcomings of the previous design.

3.2.1 Thermo-Mechanical Properties of SMPs

SMP's exhibit changes in mechanical state properties below and above a characteristic *Glass Transition Temperature*, known as T_g. Deforming the polymer and cooling it below T_g, fixes the deformation as long as the polymer is maintained below T_g. When the polymer is heated above T_g, the original shape is recovered. This recovery is thermally-induced and the deformations to which the polymer can be typically subjected to is fairly large. As a result of which SMP's are naturally suited as temperature actuated switches in thermal sensing.

For this study, the chemically-cross linked thermoset polymer tBA-co-PEGDMA, recently studied by Safranski and Gall is used [62]. The polymer was synthesized by mixing 50 mol% of the monomer tert-butyl acrylate (tBA) with 50 mol% of the crosslinking agent poly(ethylene glycol) dimethacrylate (PEGDMA) and 0.2% of the photoinitiator 2,2-dimethoxy-2-phenylacetophenone. The solution was mixed using a magnetic stir plate for 2 minutes and then degassed in a vacuum chamber for 10 minutes. The degassed solution was then UV cured for 10 minutes at an intensity of about 30 mW/cm^2. Finally, the polymer was heat-treated at 90 °C for 1 hour to complete the polymerization reaction. The polymer was then cut and polished to the desired dimensions to produce the samples used in the thermal sensing prototypes.

As has been studied in [62], T_g depends on the chemistry of the polymer. Decreasing the molar percentage of PEGDMA to tBA produces polymers with higher T_g values. This is ideal in the design of a thermal alarm sensor, because we can employ the same sensor design and manufacturing procedures to produce sensors which trigger at different temperature ranges. Note that the T_g is not a discrete value but rather a range over which the polymer's mechanical behavior changes from a rigid

state to a rubbery state. It is important to quantify this behavior because it directly affects the actuation time of the sensor at a given temperature.

In order to understand the behavior of T_g, three samples with the polymer composition mentioned above were tested using dynamic mechanical analysis (DMA). Fig. 3-8 shows the curves of storage and loss moduli for three different samples of the polymer. The storage modulus is a representation of the stored energy during deformation, while the loss modulus represents the viscous loss of energy of the material. The range of temperature over which there is a significant change in the material's ability to store energy through deformation corresponds to the material's glass transition temperature. The value of T_g is conventionally taken at the peak of the loss modulus, which occurs at approximately 15°C in Fig 3-8. As mentioned above, the glass transition temperature is not a discrete value, and it can be observed from Fig. 3-8 that the storage modulus shows significant variation from 0°C to 30°. In the design of sensors the temperature at which the onset of shape-recovery occurs is the most important property of the polymer. The onset of shape-recovery is observed to occur at the lower bound of the glass transition temperature, which is at approximately 0°C in Fig 3-8. Therefore the conclusion is that we must tailor the chemistry of the SMP such that the lower bound of T_g corresponds to the monitoring temperature of interest.

3.2.2 Design of a Temperature Threshold Sensor that implements Non-Electric Memory with SMP Actuation

The temperature threshold sensor consists of a plastic jacket with two UHF Alien Squiggle tags as shown in Fig 3-9(a). A metal plate is held in position behind one of the two tags using a SMP bridge. As we can see from the figure, the sensor has two states. In the first state, the threshold has not been exceeded and the metal plate detunes tag A. In the second state, the threshold has been exceeded and the metal plate detunes tag B. Fig 3-9(b) illustrates the temperature sensor in cross-section. As we can see, the base of the plastic jacket has a metallic isolation backplate. This

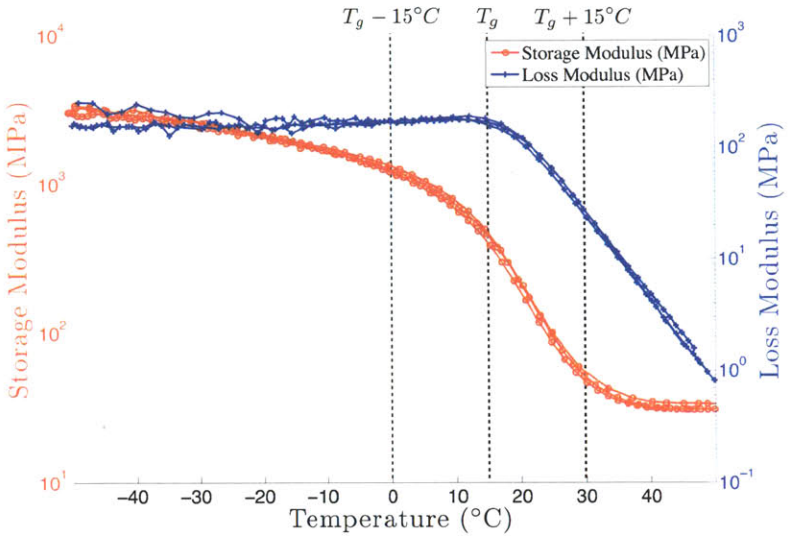

Figure 3-8: DMA curves of 50 mol% tBA co 50 mol% PEGDMA indicating glass transition temperature ranges (courtsey: C. Di Leo, *Department of Mechanical Engineering, MIT*)

metal isolator is introduced to shield the sensor from the material of deployment — one of the criticisms of the design proposed in Section 3.1. Fig 3-10 shows a prototype of the sensor.

Fig 3-11 outlines the working concept. As we can see from Fig 3-11-(A), the SMP bridge is initially deformed so that the detuning metal plate is held in position behind the lower tag. The sensor is initialized by placing it on the goods to be monitored in the cold room and pulling the arresting pins free. As shown in Fig 3-11-(B), if the temperature in the cold room remains at or lower than T_g, the polymer remains in the rigid, locked position with the metal plate detuning the lower tag. However, if the sensor is placed at an external temperature higher than T_g, the polymer starts actuating (c.f Fig 3-11-(C)) and the detuning metal plate is now held in position behind the upper tag as seen in Fig 3-11-(D).

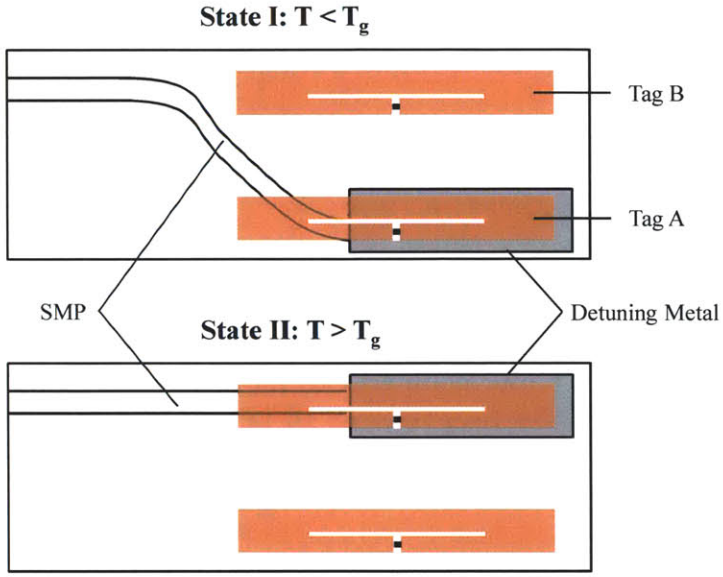

(a) Plan view of SMP actuation-based temperature threshold sensor

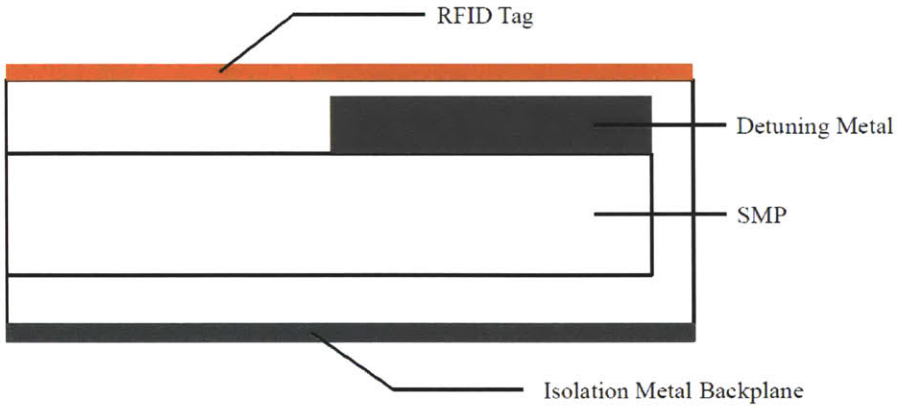

(b) Cross sectional view of SMP actuation-based temperature threshold sensor

Figure 3-9: Temperature threshold sensor that makes use of SMP actuation for non-electric memory

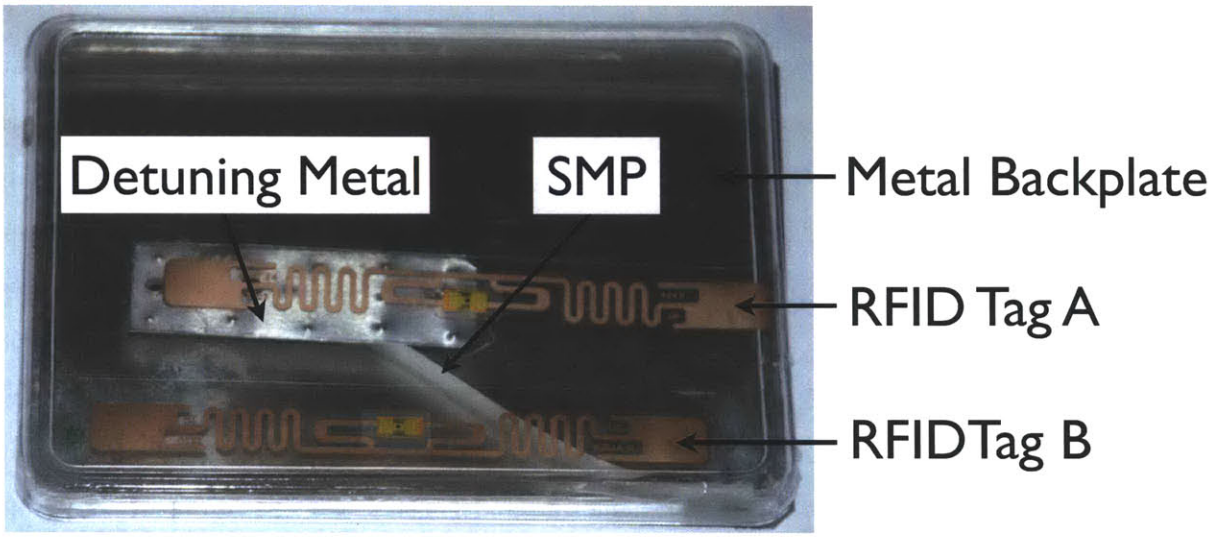

Figure 3-10: Prototype of the SMP actuation-based temperature threshold sensor

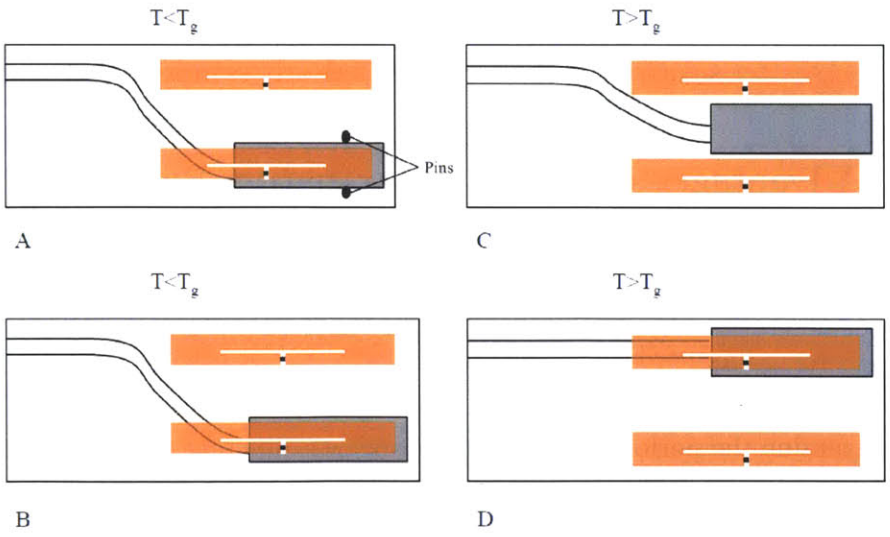

Figure 3-11: Working concept: Temperature induced actuation of SMP records temperature threshold crossovers

3.2.3 Results of Field Testing the SMP Actuation-Based Temperature Threshold Sensor

To demonstrate that the sensor design works, a shape memory polymer designed to actuate at a mean temperature of 7°C (with an actuation range of ±7.5°C) was subjected to a heating cycle test. The temperature sensor was initialized by placing it in a refrigerator unit at −10°C for 30 mins to ensure that the polymer hardens and then at an outside temperature of 28°C for a period of about 5 mins. To allow rapid testing, the prototype dimensions were selected so that the polymer bridge would actuate after about 3-5 mins at these temperature conditions. The experiments were conducted using the Impinj Speedway UHF RFID reader.

Fig. 3-12 illustrates the backscatter signal strength received from the tags A and B, described in Fig. 3-9(a), as a function of time for a reader-sensor separation of 1 m. The tags are queried at the rate of 40 reads per second and average values are plotted every 3 s, which would correspond to an average over approximately 120 data points. As we see, initially Tag A has the metal plate behind it and responds with a weak signal relative to Tag B, but as the polymer actuates, the metal plate shifts from a position behind Tag A to a position behind Tag B. This manifests itself in a swap in backscatter signal amplitude and this is clearly seen in Fig. 3-12.

3.2.4 Advantages of the SMP Actuation-Based Design Approach

This sensor design has several advantages over the fluid phase-based design proposed in the previous section:

- To examine the performance of the sensor over different read ranges, I examine the performance of the sensor over 0.5, 1, 2 and 3 m. Fig 3-13 represents a plot of differential backscatter power (Tag A relative to Tag B) as a function of time for different read ranges. As we observe from the figure, the flip in differential backscatter signals can be observed over all read ranges demonstrating that the sensor state can be unambiguously determined over a range of 3 m.

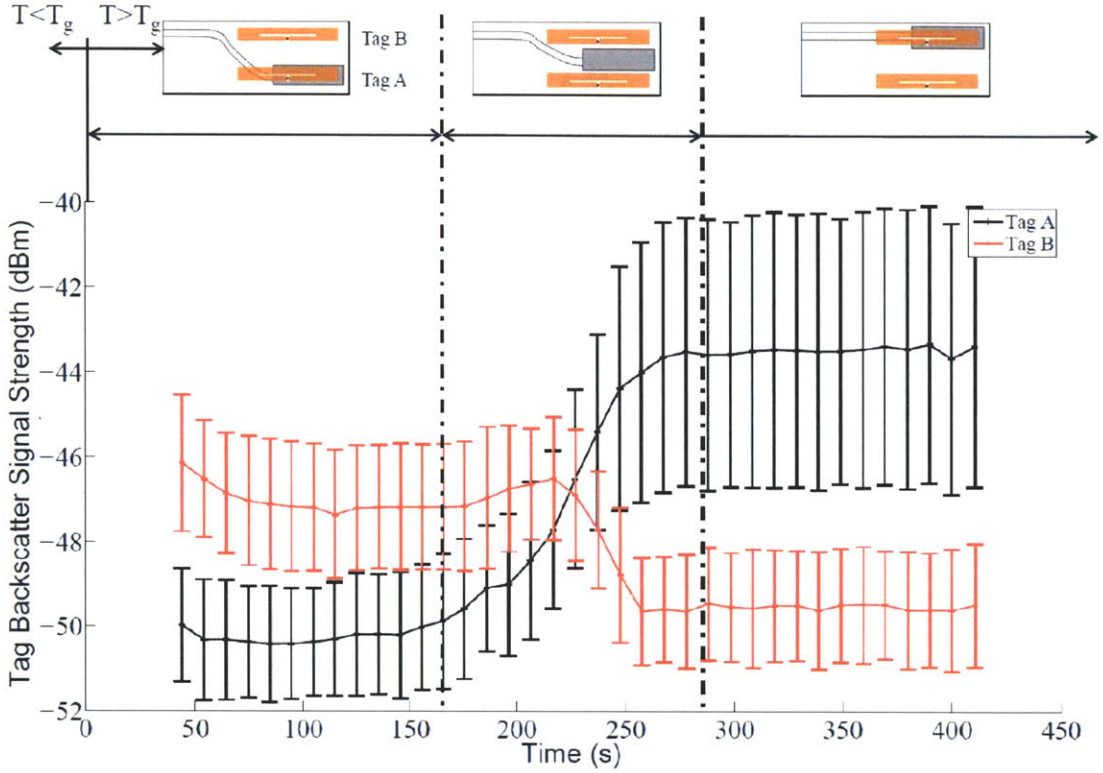

Figure 3-12: Backscatter response from the two RFID tags as the SMP actuates for a reader-sensor separation of 1 m

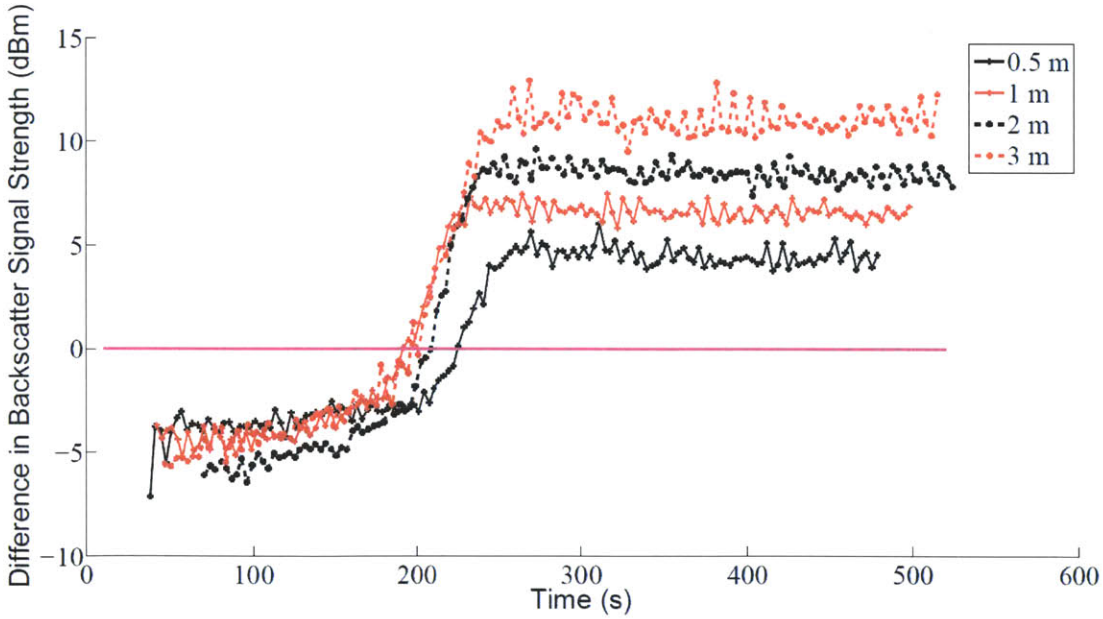

Figure 3-13: SMP actuation-based temperature threshold sensor performance over different read ranges

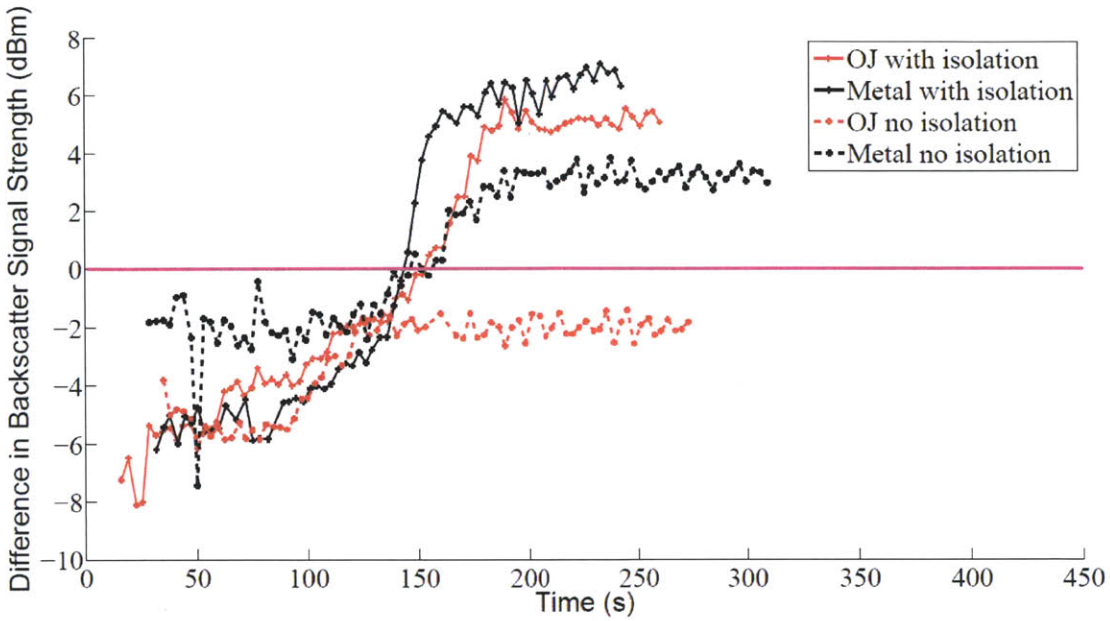

Figure 3-14: SMP actuation-based temperature threshold sensor performance when deployed on different materials

- The metal isolation plate (c.f Fig 3-9(b)) was added to the design to make sensor performance independent of the material on which the sensor is deployed. Fig 3-14 illustrates the performance of the sensor when it is deployed on a metal surface and on an orange juice carton with and without the isolation plate. As we can see from the figure, the sensor works reliably on both materials when the isolator is employed. However, the sensor fails to perform correctly when deployed on the juice carton when the isolator is removed.

- The SMP actuation is thermally induced and independent of the orientation of the sensor. We need to verify that the state changes occur reliably irrespective of whether the SMP is actuating in the direction, or against, the force of gravity. The experiment is performed in several different orientations (c.f Fig 3-15(a)), some of which occur in the direction of the gravitational force and some which occur against gravity. Fig 3-15(b) shows that sensor orientation does not affect the sensor performance. Note that the test conducted for the sensor orientation of 90° was conducted with a polymer bridge that was slightly thicker than

that used for the other orientation tests. This is why the actuation time is correspondingly longer (*c.f* Fig 3-15(a)).

- The SMP actuation is one-way implying that with appropriate tamper proof packaging, it is very difficult to inadvertently or deliberately reset the sensor once the threshold has been exceeded.
- The problem of condensation is solved since the design does not include any fluid medium. This has the added advantage of reducing the weight and form factor of the sensor.
- The SMP itself is quite inexpensive — the estimated cost of the SMP switch used in this design is O($0.1). Thus SMPs lend themselves well as low-cost, thermo-mechanical switches in pervasive sensor design.
- Finally, by appropriately controlling the polymer chemistry, sensors can be designed for a broad range of values of T_g — both above and below 0°C.

3.2.5 Scope for Future Work

While this design has been shown to solve many of the limitations outlined in Section 3.1.3, there are four open issues that still require to be addressed as part of future work:

- First, the sensor still has a cumbersome initialization step that needs to be simplified — the arming pins need to be pulled off each individual sensor once the sensor has been deployed in the cold room and the SMP has had a chance to cool below T_g.
- Second, it is necessary to quantify the expected variation in the lower bound of the glass transition temperature range described in Fig 3-8. Our analysis shows that there is not much variation across the three samples produced from the same batch of polymer, however quantifying the expected variation across different batches and in different laboratory conditions is necessary to understand the precision we can expect from these threshold sensors.

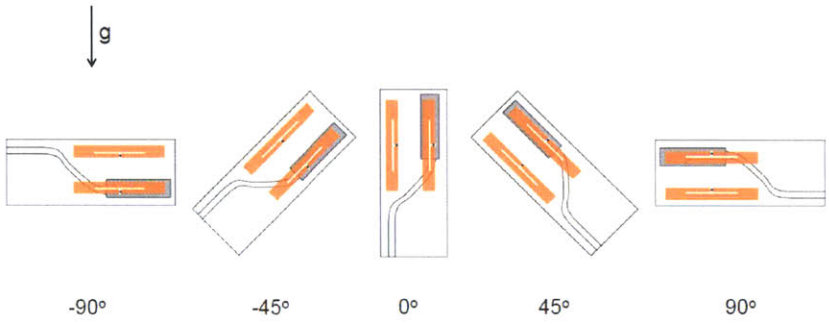

(a) SMP actuation-based temperature threshold sensor in different orientations

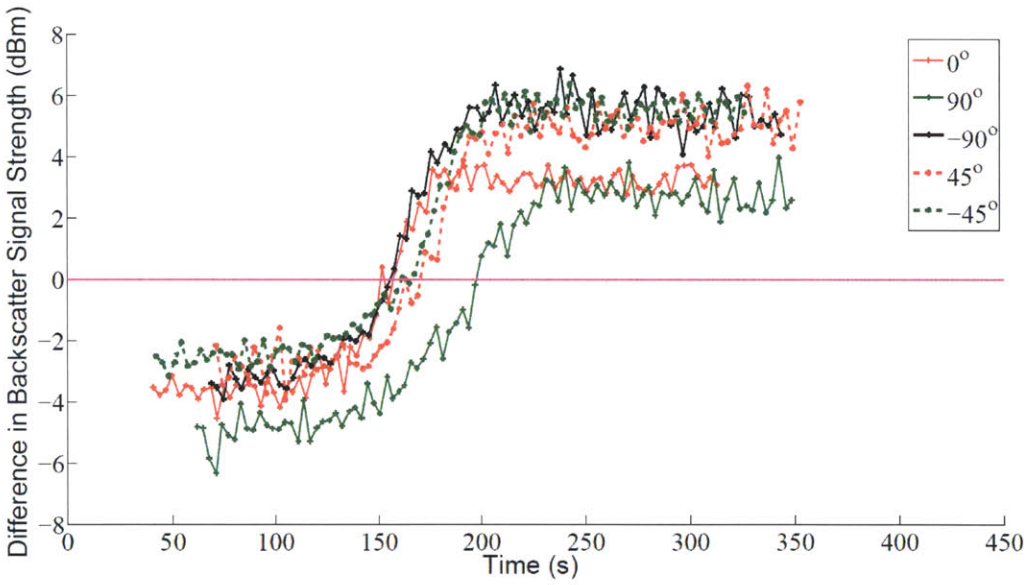

(b) SMP actuation-based temperature threshold sensor performance for different orientations

Figure 3-15: SMP actuation-based temperature threshold sensor performance for different orientations: In some orientations, the polymer actuates against gravity and in others the polymer is assisted by gravity

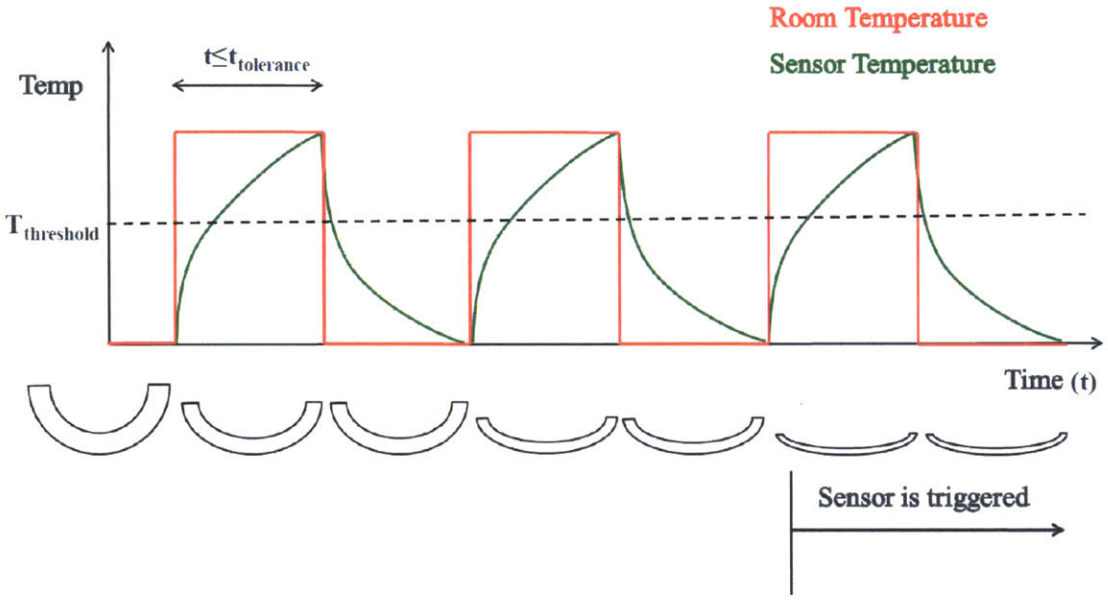

Figure 3-16: Effect of partial actuation of the SMP on the temperature threshold sensor performance

- Third, it is necessary to relate the tolerance interval $t_{tolerance}$ of the sensor to food quality degradation. The relationship between $t_{tolerance}$ and temperature can be modeled using heat transfer principles while temperature dependent food quality degradation has been modeled as a first order Arrhenius decay [63] in the literature. In [30], I hypothesize how both these concepts can be utilized so that the design value of $t_{tolerance}$ can serve as a conservative estimate of food quality degradation. However designing and field testing temperature sensor prototypes that verify this hypothesis is an open engineering question.

- Finally, it is necessary to understand the cumulative effect of partial actuation cycles of the SMP. Specifically, a temperature impulse with duration slightly less than or equal to $t_{tolerance}$, such as the one in Fig 3-16, may trigger a state change alert after a finite number of cycles. It is important to understand the probability of occurrence of such an event so that the frequency of false alarms can be quantified.

3.3 Related Work in Smart Materials and Sensing

I conclude this section by emphasizing the multi-disciplinary facet of TABS based sensing, particularly with regards the integration of antenna engineering and material science. TABS based sensors that make use of smart sensing materials has been gaining popularity in the research community and in this section I highlight some of the recent advancements. In work very similar to that outlined in Section 3.2, Caizzone *et.al* demonstrate how the actuation of shape memory alloys can be used for temperature threshold sensing [31]. They propose the design of a custom antenna optimized for read range performance in both states and demonstrate that it works reliably for low (0°C) and high (80°C) temperature thresholds.

Researchers from GE have developed an HF RFID TABS sensor that can detect the concentration of volatile organic compounds [64]. The basis of their sensor is a chemically responsive underlying surface that causes shifts in the resonant and anti-resonant frequencies of an HF tag antenna. The degree of shift is proportional to the concentration of the organic compound. Besides detecting the concentration of an individual compound, the sensor can also differentiate between mixtures of organics in the presence of varying amounts of relative humidity. The sensor is capable of monitoring concentrations down to the ppb (parts per billion) level.

Hasan *et.al* discuss the concept of a low-cost, RFID-based Reflected Electro-Material Signature (REMS) sensor [65]. The sensor essentially consists of an RFID tag antenna connected to the IC via a variable impedance transmission line. The transmission line is made of a material that is sensitive to the physical parameter of interest such as a temperature sensitive polymer. The authors use variations in the reflection coefficient (as the incident EM wave passes through the transmission line) in tandem with pattern classification techniques like neural networks to predict changes in the dielectric material of the transmission line. This in turn can be related to the parameter of interest. In [65], the authors envision a REMS-based temperature sensor to be able to reconstruct the time temperature profile of the sensor as it passed through the supply chain. This would enhance the information gained since the ques-

tion of 'when' a critical temperature threshold was exceeded can also be addressed by this approach — an advantage over the non-electric memory proposed in this chapter which can only answer the question of 'if' the threshold was ever exceeded.

Chapter 4

Frequency Modifying TABS

The American unlicensed industrial, scientific and medical (ISM) UHF RFID band has a relatively broad bandwidth of 902-928 MHz and this presents an excellent opportunity for implementing frequency domain-based sensing approaches. In this chapter, I introduce the concept of Frequency Modifying (FM) TABS - a frequency domain based transduction strategy that correlates a change in the parameter of interest to a shift in the optimal operating frequency at which the RFID tag responds to reader interrogation.

The rest of this chapter progresses as follows. I first introduce the concept of FM TABS in the context of a temperature threshold sensor design [33]. I discuss the design of the thermally actuated switch as well as a custom narrow band antenna that will be used to implement frequency domain-based state detection. The results of testing the sensor design concept in a laboratory setting are next outlined. Finally, I discuss another application of FM TABS to fluid level sensing and provide an outline of closely related work in the literature.

4.1 FM TABS: Using Frequency Shifts for Sensing

The Friis transmission equation governs radiative power transfer in the far field and determines tag read range performance. Eq 2.5 summarizes the power supplied to

the RFID tag's IC, assuming free space conditions

$$\begin{aligned} P_{chip} &= \frac{P_t G_{reader} G_{tag} \lambda^2 (1 - |\Gamma|^2)}{(4\pi d)^2} \\ &= \frac{P_t G_{reader} G_{tag} \lambda^2 \tau}{(4\pi d)^2} \end{aligned} \tag{4.1}$$

Here τ, known as the *power transfer efficiency*, is a measure of how well the IC is impedance-matched to the antenna as is expressed as

$$\begin{aligned} \tau &= 1 - |\Gamma|^2 \\ &= \frac{4 R_{antenna} R_c}{|Z_{antenna} + Z_c|^2} \end{aligned} \tag{4.2}$$

where $R_{antenna}$ is the combination of the antenna radiating and loss resistance, R_c is the chip resistance and $Z_{antenna}$ and Z_c are the antenna and chip impedances respectively. It is easy to see that $0 \leq \tau \leq 1$. We know that $\tau = 1$ when $Z_c = Z^*_{antenna}$. We normally desire $\tau \approx 1$ over the 860-960 MHz operating band for worldwide UHF RFID operations.

Both $Z_{antenna}$ and Z_c are functions of the operating frequency of the reader. An FM TABS sensing strategy can be implemented by mapping changes in a physical parameter to a controlled change in $Z_{antenna}$, which would shift the frequency band for which $\tau \approx 1$. I define this frequency band as the *Optimal Operating Frequency Band* of the FM TABS sensor. Inferences about the physical parameter of interest can then be made by observing the optimal operating frequency band. In the following section, I discuss the application of FM TABS to temperature threshold sensing.

4.1.1 FM TABS-Based Temperature Threshold Sensing

I design an FM TABS temperature threshold sensor that shifts its optimal operating frequency band when a critical temperature threshold is exceeded. Furthermore, I confine the shift to the 902-928 MHz band which allows the approach to be implemented on commercially available American RFID readers. The temperature threshold sensor is designed to exhibit the following two-state behaviour

- State 1 corresponds to the condition where the temperature remains below a given threshold. The optimal operating frequency band is designed to be 920-925 MHz and τ sharply decreases for all other frequencies in the 902-928 MHz band.

- State 2 corresponds to the condition where the temperature rises above a given threshold. The optimal operating frequency band is designed to be 905-912 MHz and τ sharply decreases for all other frequencies in the 902-928 MHz band.

The implementation of this approach requires the design of a custom RFID tag antenna and a mechanism of inducing a controlled change to $Z_{antenna}$ whenever a temperature threshold is exceeded. In the next section, I discuss the design of an SMP actuation-based temperature threshold sensor along with the design of a frequency shifting antenna that is used to implement the FM TABS approach.

4.1.2 Design of the FM TABS Temperature Threshold Sensor

Fig. 4-1(a) and Fig. 4-1(b) illustrate the design of the sensor. As seen from the figures, the temperature sensor consists of an RFID tag on a plastic jacket separated from a metal plate. An SMP bridge controls the relative distance, h, between the RFID tag and the metal plate. The SMP is designed for a glass transition temperature, $T_g = 7°C$. The metal plate serves a dual purpose in the sensor design:

- First, it acts as an isolator, shielding the tag antenna from the material on which the sensor is deployed. This is necessary since the tag sensor performance should not arbitrarily be influenced by the material on which it is deployed.

- Second, the height of the isolation plate from the tag controls the optimal operating frequency of the RFID tag antenna.

Fig. 4-2 illustrates the sensor working concept. As seen from Fig. 4-2(A), the temperature sensor is placed on the product to be monitored in the cold room and the

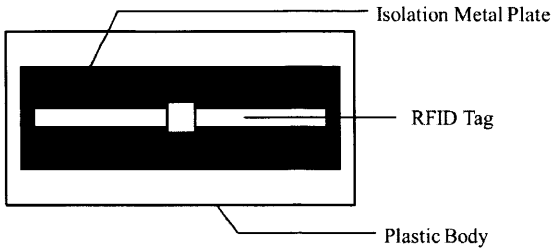

(a) FM TABS temperature threshold sensor in section

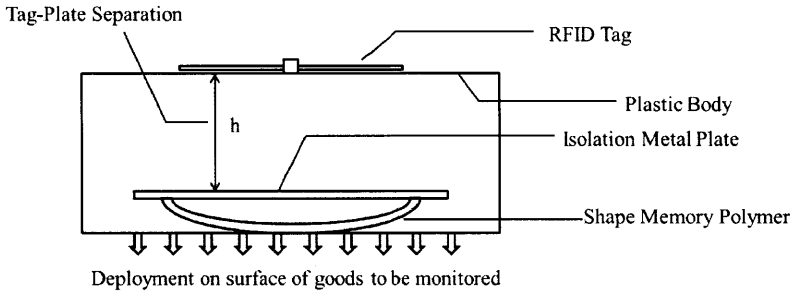

(b) FM TABS temperature threshold sensor in plan

Figure 4-1: FM TABS temperature threshold sensor that uses SMP actuation and a shift in the tag's optimal operating frequency to record temperature violations

arming pins are pulled free. As seen from Fig. 4-2(B), if the temperature remains below 7°C, the polymer remains in the rigid state and the isolation plate is kept at a constant h=10 mm distance from the RFID tag. If however, the temperature rises above 7°C, seen in Fig. 4-2(C), the polymer starts to actuate and this moves the metal plate closer to the tag. In the completely actuated state, seen in Fig. 4-2(D), the metal plate is h=3 mm from the tag. The shift in the metal plate position controls the optimal operating frequency band of the tag antenna and the SMP actuation is used to record temperature threshold violations.

The metal plate moving closer to the tag introduces an increased parasitic capacitance to the tag antenna while reducing its radiating resistance. For a sufficiently narrow-band tag, this would correspond to a reduction in the optimal operating frequency. Precisely controlling the extent of this shift in frequency so that it conforms to the design specifications, outlined in Section 4.1.1, is the subject of antenna design and this is discussed in the following section.

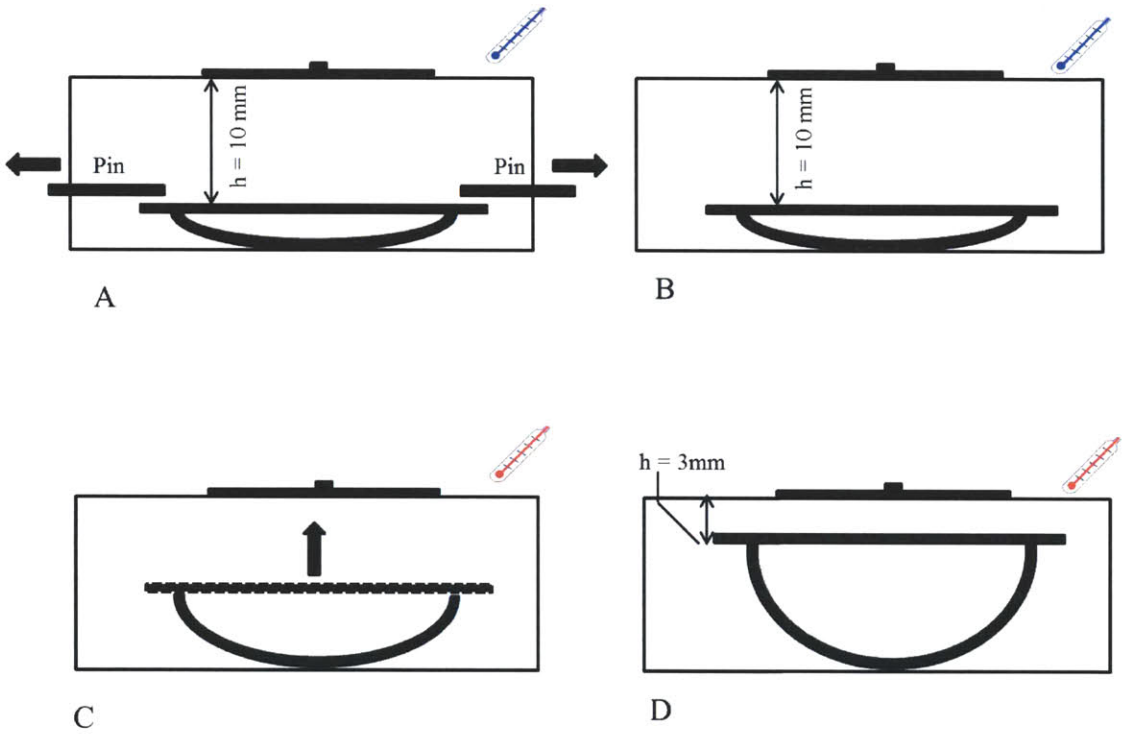

Figure 4-2: Using SMP Actuation to trigger position changes of the isolation metal back plate; the change in h results in a shift in the optimal operating frequency band of the RFID tag-sensor

4.1.3 Design of a Frequency Shifting RFID Tag Antenna

In this section, I discuss the procedure used to design a tag antenna that exhibits an appropriate shift in optimal operating frequency upon violation of the temperature threshold of interest. To aid in the design process, I reiterate the requirements of such an antenna design:

- **Narrow Bandwidth**: I design the antenna such that the optimal operating frequency band is between 920-925 MHz in State 1, 905-912 MHz in State 2 and decreases sharply at all other frequencies in the 902-928 MHz range.

- **Frequency Shift in the 902-928 MHz band**: The optimal matching frequencies for both states of the sensor need to be within a 26 MHz band of 902-928 MHz allocated for US RFID operations. This is because commercial RFID readers, which will be utilized to interrogate the tag sensor, are only capable of detecting frequencies in this operating range.

- τ **near 1 at Optimal Matching Frequencies**: For a given reader transmitted power, the range over which a tag can be read is directly related to τ. For both states of the sensor, at the optimal operating frequency, τ should be as close to 1 as possible. This will ensure a long read distance for the sensor.

Selection of an Embedded T-Match Antenna Design

I make use of the embedded T-match antenna design since it has been well documented in the literature and has a limited number of design parameters — the length L, width W, slot width s, slot height w_1 and slot thickness t as seen in Fig. 4-3.

Deavours *et.al* [66] present a comprehensive analysis of the T-match antenna explaining how the different geometrical parameters influence antenna impedance. In this section, I briefly highlight only those aspects of their analysis that helps me select an antenna with the desired performance.

My analysis procedure involves finding whether there exists a set of parameters (L, W, w_1, s) for which the optimal operating frequency band is 920-925 MHz, when

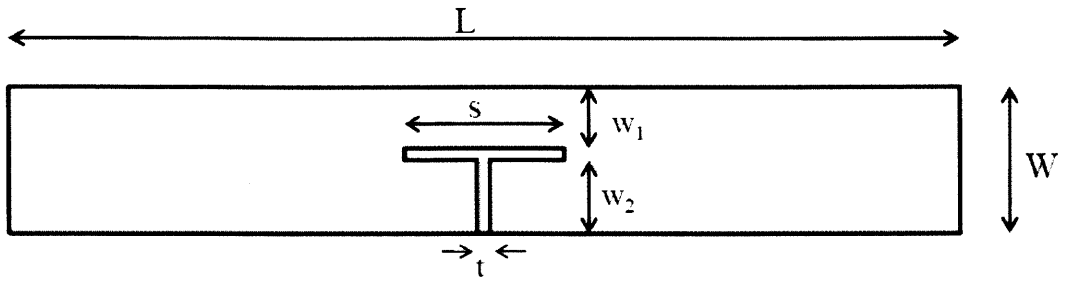

Figure 4-3: Geometric parameters of the embedded T-match antenna

the plate-tag separation is h=10 mm, and 905-912 MHz when h=3 mm. To limit the design space, I fix t=1 mm in the design. The analysis is a three step procedure and is outlined below:

- For h=10 mm, I find a set, S=(L_i,W_i), for which impedance matching between the antenna and a given IC is possible.

- For all i in S, I find corresponding values of (w_1,s) for which the optimal operating frequency band is 920-925 MHz. Let this set be denoted as G

- For all i in G, I determine if there exists an i such that the optimal operating frequency shifts to 905-912 MHz when h=3 mm, without compromising τ significantly.

I follow this design procedure and attempt to find a set of feasible antenna dimensions.

For a given L and W at 922 MHz, it is possible to compute the impedance, $Z_{com} = R_{com} + jX_{com}$, of an equivalent dipole antenna at h=10 mm from a metal surface. This can easily be done using appropriate numerical simulation software such as Ansys' HFSS [67]. The impedance of the equivalent dipole antenna is known as the *Common Mode Antenna Impedance*. For a given IC impedance $Z_c = R_c + jX_c$ and Z_{com}, Deavours *et. al* [66] present a term known as the *splitting factor*, which is a function of how w_1 needs to be selected to achieve an impedance match between the antenna and Z_c. I call this parameter, α_{match}, indicating its relationship to impedance

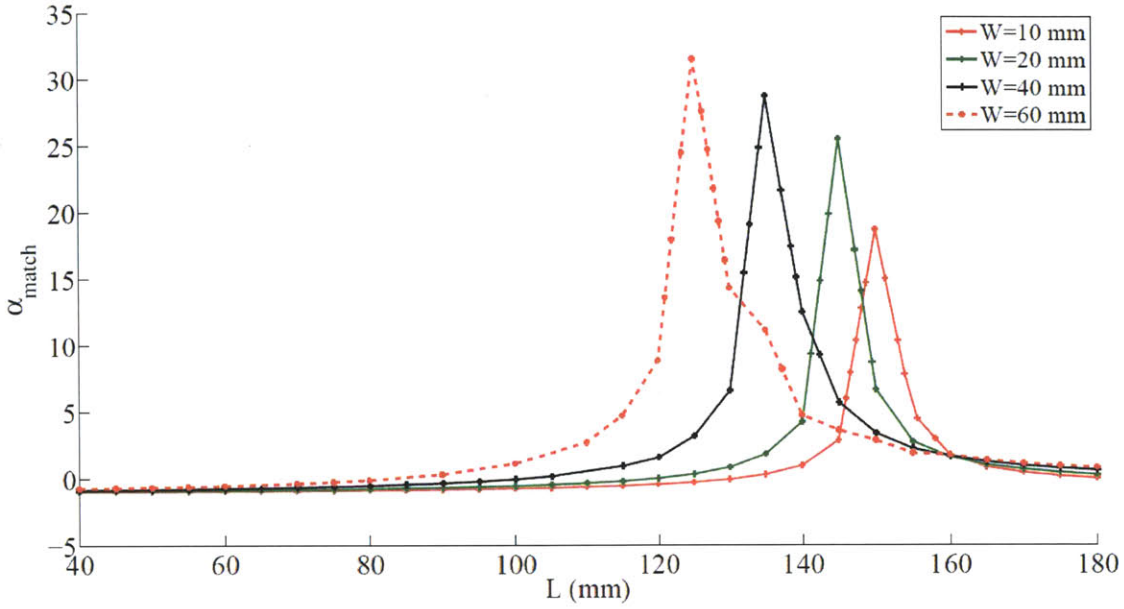

Figure 4-4: Variation of α_{match} with antenna length and width

matching:

$$\alpha_{match} = \sqrt{\frac{R_{com}(R_c^2 + X_c^2)}{R_c(R_{com}^2 + X_{com}^2)}} - 1 \tag{4.3}$$

Fig. 4-4 illustrates a plot of the simulated values of α_{match} as a function of L, for a family of W, when h=10 mm. The operating frequency is chosen to be 922 MHz. As we can see from the figure, for each (L, W), there exists a unique α_{match} and it is necessary to reduce this design space. Recollect that the splitting factor is a function of w_1. Deavours *et. al* describe this relationship [66] as illustrated in (4.4)

$$\alpha_{w_1} = \frac{ln(v)}{ln(v) - ln(u)} \tag{4.4}$$

where $u = \frac{w_1}{w_2}$ and $v = \frac{4(t+\frac{w_1+w_2}{2})}{\frac{w_2}{2}}$. For manufacturing feasibility, we impose a constraint that $w_1 \geq 1$ mm and $w_2 \geq 1$ mm. We can then verify that in order to meet these constraints, $\frac{1}{3} \leq \alpha_{w_1} \leq 3$. I make use of (4.4) to impose bounds on the values of α_{match} to highlight only those values of L that are feasible from both the manufacturing and impedance matching points of view. This is shown in Fig. 4-5.

As seen from the graph, for each W, there exists at least one long and one short L

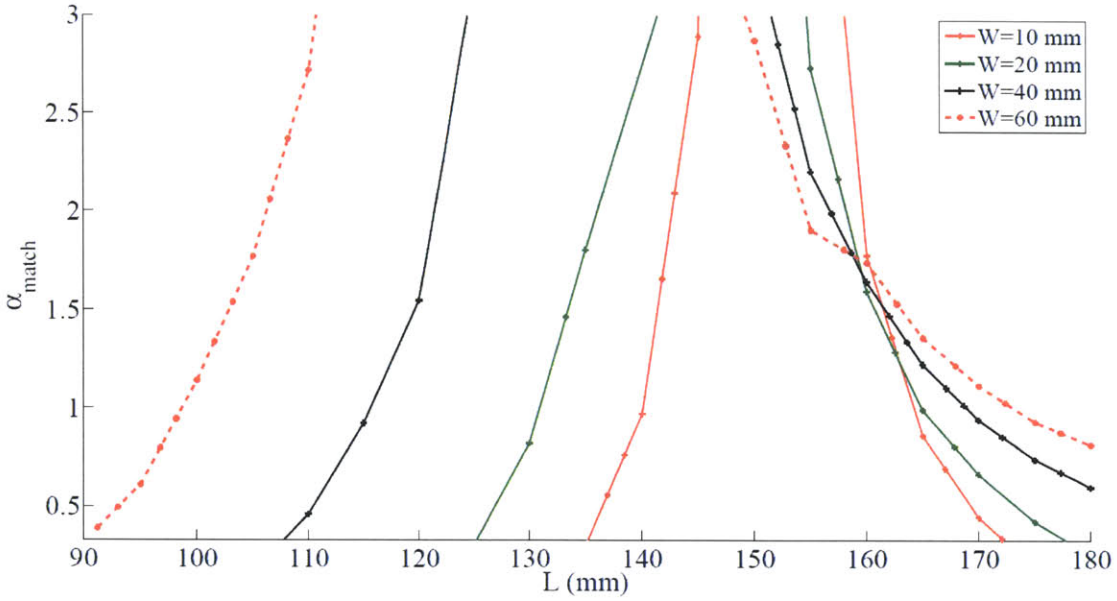

Figure 4-5: Variation of α_{match} with antenna length and width considering manufacturing limitations

for which chip matching is feasible. For example, for the antenna with W=40 mm, a short matching length of 110 mm and a long matching length of 160 mm is feasible.

Embedded T-Match Antenna Bandwidth Characteristics for Longer Antenna Lengths

As observed in Fig. 4-5, for L=160 mm, all the antennas have an α_{match} value of 1.5-1.6. Referring to (4.4), I determine that $\frac{w1}{W} \approx 0.7$. Thus for a given W and for h=10 mm, impedance matching to a given tag IC involves varying the slot width, s, shown in Fig. 4-3. For each antenna width W, I select a slot width that matches the tag antenna to a given tag IC impedance in the 902-928 MHz frequency range. Once this has been achieved, I change the antenna-metal plane separation to 3 mm, corresponding to State 2 of the sensor, and observe the effect on the antenna impedance. The selection of appropriate s values is conducted using simulation software [67] and the results are outlined on a Smith Chart shown in Fig. 4-6.

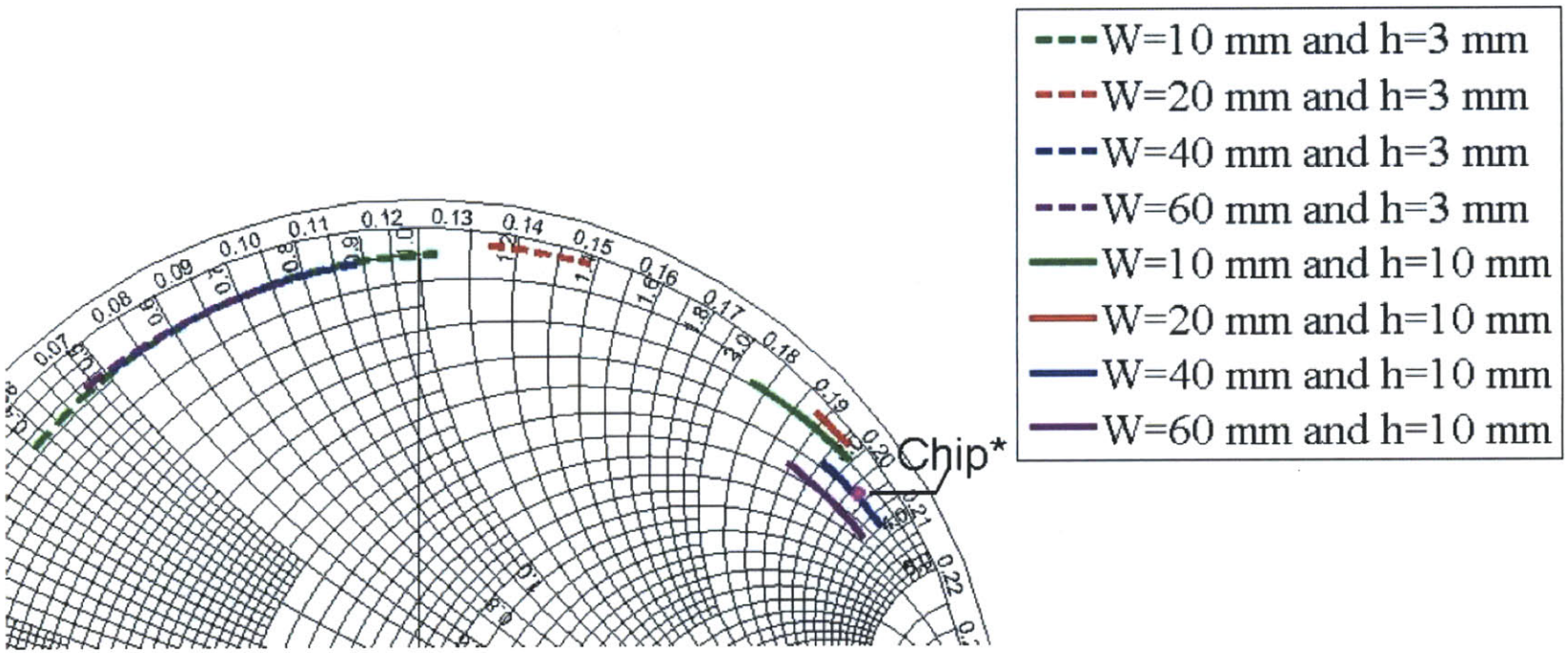

Figure 4-6: T-match antenna bandwidth characteristics for longer length antennas and multiple antenna widths; the antennas get severely detuned when the plate position changes from $h = 10$ mm to $h = 3$ mm

Table 4.1: Table of embedded T-match dimensions for shorter antenna lengths and multiple widths

L (mm)	W (mm)	W1 (mm)	α
140	10	5	1.1
130	20	7	0.8
112	40	22	1.1
96	60	34	1.1

As seen from Fig. 4-6, it is possible to select slots such that for all W, the antenna is well matched to the complex conjugate of the chip impedance for h=10 mm. However, when I change h=3 mm, the tag antennas get severely detuned from the conjugate match position. Thus the read range of the tag sensor would be severely limited by virtue of having poor τ for a tag-metal plate separation of 3 mm. Hence L=160 mm is found not to be a good candidate for our antenna design.

Embedded T-Match Antenna Bandwidth Characteristics for Shorter Antenna Lengths

Recall from Fig. 4-5 that there are shorter L values for which impedance matching is feasible. Table 4.1 highlights feasible L values for different W. Corresponding to the α_{match} values, I use Eq 4.4 to select an appropriate value of w_1. Repeating the procedure outlined for longer antenna lengths, for a plate-tag separation of 10 mm, I use numerical simulation software to obtain s values that conjugate match the chip to the antenna in the 902-928 MHz band. Once this is established, I change the plate-tag separation to 3 mm and observe the effect. The results are plotted on a Smith Chart and are shown in Fig. 4-7.

These results are much more promising than those of Section 4.1.3. When the tag-metal plate separation changes from 10 mm to 3 mm, the antenna is detuned very slightly as can be seen by the slight shift in the traces on the Smith Chart when the plate separation is changed. Thus we will be able to observe a slight shift in optimal operating frequency when the sensor changes state. Furthermore, since the detuning is not as severe as observed in Fig 4-6, we can expect reasonably high τ

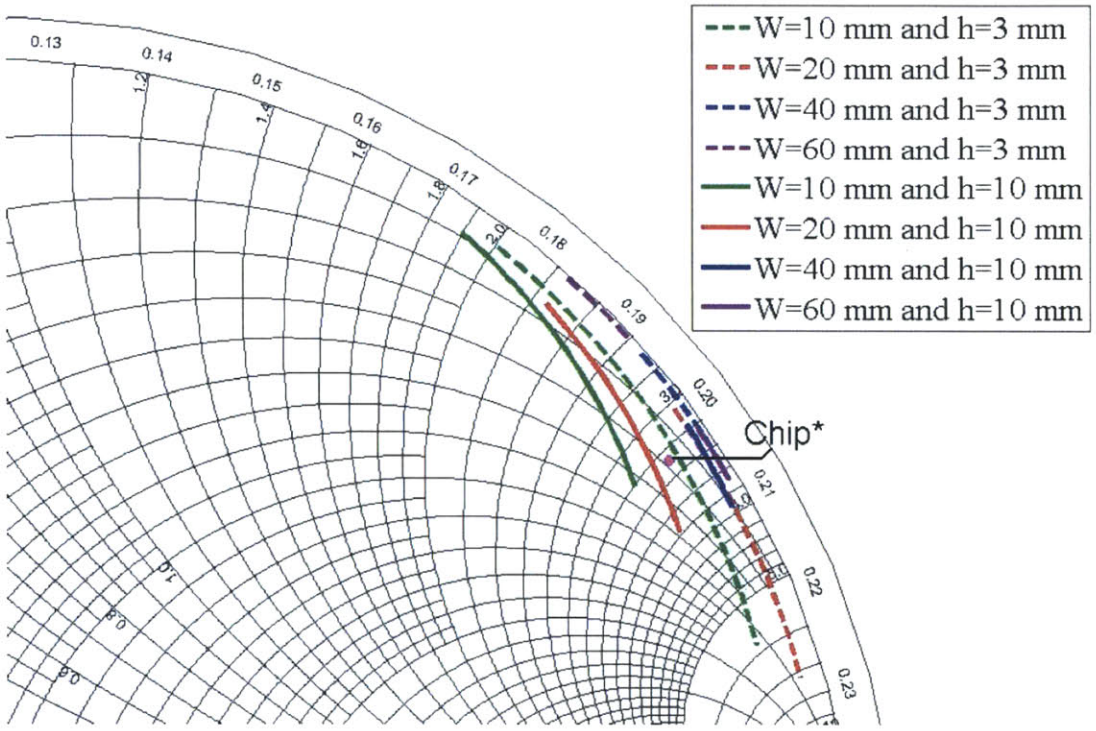

Figure 4-7: T-match antenna bandwidth characteristics for shorter length antennas and multiple antenna widths; the antenna frequency characteristics change slightly when the plate position moves from $h = 10$ mm to $h = 3$ mm

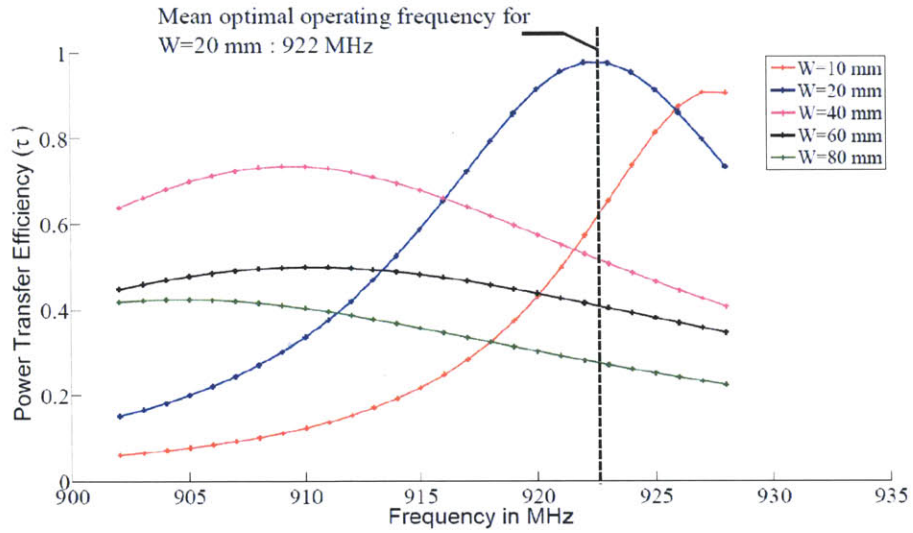

(a) τ vs frequency for h=10 mm

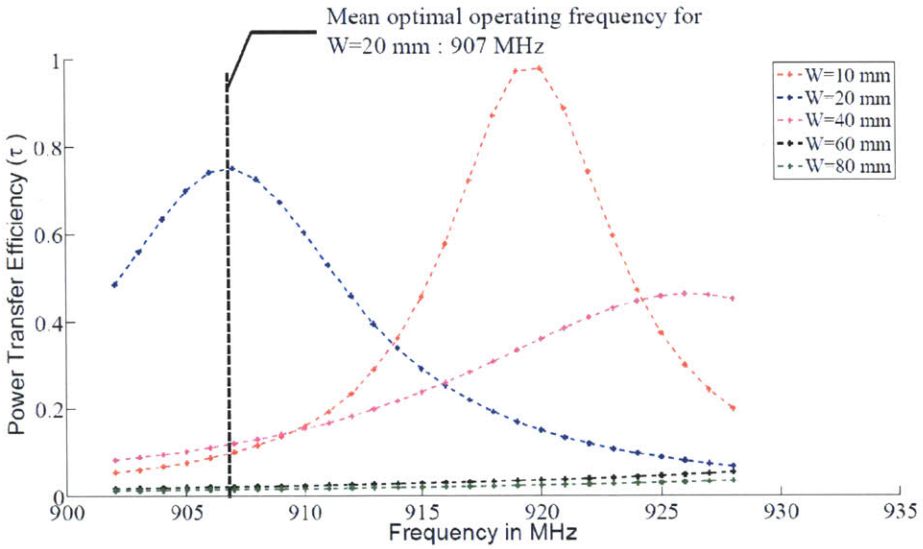

(b) τ vs frequency for h=3 mm

Figure 4-8: Variation of simulated values of τ with frequency for h=3 and 10 mm; for different antenna widths and considering shorter antenna lengths

values for both sensor states and this improves the read range of the sensor.

In order to select an optimal W presented in Fig. 4-7, I plot simulated values of τ as a function of frequency for different W and h. The simulated results are outlined in Fig. 4-8(a) and Fig. 4-8(b) respectively. As we can see from the figure, both the antennas corresponding to W=10 mm and W=20 mm exhibit the set of

requirements we are looking for — their optimal operating frequencies shift with a change in position of the metal backplane. The antenna with W=10 mm exhibits a higher power transfer coefficient for the tag-metal plate separation of 3 mm while the antenna with W=20 mm exhibits a higher power transfer coefficient for the tag-metal plate separation of 10mm.

Another difference is that the tag with W=20 mm provides a shift of 15 MHz in peak operating frequency — from 922 MHz when *h=10 mm* to 907 MHz when *h=3 mm* — as compared to 8 MHz for the case with W=10 mm, thus having better state separation in the frequency domain. I choose the tag with W=20 mm due to the greater shift in operating frequency. The following section outlines the results of field testing this prototype design.

4.1.4 Performance of the FM TABS Temperature Threshold Sensor in Laboratory Tests

Fig. 4-9 illustrates the antenna prototype that was subjected to field tests. The antenna was manufactured by precision cutting the geometry from a sheet of copper trace. I make use of an Alien Higgs 3 IC [61] and based on the specification sheets, set its nominal impedance to be $Z_{IC} = 18 - 164j$ at turn on power. I also make an assumption that Z_{IC} remains fairly constant over the 902-928 MHz operating frequency. The IC was bonded to the copper trace using silver epoxy.

In this section, I discuss the testing procedure employed and examine tag performance in terms of repeatability, read range and operating environment.

FM TABS: Testing Procedure using Commercial RFID Reader Equipment

In this study, I use an Impinj Revolution LLRP compliant RFID reader to detect tag response [68]. By choosing an appropriate implementation of the LLRP protocol stack [69], I can not only extract the operating frequency at the time of the query round, but also gradually increase the transmitted power (P_{trans}) on the reader from 15-32.5 dBm in steps of 0.25 dBm (70 discrete power levels). These two features allow me to

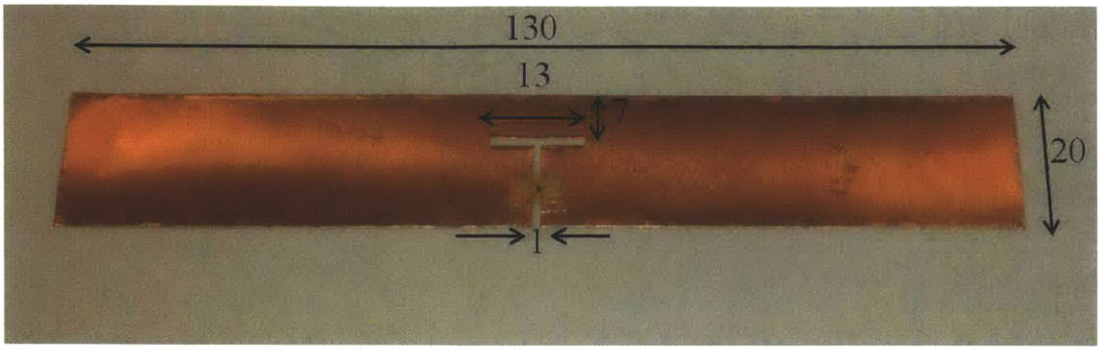

Figure 4-9: The frequency shifting embedded T-match antenna prototype used in the FM TABS temperature threshold sensor

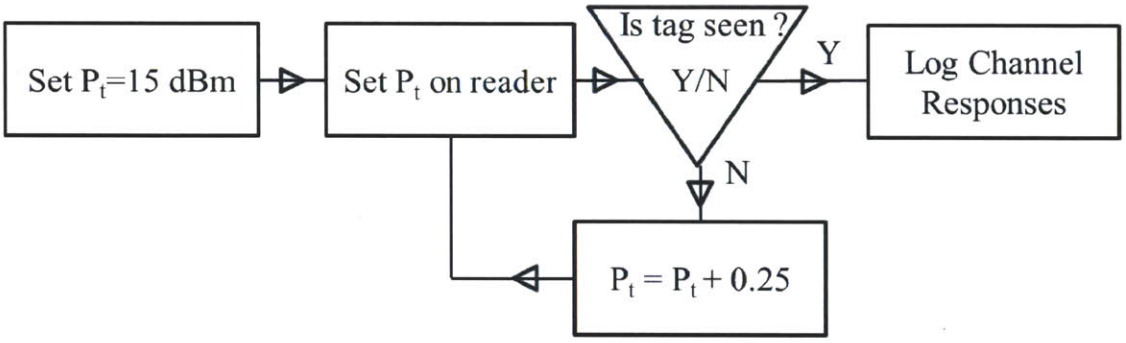

Figure 4-10: Algorithm to detect the optimal operating frequency band of an FM TABS sensor; sensor interrogated on 500 kHz carrier frequency channels in the 902-928 MHz band

design a simple testing procedure summarized in Fig 4-10. I define P^j_{thresh} (dBm) as the threshold power, the transmitted power at which the tag is just detected. The index j corresponds to either of the two states 1 or 2.

To classify state, I proceed by gradually increasing P_{trans} till I reach P^j_{thresh} and observe the set of channels, $\mathcal{F}_{thresh}$, on which the tag responds at this power setting. My classification algorithm is defined as follows:

- Set $j = 1$ if $f \geq 920$ MHz $\forall f \in \mathcal{F}_{thresh}$. In other words, if the sensor is first detected in a small band above 920 MHz then the tag is in State 1.
- Set $j = 2$ if $f \leq 912$ MHz $\forall f \in \mathcal{F}_{thresh}$. In other words, if the sensor is first detected in a small band below 912 MHz then the tag is in State 2.

The testing procedure is illustrated in Fig. 4-11. At a given transmitted power set-

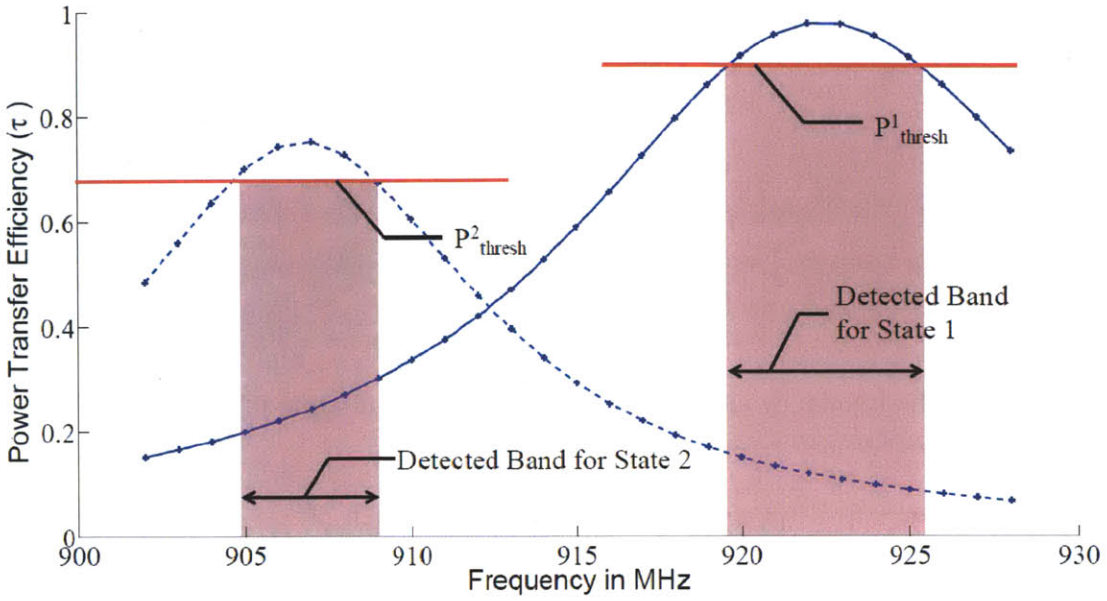

Figure 4-11: Frequency-base state detection mechanism for the temperature threshold sensor design

ting, I query the tag antenna for 60 seconds for the following reason: The Impinj Revolution reader randomly hops every 400 ms on 500 kHz channels between 902-928 MHz in order to fulfill FCC regulations in the US [70] and avoid interference between multiple readers and other RF equipment in the vicinity of the RFID reader. Assuming uniformly random hopping, it would take the reader a minimum of 20 seconds to sweep all 52 channels in the 902-928 MHz band. Therefore over the chosen time window of 60 seconds, the reader would have had enough time to query the tag on all 52 channels between 902-928 MHz. The Impinj test equipment has $N = 70$ discrete transmitted power settings. This implies that an FM TABS sensor in my experiments typically takes O($\frac{N}{2}$ x 60 = 2100 s) to be interrogated in the naive case and O(log(N) x 60 = 368 s) using a binary search technique [54]. I now present the results of laboratory testing of the tag antenna.

Results of Field Testing the FM TABS Temperature Threshold Sensor

Fig. 4-12 illustrates the results of laboratory tests. I conduct the experiment for both states of the sensor and record the *Fractional Channel Contribution*, which is

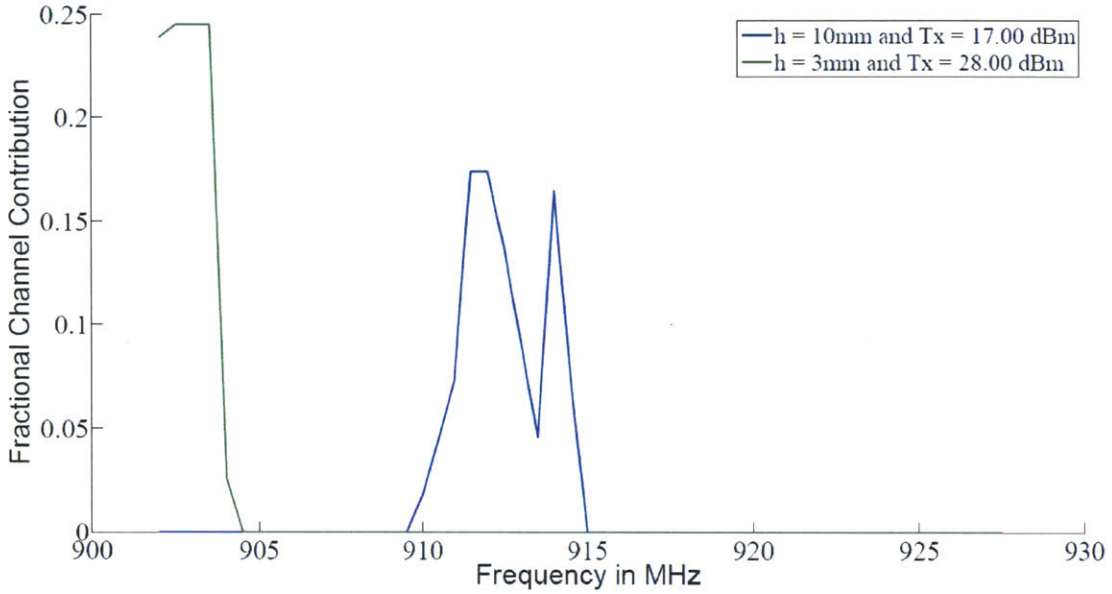

Figure 4-12: Frequency bands at which the sensor tag was detected for the two states of the FM TABS temperature threshold sensor; results are obtained using the Impinj Revolution RFID equipment and reader-tag separation was 2.5 m

the fraction of times the tag was detected in a particular frequency channel at the threshold transmitted power. The experiment was conducted in an open room, with clear line of sight between the reader and tag antenna. The reader and tag were separated by a distance of 2.5 m. No special anechoic chamber provisions were made to minimize reflections and channel fading. As we can observe from the figure, a clear distinction can be made between the two sensor states at the threshold transmitted power (T_x). Fig. 4-13 illustrates the results of repeating the test on 6 replicas of the tag prototype respectively. The purpose of repeating the test multiple times for different replicas is to assess the sensitivity of the antenna performance to variability in the antenna manufacturing process. As we can see, there is some variability between the repetitions although the direction of shift in optimal operating frequency remains consistent. We also observe a variation of as much as 3 dBm between replicas 1-5. The only anomaly is Replica 6 for which both states register significantly different optimal operating frequencies. We can conclude that the tag performance is indeed very sensitive to variability in the manufacturing process and this needs to be taken

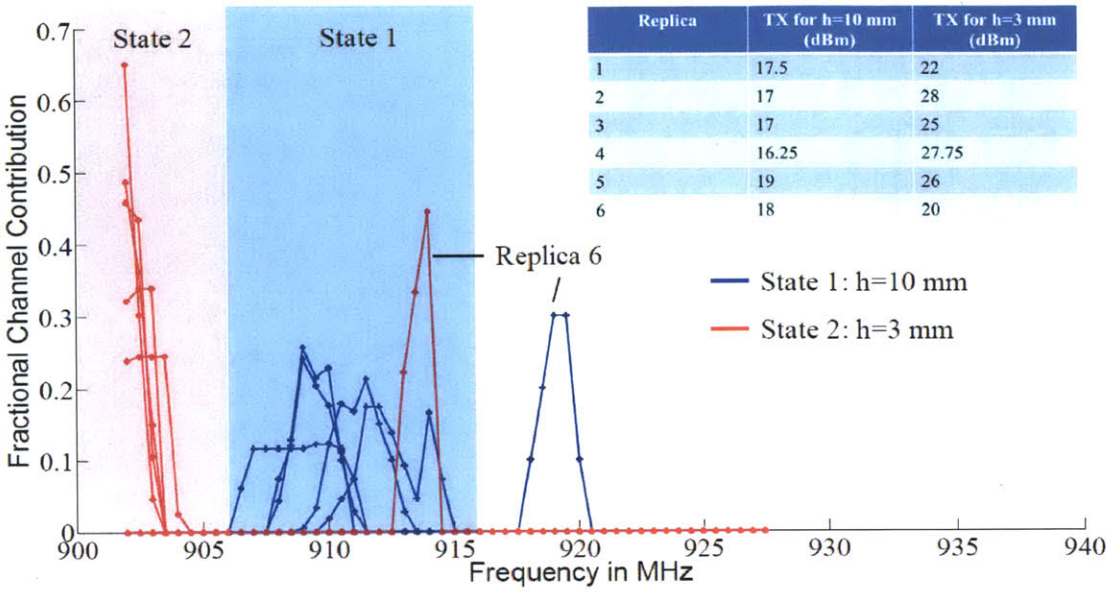

Replica	TX for h=10 mm (dBm)	TX for h=3 mm (dBm)
1	17.5	22
2	17	28
3	17	25
4	16.25	27.75
5	19	26
6	18	20

Figure 4-13: Measuring sensitivity of FM TABS to manufacturing variability by testing 6 replicas of the FM TABS temperature threshold sensor; measurements were taken using the Impinj Revolution equipment and reader-tag separation was set to 2.5 m

into account during mass production of FM TABS.

We also note that the optimal frequency band is offset by about 5-10 MHz from the simulation predictions. We propose a two-fold reason for this. First, our simulation assumes the two states of the sensor correspond to the isolation plate moving from $h = 10$ to $h = 3$ mm. In reality, there may be a slight uncertainty associated with the exact value of h for the two states of the sensor. Second, the RFID tag chip impedance is a function of frequency and input power. In our simulations, we neglect these effects and assume a fixed average value. Fluctuations in the chip impedance due to frequency and input power will also contribute to a difference between simulation and practice.

Determination of Read Range of the FM TABS Temperature Threshold Sensor

It is necessary to determine the read range over which the tag sensor can be reliably detected for both states of the sensor. I selected one of the replicas (Replica 5) and

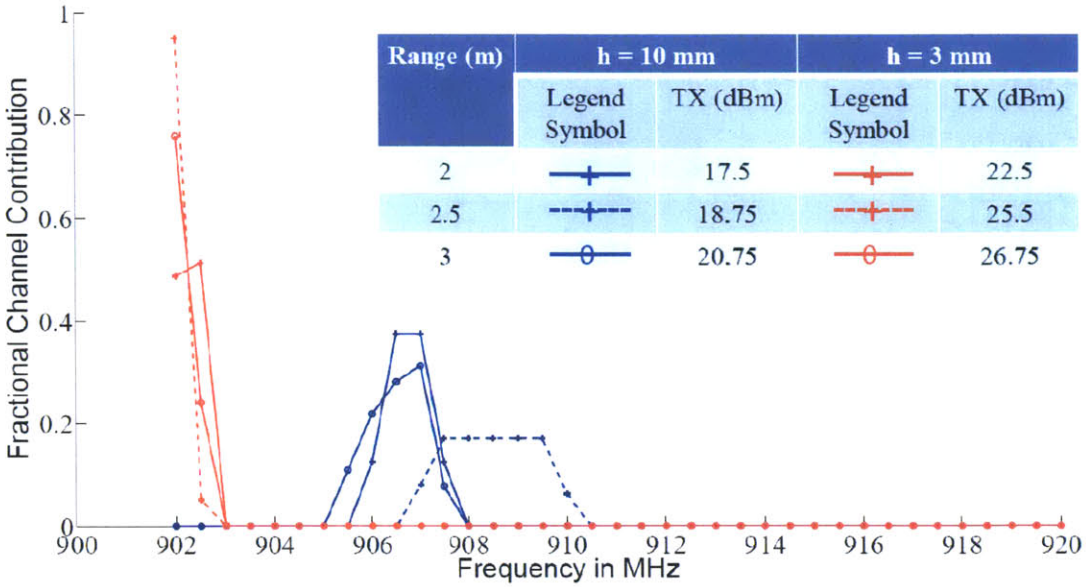

Figure 4-14: FM TABS temperature threshold sensor performance over different read distances; the experiment was conducted with replica 5

ran the state detection test for different reader-sensor separations. Fig. 4-14 illustrates the performance of the sensor for a reader-sensor separation of 2 m, 2.5 m and 3 m.

As we can see from the figure, the sensor can be reliably detected in both states over a distance of 3 m although there is a variability of 3-5 MHz observed in the position of the frequency bands corresponding to State 1. The tag IC impedance is a function of transmitted power and slight variations in the threshold transmitted power supplied to the chip due to the variable read distance can bring about this shift. However, these variations are still small compared to the frequency shifts induced by state change and thus state differences can still be successfully inferred.

We also observe that the threshold transmitted power for a plate-sensor separation of 3 mm is 26.75 dBm for a read range of 3 m which is less than the allowed maximum reader transmitted power of 32.5 dBm. This indicates that the maximum read distance of the sensor is larger than 3 m.

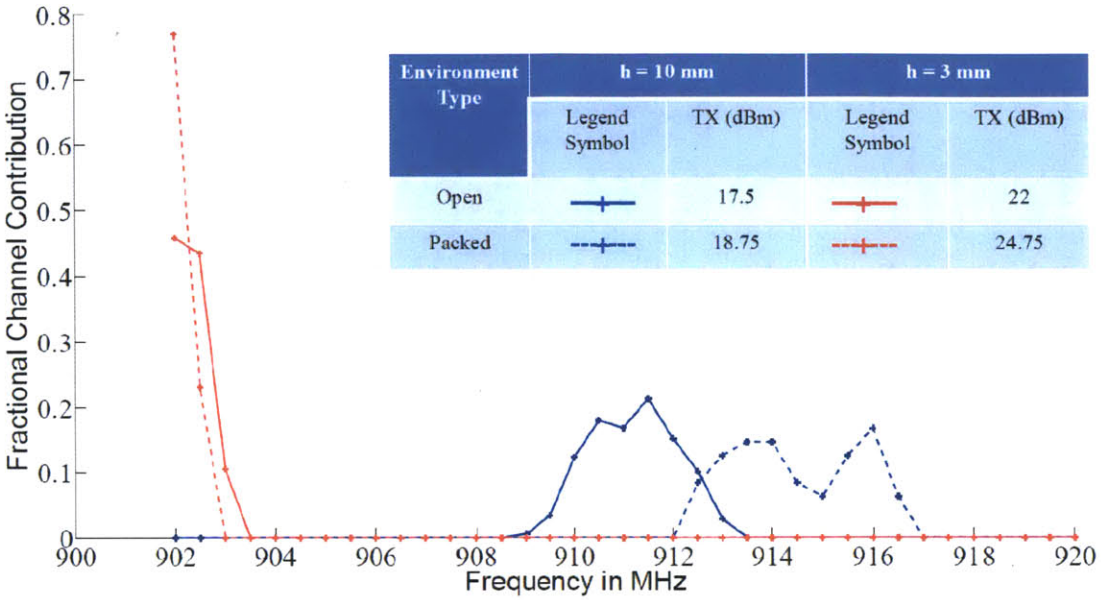

Figure 4-15: FM TABS temperature threshold sensor performance in different environments; the experiment was conducted with replica 1

Effect of Environment on Sensor Performance

The RFID tag sensor is likely to be deployed in several different environments ranging from open warehouse lots to confined storage rooms. It is necessary to assess how differences in environment affect the tag performance. I examine the tag-sensor performance in a representative room with furniture and reflecting metal surfaces in close proximity to the RFID tag. The only constraint I maintain is a line of sight between the reader and tag antennas. Fig. 4-15 illustrates the results for a reader-tag separation of 2 m. For the purposes of this experiment I make use of Replica 1.

As we can see from the figure, there is a shift of 3-5 MHz in the frequency band for the sensor in State 1, although it is still possible to differentiate between State 1 and State 2. Thus the environment does affect tag performance; however by sufficiently separating the frequency bands between State 1 and State 2, we can accommodate the slight variations caused by environmental fluctuations.

4.2 Case Study 2: Design of an FM TABS Fluid Level Sensor

FM TABS sensors can also be applied to the problem of fluid level sensing such as the detection of fluid levels in gasoline containers, overhead storage tanks and backup battery generators. One of my previous studies illustrates that fluid level TABS are best suited for binary level sensing — where N discrete fluid levels are monitored by using N TABS rather than using a single TABS antenna to assess N fluid levels [56]. Therefore, I attempt to design an FM TABS fluid binary level sensor capable of detecting the presence or absence of water in a beverage glass. The FM TABS approach makes the state detection mechanism independent of read range. Furthermore, the customized tag antenna can be designed so as to optimize tag read range. Fig 4-16(a) shows the prototype FM TABS sensor deployed on the glass.

I design the FM TABS fluid level sensor for an ordinary quartz beverage drinking glass having wall thickness 4 mm. The glass has a height of 130 mm which places a constraint on the maximum length of the antenna. I fix the antenna dimensions as shown in Fig 4-16(b) so that the tag antenna is impedance matched in the *glass full* condition. Figure 4-17 illustrates the simulated frequency characteristics of the FM TABS sensor in the presence and absence of water for the 902-928 MHz ISM band for UHF RFID operations.

As we can see from the figure, the presence of water reduces the radiating resistance of the antenna. The tag has a much narrower bandwidth when water is present and is better impedance matched to the RFID tag's IC for the frequencies in the 910-920 MHz band. When the glass is dry, the tag displays a response across a broader band and the power transfer efficiency is practically the same over all frequencies. This is confirmed by the graph of power transfer efficiency, τ, as a function of frequency (*c.f* Fig 4-18).

I make use of the frequency detection algorithm outlined in Fig 4-10. As I increase P_t, the number of channels across which the tag responds when in the empty state is expected to be higher than in the full state. As seen in Fig 4-19(a), at the threshold

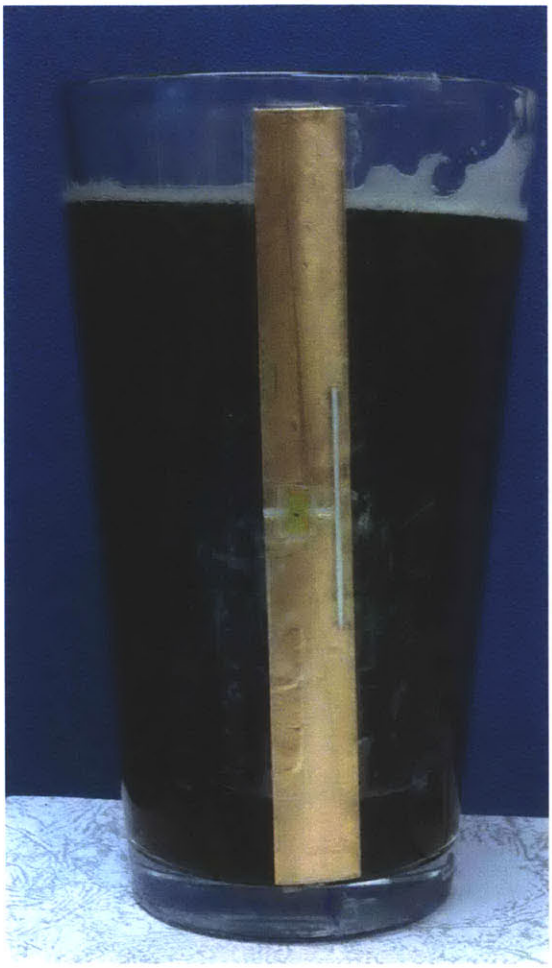

(a) FM TABS fluid level sensor deployed on beverage glass

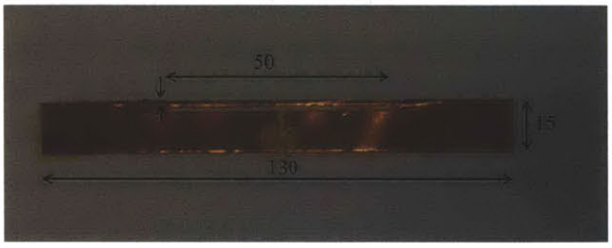

(b) FM TABS embedded T-match antenna for fluid level monitoring

Figure 4-16: Monitoring fluid level with an FM TABS sensor

transmitted power P_{thresh} the full glass is detected in a band around 920 MHz while the empty glass is seen across more channels. The fractional channel contribution used in Fig 4-19(a) is the fraction of times, the tag is detected at a specific frequency

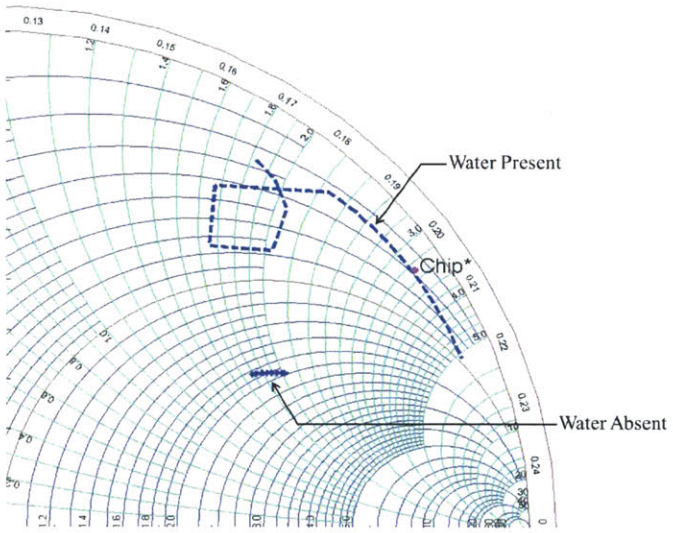

Figure 4-17: Frequency characteristics of FM TABS fluid level sensor when the beverage glass is completely full and empty

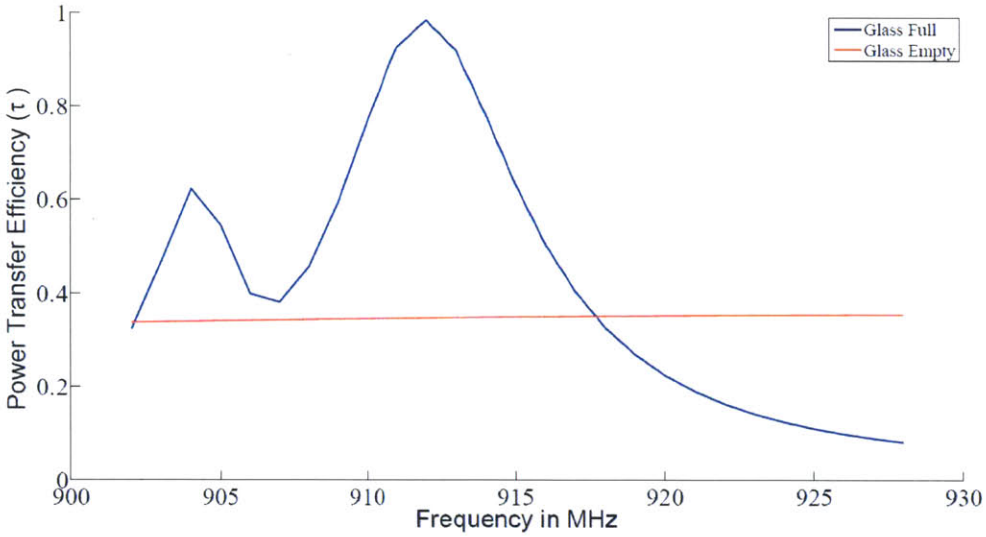

Figure 4-18: Variation of τ with frequency for the fluid level sensor in the presence and absence of water

when a frequency sweep is conducted, in this case at P_{thresh}. At $P_t = P_{thresh}+1.5dBm$, the full glass is still detected across slightly more frequencies in the 920 MHz band while the empty glass is detected across all frequencies evenly (c.f Fig 4-19(b)). Thus the frequency response at $P_t = P_{thresh} + 1.5dBm$ can be used as a metric to classify the state of the sensor.

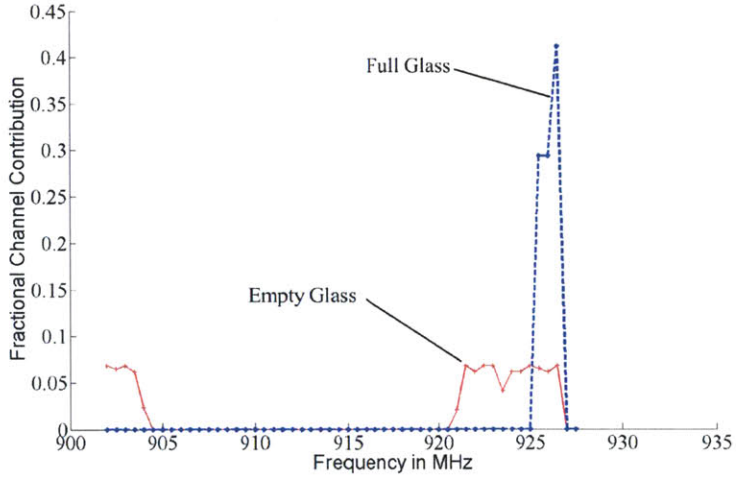

(a) Frequency response of the FM TABS fluid level sensor in the presence and absence of water at P_{thresh}

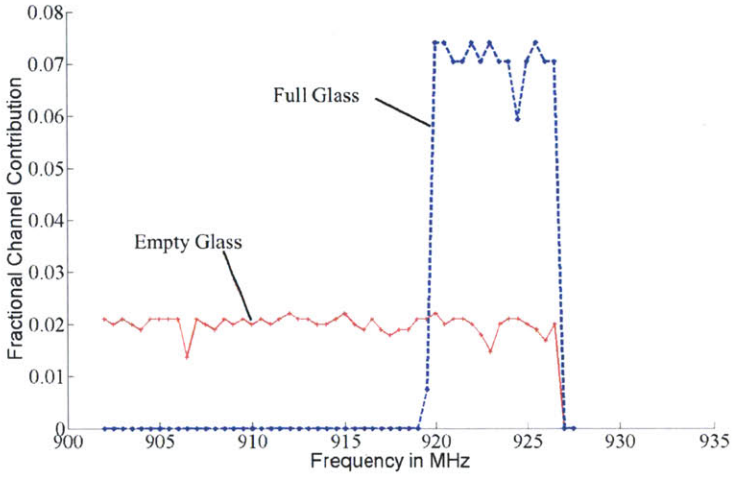

(b) Frequency response of the FM TABS fluid level sensor in the presence and absence of water at $P_{thresh} + 1.5dBm$

Figure 4-19: Frequency domain state detection of an FM TABS fluid level sensor in the presence and absence of water

I repeat the experiment for four replicas of the tag antenna to ensure repeatability. It is encouraging to note that, as seen in Fig 4-20, the results follow the same trends although subject to some variation due to manufacturing variability.

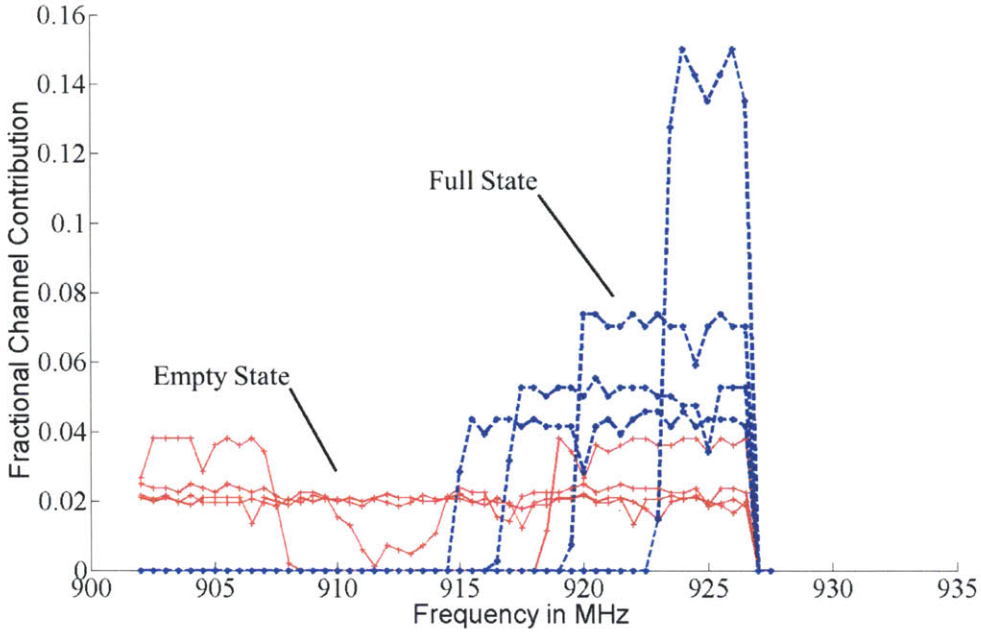

Figure 4-20: Measuring sensitivity of FM TABS to manufacturing variability by testing 4 replicas of the FM TABS fluid level sensor

4.3 Related Work in Frequency Domain-Based Sensing

Frequency domain-based sensing in its broadest interpretation is well known in the literature. For example, structural damage can be detected by relating damage states to changes in the free vibration response of a structure as discussed by Lynch *et.al* [71]. Changes in frequency have also been used in fiber-optic based sensing to sense parameters such as temperature and strain as shown by Garcus *et. al* [72].

Frequency domain methods have also been used in passive, pervasive sensor design. Fletcher *et al.* [73] propose the design of reversible and single-use temperature threshold sensors as well as continuous monitoring temperature sensors by relating temperature to changes in the frequency characteristics of magnetic materials. These sensors are very low cost and operate over a temperature range of 20-80^{0}C. However, they do not have an inherent unique identifier and have a short read range of a few inches. In related work [74], the authors also illustrate how electromagnetically re-

sponsive material structures can be used to design low cost force and position sensors.

Specific to RFID, there has been at least one instance of HF frequency domain based sensing. In their paper, Potyrailo *et.al* [64] demonstrate how a HF RFID tag vapour sensor can be used to differentiate between mixtures of volatile organics as well as concentrations of individual organics by relating these quantities to changes in the resonant and anti-resonant frequencies of an ordinary HF tag. In the UHF domain, the work described in this chapter [33] is the first known instance of how changes in a physical parameter can be related to shifts in the optimal operating frequency of an RFID tag for the 902-928 MHz ISM band for American RFID operations.

Chapter 5

Phase Modifying TABS

The previous chapters examine how RFID tag signal amplitude and operating frequency can be used for sensing. In this chapter, I introduce the concept of Phase Modifying (PM) TABS where tag signal phase can be used as a proxy for a physical parameter of interest. Recently, RFID tag phase information has been used to improve tag position estimates and the physics and factors influencing tag RF phase has been well understood and documented in the literature. I summarize this theory and build on it to propose the design of a PM TABS fluid level sensor. I demonstrate, via numerical simulation and experimentation, that while a PM TABS design is theoretically possible, its sensitivity to extraneous uncertainties make its practical implementation challenging.

5.1 Recent Interest in RFID Tag Signal Phase

Tag backscatter signal amplitude (RSSI) has been used for the triangulation of RFID tags, but is notoriously inaccurate due to channel fading effects [75]. RSSI measurements are therefore frequently used in tandem with more sophisticated sensors such as reference active RFID tags [76] or laser position sensors [77] to improve position estimation.

RFID readers perform fully coherent detection of the demodulated backscatter response of an RFID tag and are capable of extracting phase angle information in

addition to RSSI. Recent research efforts have examined using phase information in tandem with RSSI for improving the position accuracy of RFID tags [78] [79]. A thorough overview of the physics of RF phase angle changes and the factors that influence it is provided by Nikitin *et.al* [75] who use it to obtain accurate spatial position estimates of an RFID tag as it passes by a reader installed in the dock door of a warehouse. In the following sections, I build on this theory to propose the design of a PM TABS fluid level sensor.

5.2 Factors influencing RF Phase Angle

At the RFID reader, the RF phase angle is determined by I/Q demodulation of the received backscatter signal voltage [9] and each demodulated component has a DC offset and an AC component illustrated in Fig 5-1 [75]:

$$\begin{aligned} I &= I_{DC} + I_{AC} \\ Q &= Q_{DC} + Q_{AC} \end{aligned} \tag{5.1}$$

The DC offset is introduced by leakage from the transmit to receive antennas and reflections of the transmitted electromagnetic wave off background reflectors in the environment. The AC offset is determined by the relative orientations of the vectors $\vec{S_1}$ and $\vec{S_2}$. These voltage vectors correspond to the two impedance states of the RFID tag IC used in ID modulation. I assume that $\vec{S_1}$ corresponds to the *impedance matched* state where $Z_c = Z^*_{antenna}$ and $\Gamma_1 = 0$. Similarly $\vec{S_2}$ corresponds to the *poorly matched* state where Z_c is very poorly matched to $Z_{antenna}$ and $\Gamma_2 = 1$ (the reader is referred to Chapter 2 for a refresher of tag IC impedance states). RFID readers renormalize RF phase angle to factor out the DC offset [75]. The RF phase angle, ϕ, measured by the RFID reader thus depends on the AC components alone and is expressed as:

$$\phi = \arctan \frac{Q_{AC}}{I_{AC}} \tag{5.2}$$

ϕ, depends upon three factors [75]:

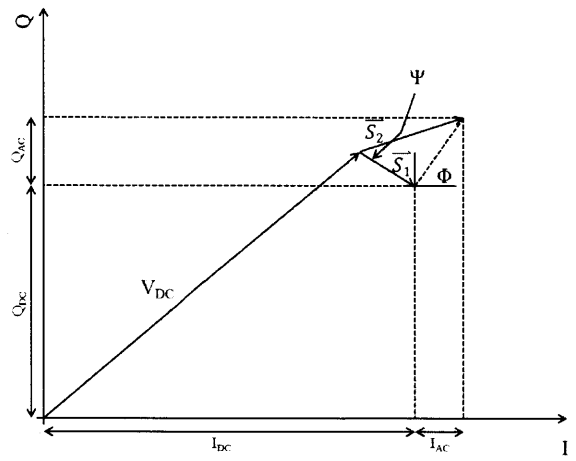

Figure 5-1: RF phase angle from the I/Q demodulation of the RFID tag signal (Adapted from: P.V Nikitin, R. Martinez, S. Ramamurthy, H. Leland, G. Spiess and K.V.S Rao, *Phase based spatial identification of UHF RFID tags*, IEEE International Conference on RFID, 2010, pp 102-109)

- The accumulated phase, ϕ_{prop} due to electromagnetic wave propagation to and from the RFID tag. ϕ_{prop} depends not only upon the distance between the reader and tag, but also the position of reflecting surfaces like the walls, ceiling and floor of a room as well as pieces of furniture and passing objects.

- The phase offsets in the RFID reader electronics, ϕ_{off}, due to the length of the transmission line between the reader and the receiving antenna as well as the phase noise in the reader's electronic components like local oscillators and mixers.

- The phase due to tag backscatter modulation, ϕ_{BS}. This parameter depends upon the impedance match between the antenna impedance $Z_{antenna}$ and the chip impedance Z_{c1}.

I now examine the sensitivity of ϕ to each of these components and the scope for developing a PM TABS based sensing strategy. Eq 5.3 illustrates the relationship between the phase components:

$$\phi = \phi_{prop} + \phi_{off} + \phi_{BS} \tag{5.3}$$

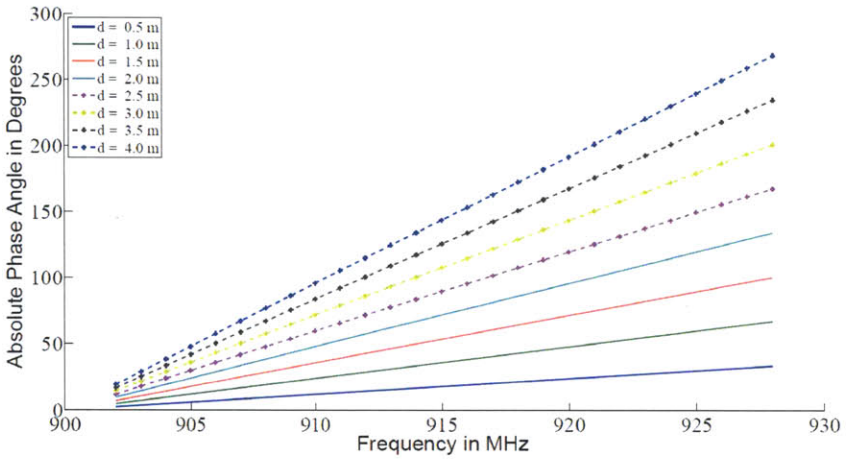

Figure 5-2: ϕ_{prop} vs. frequency for different reader-tag separations in free space

5.2.1 Effect of Wave Propagation on RF Phase Angle

In free space, ϕ_{prop} linearly varies with both the frequency of operation and distance between the RFID tag and the reader [75]

$$\phi_{prop} = 2kd \tag{5.4}$$

where k is the wavenumber at the frequency of operation and d is the reader-tag separation distance.

Fig 5-2 illustrates the variation of free-space accumulated phase with operating frequency for typical reader and passive tag separations. As we can see from the figure, the phase accumulation across the 902-928 MHz band, corresponding to American RFID operations, is less than 50° for d=0.5 m while it can be as large as 250° for d=4 m.

A real propagation environment consists of several objects such as the walls, floor and ceiling or furniture in close proximity to the reader or tag. Constructive or destructive interference from these reflections change RFID tag signal amplitude and phase unpredictably. There have been attempts to quantify these multipath effects using reflection ray models, but all these models assume some a priori understanding or simplification of the arrangement of the sources of reflection relative to the reader-

tag system.

For instance, Tam and Tran [80] present a multi-ray model to predict propagation path loss of an electromagnetic wave in an indoor environment. Their approach assumes that parallel surfaces such as the floor and ceiling or walls contribute most to multipath effects. Results show that the model predicts path loss reliably over a distance of 12 m but is very dependent upon understanding the 3-D geometry of the propagation environment.

Similarly, Nikitin *et.al* [75] outline the challenges associated with accurate RF phase measurement in a real environment with multipath effects. They emphasize the need for tightly controlled experimental conditions and propose a wave reflection model to predict the effect of environment on RF phase angle. Furthermore, they make use of a custom designed RFID reader which would allow them to characterize the expected phase noise in the internal reader electronics. Their wave reflection model makes several simplifying assumptions for analytical simplicity but is shown to be in good agreement with experiments conducted using the custom RFID reader. While describing the model, the authors introduce a parameter, H, which quantifies the effect of reflections off the walls, floor and ceiling on RF phase angle [75]. This parameter depends primarily upon the position of the reflecting surfaces relative to the reader-tag set up. The factor H is shown to relate to ϕ_{prop} as [75]

$$\phi_{prop} = 2kd - 2arg(H) \tag{5.5}$$

From Eq 5.5, we note that the propagation environment can arbitrarily influence ϕ_{prop}. In Section 5.4, I provide a more detailed summary of their wave reflection model and make use of it to determine the practical applicability of PM TABS.

5.2.2 Effect of Reader Electronics on RF Phase Angle

The cabling between the reader antenna and transceiver presents a transmission line of finite length L for which ϕ_{off} varies in direct proportion with the wavenumber and length. In addition, the phase noise due to electronic components like the mixers

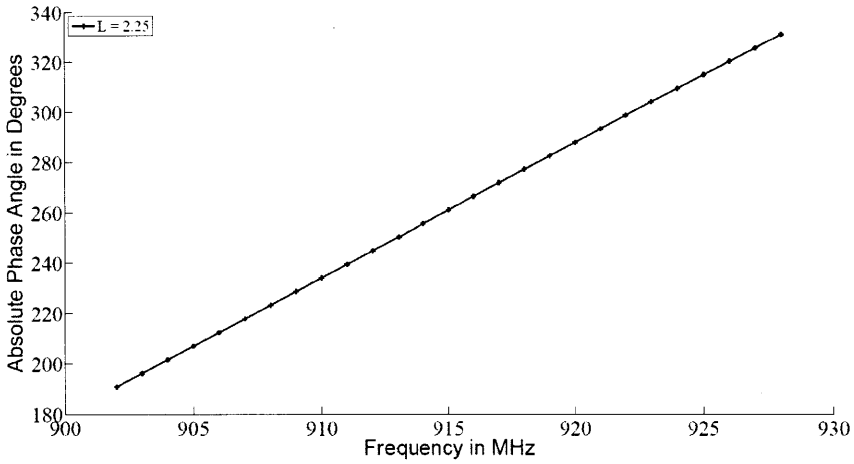

Figure 5-3: ϕ_{off} induced due to length of transmission line cabling between the reader and receiving antenna

and oscillators, adds additional noise, η_f, to ϕ_{off}. Thus ϕ_{off} is modeled as per the following equation

$$\phi_{off} = 2kL + \eta_f \tag{5.6}$$

For the reader used in our experiments, the transmission line cabling length is approximately 2.25 m which induces a phase offset difference of about 140° across the 902-928 MHz band as seen in Fig 5-3. Furthermore once the frequency dependence of η_f is factored into Eq 5.6, this linear trend may no longer hold.

5.2.3 Effect of RFID Tag Antenna Impedance

The phase component ϕ_{BS} depends upon the tag backscatter modulation. As observed in Fig 5-1, the angle ϕ is related to the relative orientation of $\vec{S_1}$ and $\vec{S_2}$ - which is defined by the angle ψ. Let us assume that $\vec{S_1}$ corresponds to the tag IC impedance state Z_{c1} while $\vec{S_2}$ corresponds to the tag IC impedance state Z_{c2}. Z_{c2} corresponds to an open or short circuit condition and thus $\Gamma_2 = \pm 1$. Thus for a constant reader-tag separation and operational environment, the position of $\vec{S_2}$ remains fixed for all operating frequencies.

Z_{c1} corresponds to the chip's impedance state when the tag is scavenging power from the RFID reader. For a broadband RFID tag, ideally $|\Gamma_1| \approx 0$, corresponding

to the *impedance matched condition*, across the 860-960 MHz frequency range of operations or the 902-928 MHz band for American UHF RFID operations. For a narrow band tag, such as the frequency selective antennas designed in Chapter 4, the value of $|\Gamma_1|$ could fluctuate significantly depending upon the frequency dependence of $Z_{antenna}$.

Fig 5-4(a) illustrates the change in the angle ψ for a broad band RFID tag as the reader frequency of operation changes for a fixed reader-tag separation and operational environment while Fig 5-4(b) captures the corresponding change in the angle ψ for a narrow band tag. The phase angle $\phi_{BS}(f_i)$ manifests itself as the difference between the vectors $S_1(\vec{f_i})$ and $S_2(\vec{f_i})$ as follows

$$\phi_{BS}(f_i) = \arctan\left[S_1(\vec{f_i}) - S_2(\vec{f_i})\right] \tag{5.7}$$

Here i is a index indicating the operating frequency at which the measurements are taken. The effect of tag modulation on RF phase is contained in the tag differential backscatter power. From Eq 2.16, the real and imaginary components of the backscattered power are proportional to $(\Gamma_1 - \Gamma_2)^2$. Eq 5.7 can then be modified as

$$\begin{aligned} \phi_{BS}(f_i) &= \arctan\left[S_1(\vec{f_i}) - S_2(\vec{f_i})\right] \\ &= \arctan\left[(\Gamma_1 - \Gamma_2)^2\right] \end{aligned} \tag{5.8}$$

In the following section, I attempt to precisely quantify the extent by which $\phi_{BS}(f_i)$ can be made to fluctuate and examine the possibility of developing a phase-based state detection technique using this fluctuation.

5.3 Using Tag Backscatter Phase Modification for Sensing

From the theory outlined in Section 5.2.3, I propose the design of a PM TABS sensing strategy that utilizes antenna change from broadband to narrow band performance

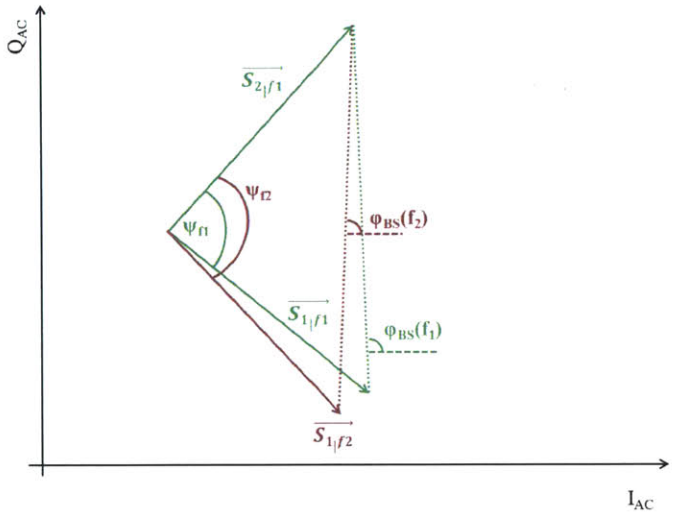

(a) Small changes in ψ with operating frequency for a broadband antenna

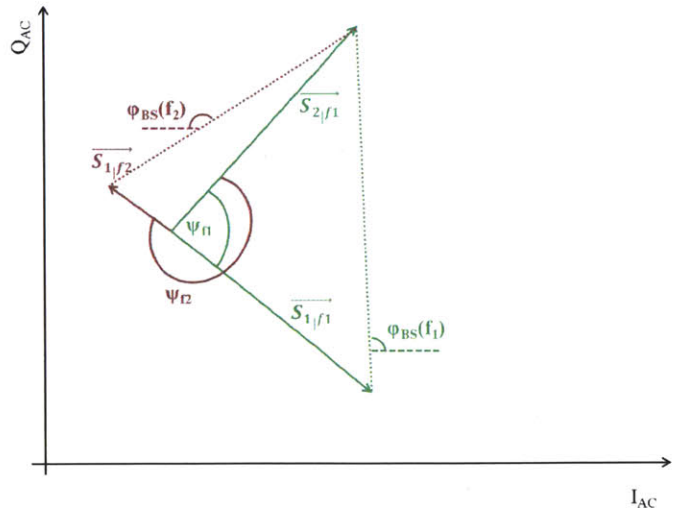

(b) Large changes in ψ with operating frequency for a narrow band antenna

Figure 5-4: Effect of antenna band characteristics on RF Phase

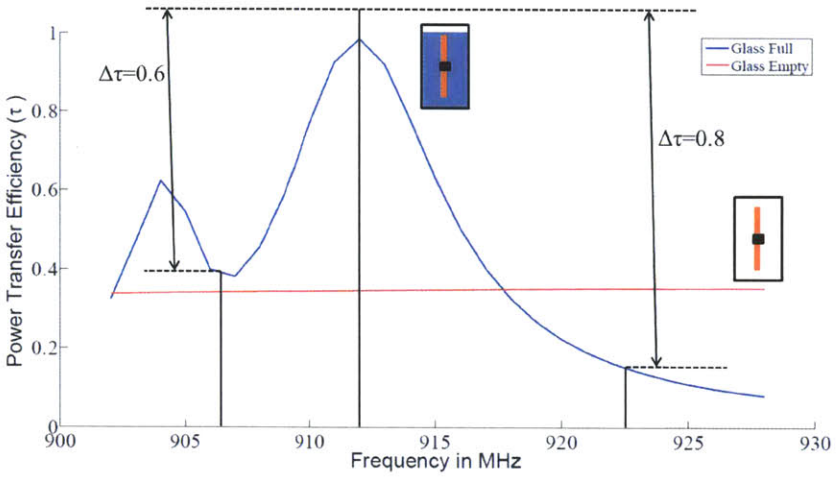

Figure 5-5: Power transfer efficiency (τ) vs. frequency of the antenna for two states of the glass: completely empty and full

depending upon a change in the physical parameter of interest. I consider the design of a PM TABS fluid level sensor to determine whether or not a beverage glass is completely empty or completely full.

I make use of the tag antenna proposed in Section 4.2. Fig 5-5 illustrates the band characteristics of the tag antenna, obtained from simulations, when the glass goes from the empty to the completely full state. As we see from the figure, there is no significant variation in the degree of impedance match (τ) when the glass is empty indicating a broadband performance in the 902-928 MHz band. On the other hand, when the glass is full, we observe a change of $\Delta\tau$=0.6 in the 907-912 MHz band and a change of $\Delta\tau$=0.8 in the 912-922 MHz band — indicative of narrow band performance. Using the values of Γ_1 obtained from simulation and assuming Γ_2=1 (corresponding to Z_{c2} open circuit condition), I use Eq 5.8 to predict the change in $\phi_{BS}(f_i)$ for the full and empty glass states. Fig 5-6 illustrates the change in computed phase angle from the antenna for the two states of the beverage glass. As we can see from the figure, $\phi_{BS}(f)$ remains more or less constant over the entire 902-928 MHz band for the empty glass while there is a significant variation in $\phi_{BS}(f)$ for the glass in the full state. Thus the state of the glass (full or empty) can be inferred by examining the frequency dependence of $\phi_{BS}(f)$.

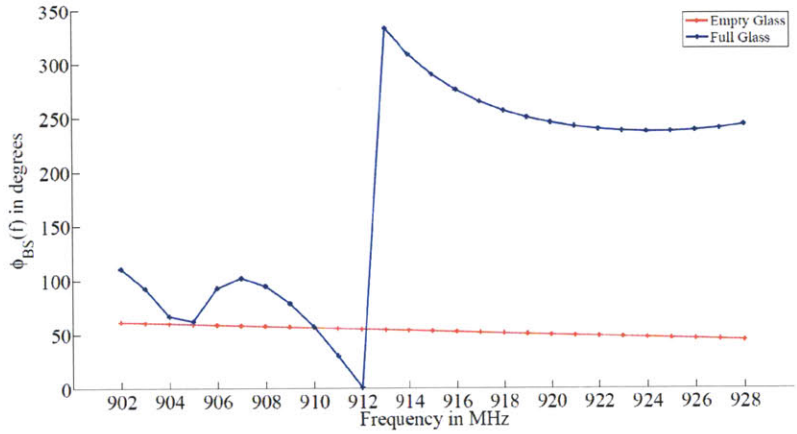

Figure 5-6: ϕ_{BS} vs frequency for the two states of the glass: completely empty and full

5.4 The Practical Applicability of PM TABS

From Section 5.3, we observed that state differentiation based solely on $\phi_{BS}(f)$ is feasible. However, it is the parameter ϕ_f that is measured at the RFID reader, which in addition to $\phi_{BS}(f)$, also includes components such as ϕ_{prop} and ϕ_{off} as seen in Eq 5.3. These components introduce distance and frequency dependent rotations to $\vec{S_1}$ and $\vec{S_2}$. Precisely determining the sensitivity of ϕ_f to these quantities is difficult due to the following reasons:

- As observed in Section 5.2.1, ϕ_{prop} can vary considerably depending upon reader-tag separation, operating frequency and real world environmental conditions.

- ϕ_{off} introduces a frequency dependent phase offset as shown in Section 5.2.2. There is some uncertainty associated with precisely determining the length of the transmission line cabling between the reader and receiving antenna. In addition, the phase noise in the mixers and local oscillators of the RFID reader present an additional source of uncertainty in ϕ_{off}.

- Simulation assumes that $\phi_{BS}(f)$ is known precisely. As noted in Chapter 4 there is manufacturing uncertainty associated with $Z_{antenna}$, and thus Γ_1, that will change $\phi_{BS}(f)$ from the expected value.

- The chip impedance, Z_{c1}, varies with the input power and operating frequency. This causes variations in Γ_1 and thus $\phi_{BS}(f)$.

- ϕ_f is subject to a phase wrap for every multiple of 360°.

The effectiveness of phase-based state detection will be determined by whether the phase changes in $\phi_{BS}(f)$ are overwhelmed by the sensitivity of ϕ_f to these uncertainties. In the following sections, I first discuss the scope of using ϕ_f for sensing under highly idealized conditions. I then compute the effect of progressively adding uncertainty in the determination of $\phi_{BS}(f)$, ϕ_{off} and ϕ_{prop}. Finally, I verify the applicability of PM TABS experimentally.

5.4.1 Estimation of ϕ_f in Free Space Conditions

I first examine the effect of ϕ_{BS}, ϕ_{prop} and ϕ_{off} in idealized conditions. I make the following assumptions:

- I ignore the effect of multipath and assume free space propagation conditions.

- I assume the antenna receiver cabling length is known precisely and the phase noise, η, in the RFID reader electronics is negligible.

- Manufacturing uncertainty in $Z_{antenna}$ and uncertainties in Z_{c1} due to variations in input power and operating frequency are neglected and I assume that the simulated values of Γ_1 represent reality.

I compute ϕ_f as per the following equation

$$\phi_f = mod(2kd + 2kL + \phi_{BS}(f), 360) \tag{5.9}$$

Fig 5-7 highlights how ϕ_f varies for the two states of the glass for free space wave propagation conditions and for a reader-tag separation of between 0.5 and 1 m. As we observe from the figure, in the case of the empty glass, the phase dependence on frequency is linear with the exception of the distance dependent phase wrap. In the

case of the full glass, the phase dependence on frequency is non-linear. It is possible to differentiate between the two states of the glass based on the linear vs. non-linear trend of ϕ_f, even though the absolute shapes of the curves may differ depending upon the reader-tag separation.

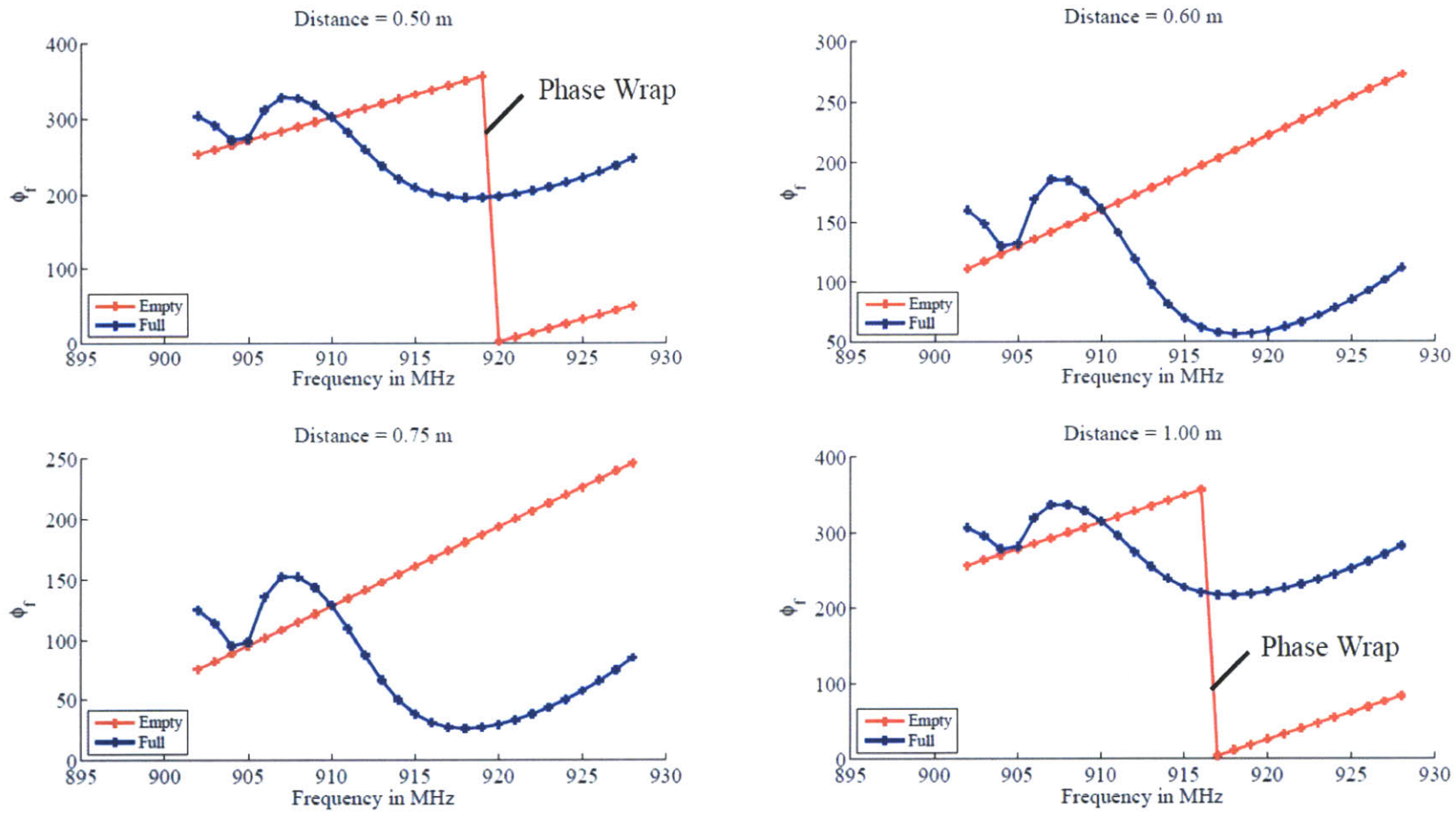

Figure 5-7: Variation of ϕ with frequency for the PM TABS antenna for the full and empty states of the beverage glass for read distances of 0.5-1 m: ϕ_{BS} is computed by simulation, ϕ_{off} is assumed known precisely and free space propagation is assumed

Effect of Uncertainty in Γ_1

As outlined in Section 5.4, Γ_1 is prone to uncertainty in $Z_{antenna}$ and Z_{c1}. To quantify the sensitivity of ϕ_f to uncertainty in Γ_1, I introduce between 10 - 20% random noise in the simulated values of Γ_1 and run six simulations to predict ϕ_f under these conditions and for a reader-tag separation of 0.6 m. The results are shown in Fig 5-8. As we observe from the figure, the introduction of noise increases the variation in both curves. However the phase response of the empty glass still follows a linear trend. State inference is thus possible for a known reader-tag separation.

I next examine the effect of randomly varying the read distance. Fig 5-9 illustrates the results of six simulations given a 20% random noise in the simulated value of antenna impedance as well as a random reader-tag separation of between 0.5 and 1 m. As observed from the figure, in at least one instance, corresponding to a reader-tag separation of 0.7 m, it is difficult to differentiate between the two states of the glass based purely on shape of the phase profiles alone.

Effect of Uncertainty in Γ_1 and ϕ_{off}

In this section I introduce ambiguity in the exact value of ϕ_{off} due to uncertainty in the precise length of transmission line cabling of length L = 2.25 m discussed in Section 5.2.2. I subject L to a position uncertainty δL which varies from 0 cm to 16 cm in steps of 2 cm. Further, I make the assumption that η_f in Eq 5.6 can be neglected in our analysis. Fig 5-10 illustrates how ϕ_f varies in the presence of uncertainty in both ϕ_{off} and Γ_1 and for a reader-tag separation of 0.6 m. As we observe from the figure, state differentiation based purely on the shape of the curves is difficult in this case.

Similarly, Fig 5-11 illustrates the sensor performance when L varies from 2.25 - 2.39 m with random reader-tag separation of between 0.5 and 1 m. We observe that state discrimination in the presence of uncertainty in ϕ_{off}, Γ_1 and reader-tag separation is not possible.

I conclude that the sensitivity of ϕ_f to uncertainty in Γ_1, ϕ_{off} and reader-tag

separation, even in free space conditions, makes the practical implementation of PM TABS challenging.

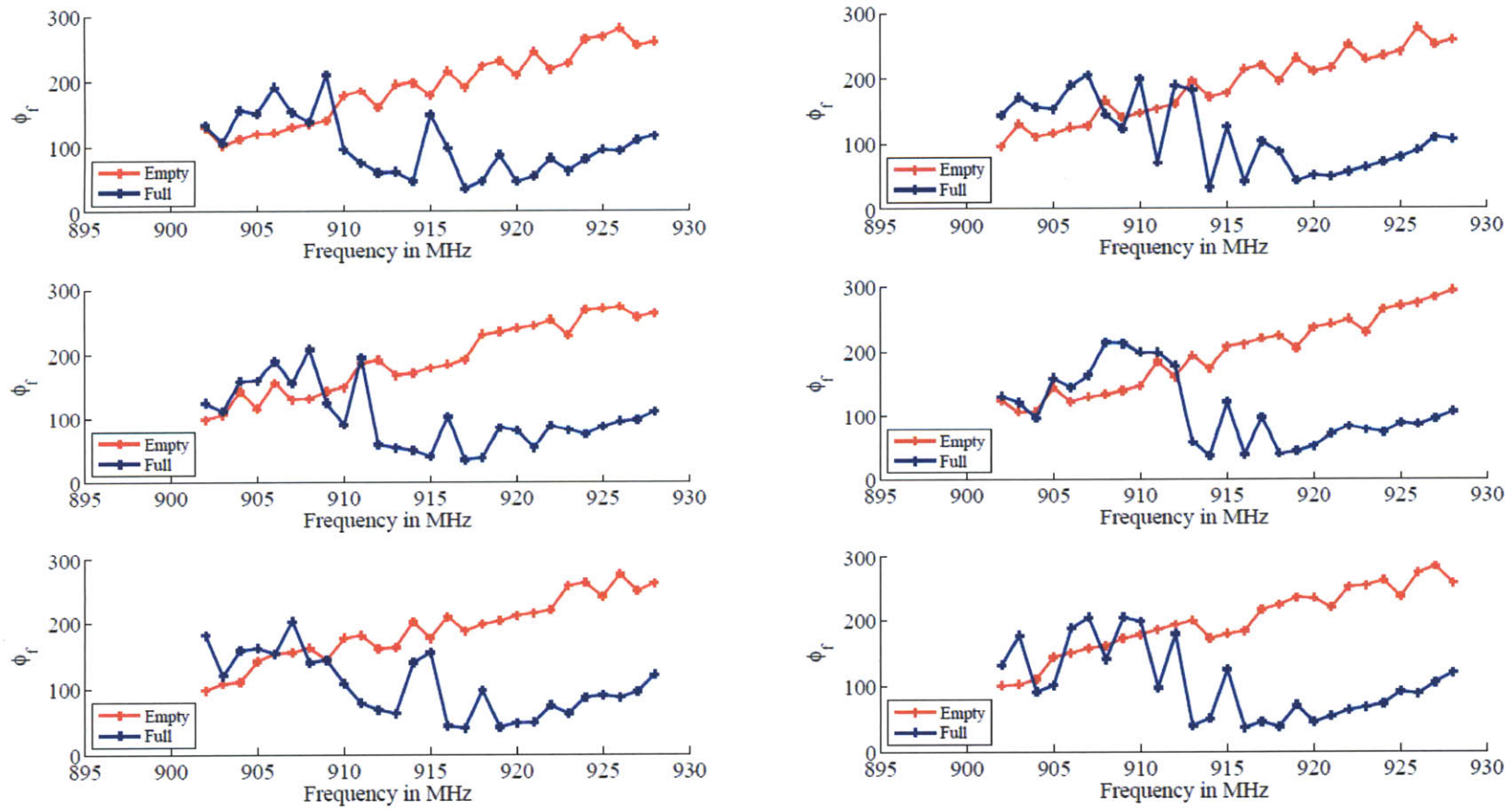

Figure 5-8: Variation of ϕ_f for the PM TABS antenna for the full and empty states of the beverage glass: Γ_1 is contaminated with up to 20% noise, ϕ_{off} is assumed known precisely and the reader-tag separation is 0.6 m under free space conditions

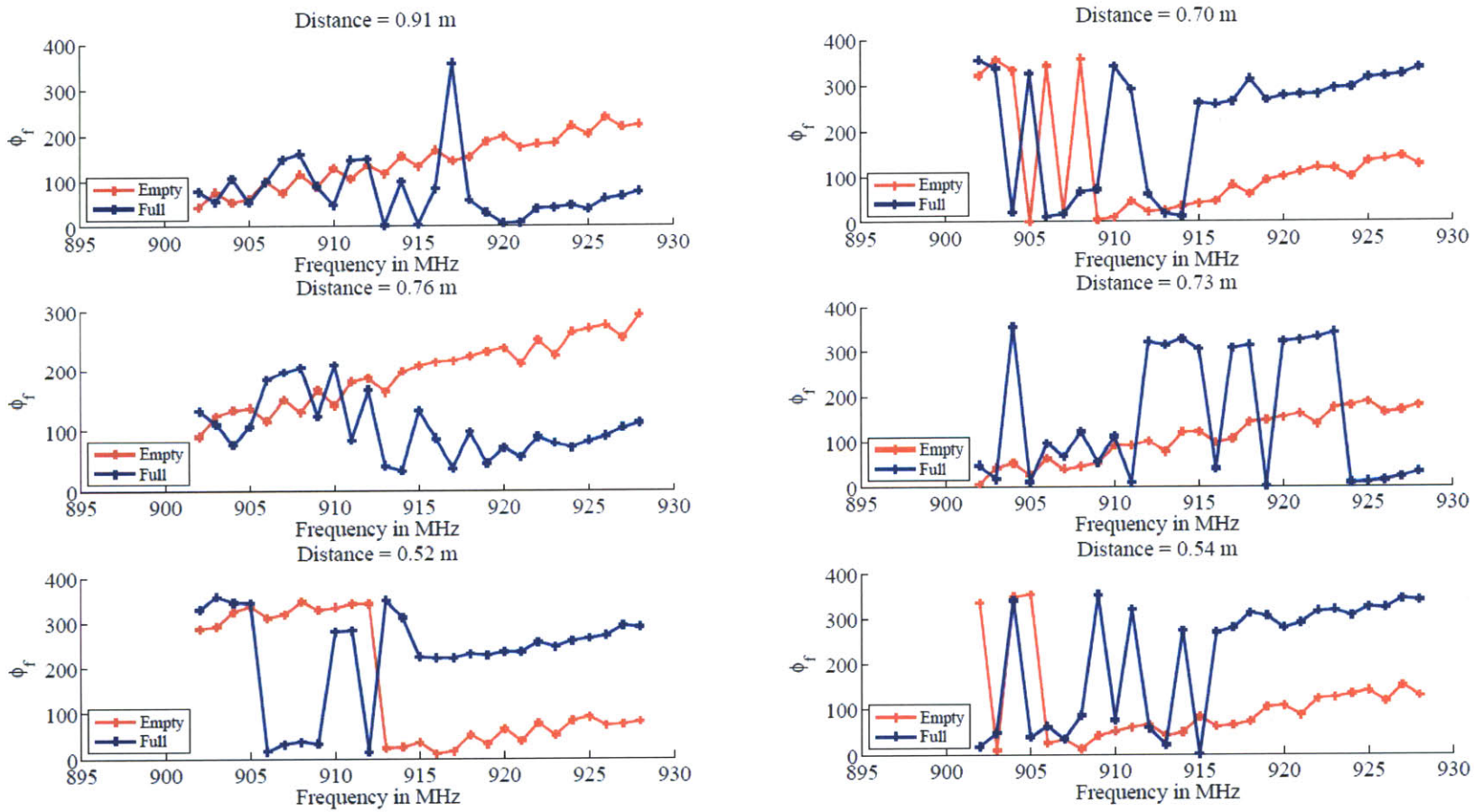

Figure 5-9: Variation of ϕ_f for the PM TABS antenna for the full and empty states of the beverage glass: Γ_1 is contaminated with up to 20% noise, ϕ_{off} is assumed known precisely and the reader-tag separation is randomly selected between 0.5 and 1 m under free space conditions

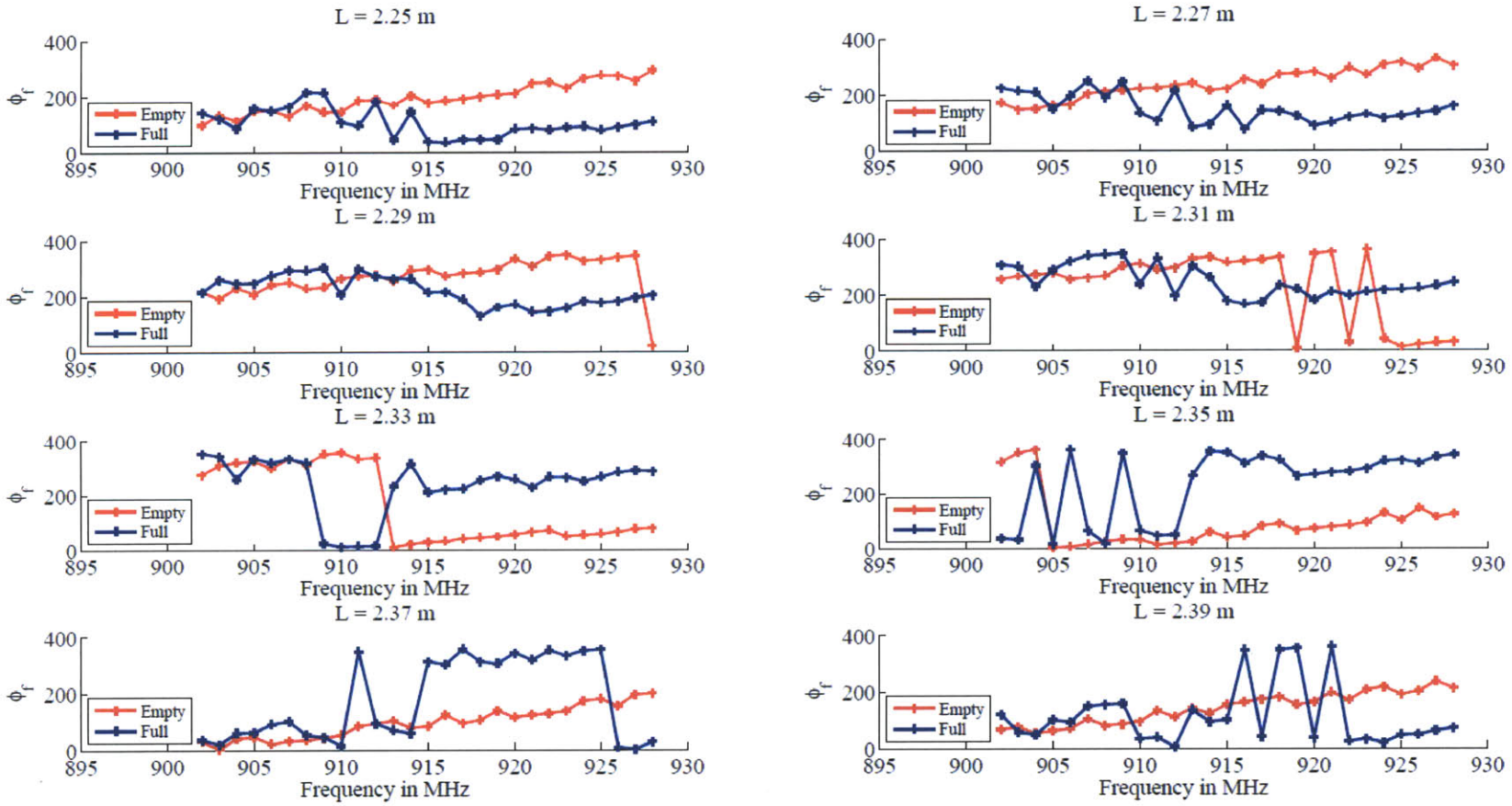

Figure 5-10: Variation of ϕ_f for the PM TABS antenna for the full and empty states of the beverage glass: Γ_1 is contaminated with up to 20% noise, ϕ_{off} depends on L varying from 2.25 - 2.39 m and the reader-tag separation is 0.6 m under free space conditions

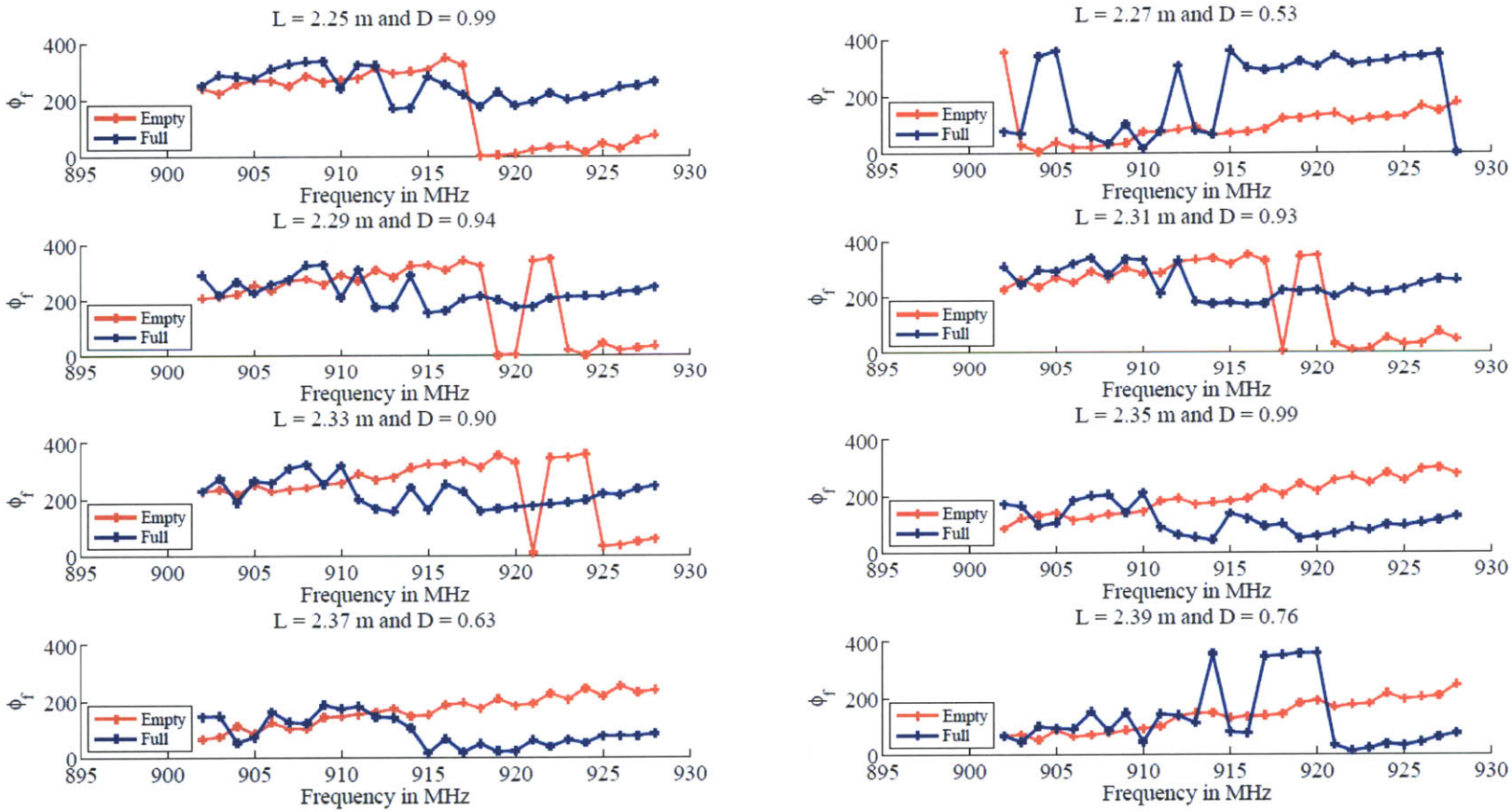

Figure 5-11: Variation of ϕ_f for the PM TABS antenna for the full and empty states of the beverage glass: Γ_1 is contaminated with up to 20% noise, ϕ_{off} depends on L varying from 2.25 - 2.39 m and the reader-tag separation varies randomly between 0.5 and 1 m under free space conditions

5.4.2 Estimation of ϕ_f in Laboratory Conditions

Free space represents a highly idealized condition for wave propagation. In reality, the geometrical arrangement of reflectors such as the walls, floor and ceiling change ϕ_{prop}. In [75], Nikitin *et.al* attempt to model environmental reflections by introducing a parameter, H, that I summarize below:

$$H = 1 + \sum_{i=1}^{n} G^i_{reader} G^i_{tag} R_i \frac{d}{d_i} e^{-jk(d-d_i)} \tag{5.10}$$

Here G^i_{reader} and G^i_{tag} are the angle dependent reader and tag gains, R_i is the reflection coefficient off the i^{th} reflector, d is the length of the direct path between the reader and the tag, d_i is the length of the i^{th} reflected path, and k is the wavenumber that depends on the reader operating frequency.

Fig 5-12(a) and Fig 5-12(b) illustrate the top and front views of the laboratory environment. Our experimental setup ensures that there is direct line of sight between the reader antenna and the tag. I assume that the only significant sources of reflection are the walls, the ceiling and the floor of the room. The reflection paths are shown in the figures.

For the purposes of computing the parameter H, I assume a single ray reflection off the walls, floor and ceiling. Furthermore, the reflecting surfaces are assumed to be perfect electrical conductors - i.e the parameter R_i in Eq 5.10 is set to be -1 for all reflections. I assume G^i_{tag} is constant at 1.6 dBi and the angle dependent G^i_{reader} is determined from the reader antenna manufacturing specification sheet [81]. After computing the parameter H, Eq 5.9 can then be modified as

$$\phi_f = mod(2kd - 2arg(H) + 2kL + \phi_{BS}(f), 360) \tag{5.11}$$

Table 5.1 summarizes the single reflection path lengths considered in Eq 5.10 and described in Fig 5-12. I make use of these path lengths while computing the parameter, H, in Eq 5.11: Fig 5-13 shows the phase response of the two states

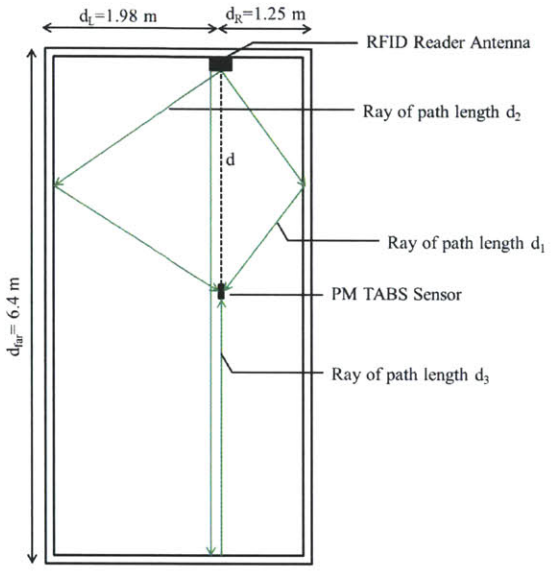

(a) Plan view of the laboratory environment where the PM TABS sensor was tested: d_1,d_2 and d_3 are the single reflections off the walls

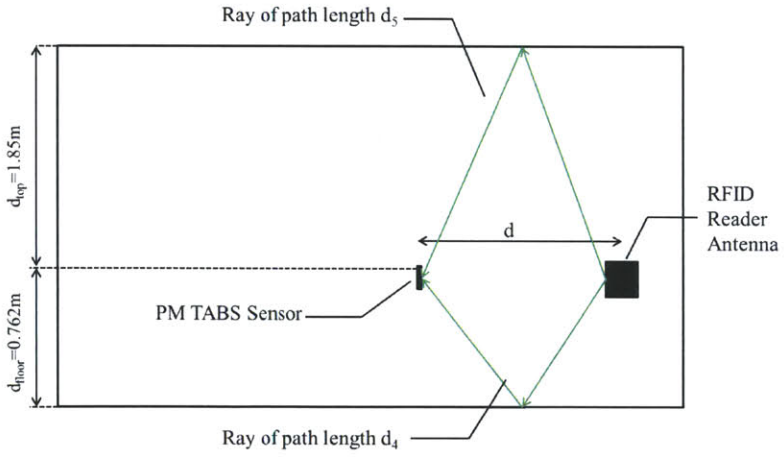

(b) Elevation view of the laboratory environment where the PM TABS sensor was tested: d_4 and d_5 are the reflections off the floor and the ceiling

Figure 5-12: Dimensions of the laboratory environment where the PM tests were conducted

Table 5.1: Path lengths due to wave reflections off the reflecting surfaces in the laboratory environment

Path Length)	**Mathematical Expression**	**Comments**
d	–	Direct path
d_1	$2\sqrt{(\frac{d}{2})^2 + d_r}$	Wall reflection
d_2	$2\sqrt{(\frac{d}{2})^2 + d_l}$	Wall reflection
d_3	$2d_{far} - d$	Wall reflection
d_4	$2\sqrt{(\frac{d}{2})^2 + d_{floor}}$	Floor reflection
d_5	$2\sqrt{(\frac{d}{2})^2 + d_{top}}$	Ceiling reflection

considering multipath effects in addition to the uncertainty in Γ_1, ϕ_{off} and for a random reader-tag separation of between 0.5 and 1 m. As we can see from the figures, the phase changes in $\phi_{BS}(f)$ are overwhelmed by the sensitivity of ϕ_f to the uncertainties in these parameters making PM TABS difficult to implement in practice.

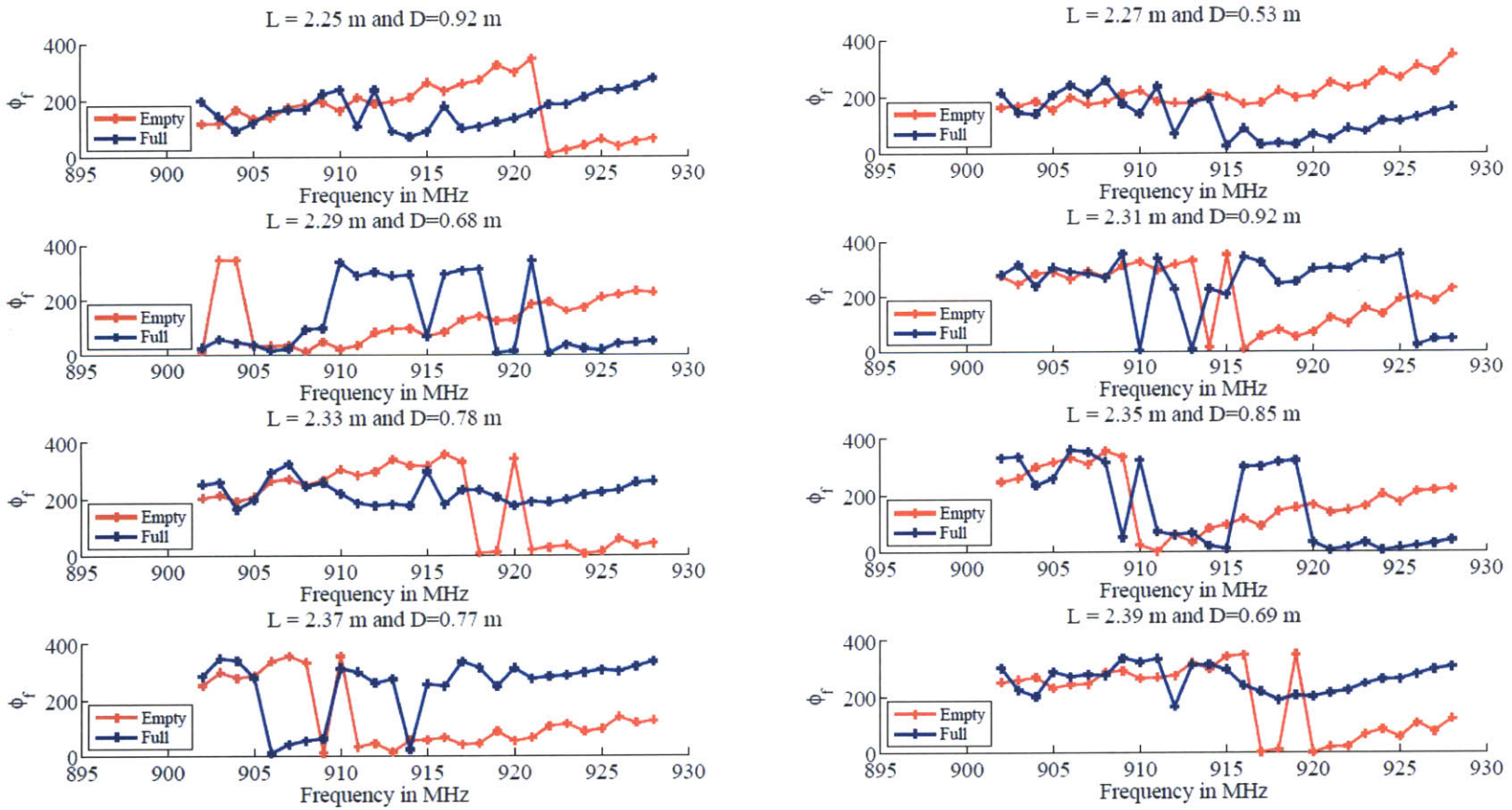

Figure 5-13: Variation of ϕ_f for the PM TABS antenna for the full and empty states of the beverage glass: Γ_1 is contaminated with up to 20% noise, ϕ_{off} depends on L varying from 2.25 - 2.39 m and the reader-tag separation is randomly selected between 0.5 and 1 m in the presence of simulated multi-path conditions

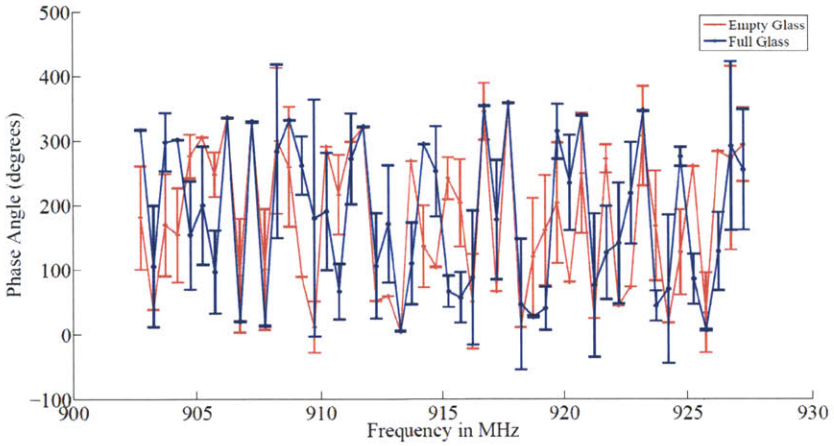

Figure 5-14: Variation of ϕ_f for the full and empty states of the beverage glass: phase measurements are conducted using the Impinj Revolution RFID reader in laboratory conditions for a reader-tag separation of d=0.75 m

5.4.3 Experimental Verification of PM TABS

I make use of the Impinj Revolution RFID reader [68] to extract ϕ_f information from the PM TABS sensor when it is deployed on the beverage glass in the completely full and empty states. The reader-tag separation, d, is chosen to be 0.75 m as seen in Fig 5-12(a). Each test is conducted at a reader transmitted power of 36 dBm EIRP and at least 30 phase data points are gathered per frequency channel. Fig 5-14 illustrates the phase response for the two states of the PM TABS sensor. The response of both states has no discernible trend. Clearly, the sensitivity of ϕ_f to ϕ_{prop} and ϕ_{off} dominates the sensitivity to $\phi_{BS}(f)$. I further verify the sensitivity of ϕ_f to ϕ_{prop} by changing the distance, d, in Fig 5-12(b) from 0.75 to 0.83 m in steps of 20 mm corresponding to a position change (Δd) of approximately 0 to $\frac{\lambda}{4}$ in steps of $\frac{\lambda}{16}$. Thus, I consider a set of reader-tag separations given by:

$$S = [0.75, 0.77, 0.79, 0.81, 0.83] \tag{5.12}$$

I modify Eq 5.11 to predict the expected change in ϕ_f. For a specific reader operating frequency:

$$\delta\phi_f(d_i) = mod([2k[d_i - d] - 2[arg(H(d_i)) - arg(H(d))], 360) \tag{5.13}$$

Here $d_i \in S$ and d corresponds to 0.75 m. I assume that over such a small distance, the environment should not affect measurements significantly and there should be good agreement between the $\delta\phi_f(d_i)$ computed experimentally and from Eq 5.13. Note that Eq 5.13 also implicitly assumes that ϕ_{off} and $\phi_{BS}(f)$ do not vary significantly over the small incremental distances in S.

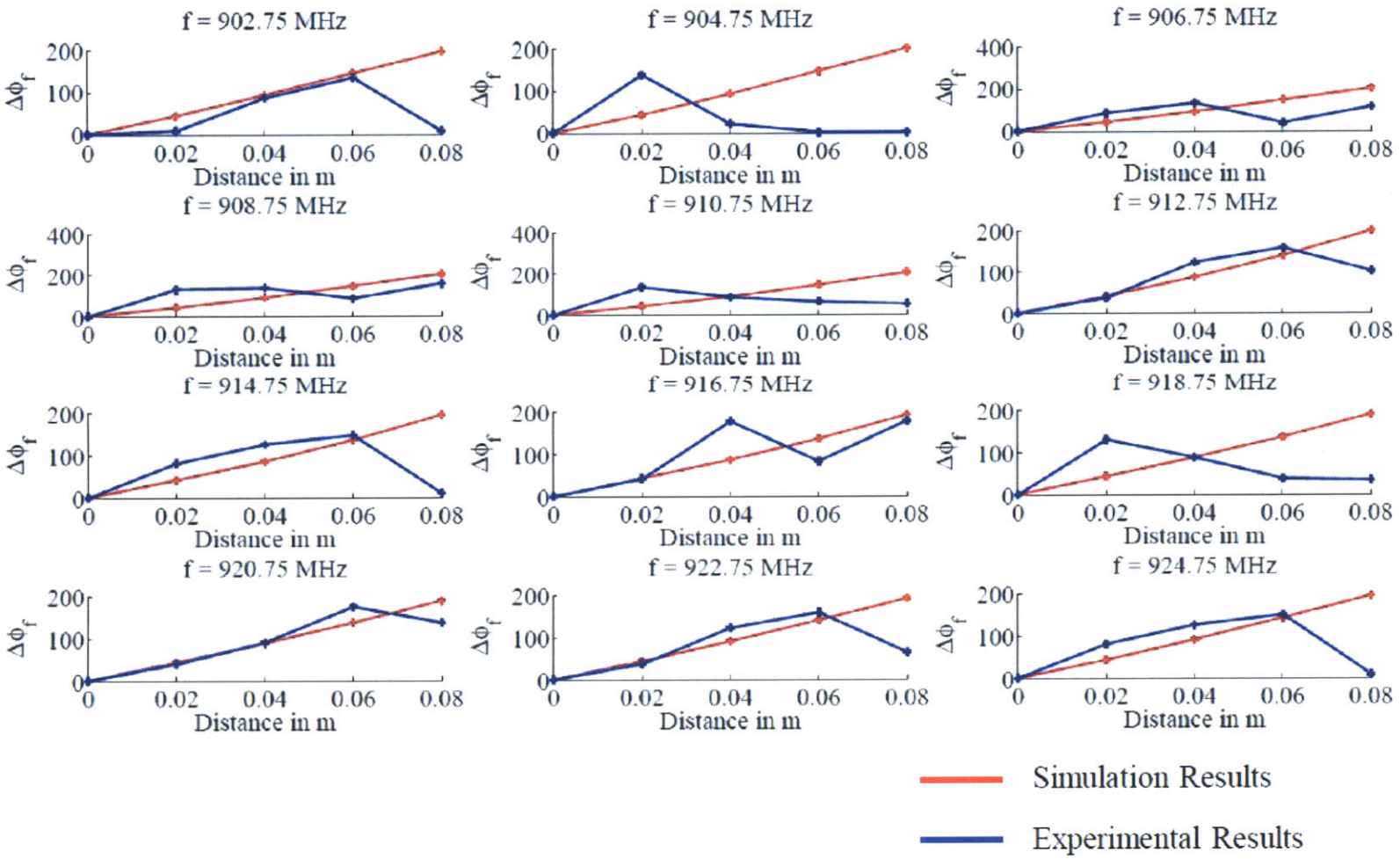

Figure 5-15: Variation of ϕ_f when the tag is shifted from its position of d=0.75 m in front of the reader antenna from d-$d + \frac{\lambda}{4}$ in steps of $\frac{\lambda}{16}$ at different reader operating frequencies: phase measurements are conducted using the Impinj Revolution RFID reader in laboratory conditions

As observed from the figure, there is a wide variation between the modeled and experimentally obtained values. This could be due to several possible reasons, which are enumerated below:

- The simple single-reflection multipath model, proposed in Section 5.4.2, which ignores the effect of furniture and other reflectors in the environment is insufficient to model ϕ_{prop}.
- The assumption that η in Eq 5.6 is negligible may not hold for the Impinj RFID reader used in our experiments [68]. In general, it is necessary to quantify the effect of η on ϕ_f for popular commercial RFID readers that would be used to interrogate the PM TABS sensors.
- The modeled variation of 10-20% in Γ_1 that simulates uncertainties due to tag manufacturing variability and due to approximations in RFID tag IC impedance may not adequately represent reality. There is a need to rigorously quantify the expected variation in Γ_1 due to fabrication. It is also necessary to quantify the effect of carrier frequency and input power on the tag IC impedance.

I do not address these issues any further in this thesis but present them as good opportunities for further investigation that will help better determine the scope of this sensing methodology.

Chapter 6

Discussion

In this thesis, I have introduced the concept of *RFID tag antenna-based sensing (TABS)* and have examined how RFID tag-sensors could be used to enable pervasive sensing in several applications where the monitoring needs cannot be met by today's wireless sensors. There is a four-fold motivation for using RFID to address this sensing requirement: First, the RFID infrastructure is a mature, standardized and reliable wireless communication technology. Second, there is a well-established infrastructure to mass produce low-cost RFID tag-sensors. Third, RFID has a proven track record for pervasive deployment for object identification in the supply chain and apparel industry. Finally, the RFID tag-sensors can be integrated into RFID-enabled business processes at trivial additional setup cost.

My thesis has made two main contributions. First, I have examined how three reader-tag signal communication properties can be used to encode sensing information. Second, I have introduced the the concept of low-cost, non-electric memory to record critical threshold crossovers in a sensed parameter that may occur even when the passive tag-sensor is unpowered. I have demonstrated how this can be done without compromising on sensor cost. I have framed my contributions by designing illustrative sensor prototypes in three application areas.

In this chapter, I summarize the thesis contributions, compare and contrast the three classes of TABS and motivate additional signature applications for non-electric memory. I also discuss areas in which further contributions can be made to this

field. Finally, I propose two preliminary TABS design ideas for extensions to other application scenarios.

6.1 Sensing using Tag and Reader Signal Parameters of Passive UHF RFID Tags

In the process of decoding EPC ID information, RFID readers also log three fundamental communication signal parameters — tag signal power, operating frequency and tag backscatter phase. I have demonstrated how each of these signal parameters could be used to encode sensing information and proposed the following classes of TABS:

- *Amplitude Modifying* (AM) TABS use reader transmitted power and tag backscatter power for sensing. I have demonstrated proof of concept using a displacement sensor and have showed that both power metrics could be reliably used to sense structural displacement. I have examined the sources of uncertainty in the measurements and concluded that backscatter power-based AM TABS are better suited for applications that require quick state estimates while threshold transmitted power-based AM TABS enable applications in which better sensor precision is desired.

- *Frequency Modifying* (FM) TABS use shifts in RFID tag optimal operating frequency for sensing. I have extended prior art in antenna theory and presented the design methodology for an RFID tag antenna that shifts its optimal operating frequency whenever there is a change in its boundary conditions. Changes in a sensed parameter can be related to a controlled change in the boundary condition of an RFID tag — and hence a change in its optimal operating frequency. I demonstrate how this frequency shift can be confined to the 902-928 MHz band for UHF RFID operations in the Americas. I have illustrated proof of concept by implementing a temperature threshold sensor and a fluid level sensor. The FM TABS strategy has good read range performance, lower cost,

smaller tag sensor size and is reasonably robust to differences in environmental conditions. However, sensitivity to variations in the tag manufacturing process and the slow interrogation speed — associated with determining the threshold transmitted power level and the implicit frequency sweep at each power level — adversely impacts sensor performance and applicability.

- I have proposed a class of *Phase Modifying* (PM) TABS that uses RFID tag backscatter phase for sensing and the design of a PM TABS fluid level sensor. Using numerical simulation and preliminary experimental results, I have demonstrated that the sensitivity of RF phase to extraneous factors — the operating environment, variability in antenna-IC impedance matching, and phase noise in reader electronics — made the practical implementation of PM TABS challenging. I have proposed three open questions that could better quantify the effect of these extraneous factors on RF phase and help determine the scope of PM TABS.

6.2 Implementation of Non-Electric Memory in RFID TABS to Record Critical Threshold Crossovers

The TABS sensors discussed in this thesis were based on passive UHF RFID tags and thus have a limited read range of a few meters. Where continuous monitoring with a dedicated reader is not possible, it may be necessary to conduct periodic monitoring using a mobile reader. There may be instances where critical thresholds in the sensed parameter may be crossed when the sensor is unpowered by the reader. Recording these impulse events without compromising on the cost of the TABS node was a design challenge.

I have introduced the concept of *non-electric memory* to detect and record the crossing of a critical threshold in the parameter of interest that might occur even when the tag is unpowered. This can be achieved by triggering a controlled permanent change in the geometry or boundary conditions of the RFID tag whenever

a critical threshold in the sensed parameter is crossed. I have demonstrated how non-electric memory can be implemented in a low-cost manner via the evolutionary design of a temperature threshold sensor. The sensor designs used fluid phase changes and shape memory polymer actuation to make permanent changes to the boundary condition of an RFID tag without adding significantly to sensor cost. While the non-electric memory concept can unambiguously detect *if* a threshold was crossed, it cannot provide time history information as to *when* the crossover occurred — a tradeoff between cost and functionality. Therefore, non-electric memory lends itself for those applications which do not require instantaneous alarm triggering but where it is sufficient to detect the critical threshold crossover at the subsequent reader interrogation cycle.

6.3 A Comparison of AM, FM and PM TABS

I summarize the advantages and shortcomings of the three classes of TABS. I then compare and contrast the TABS classes along several dimensions that impact their practical applicability.

AM TABS using Tag Backscatter

AM TABS using tag backscatter power have two main advantages. First, for any arbitrary reader transmitted power and given reader-tag separation, changes in a physical parameter of interest can be inferred simply by observing changes in sensor-tag backscatter power. Thus, this approach has the fastest state detection speed, nearly instantaneous, as long as the sensor is within range of the reader. Second, the technique can also be reliably implemented using commercial RFID tags [27] [26].

However, there are several sources of uncertainty in backscatter power measurements:

- Multipath fading affects tag backscatter measurements in the forward and reverse power transmission links.

- FCC mandated frequency hopping introduces additional uncertainty in the chip and antenna impedance since both are functions of frequency.

- Chip impedance is also a function of received input power which varies depending upon the reader-tag separation and reader transmitted power.

All these sources jointly contribute to backscatter power measurement uncertainty. Still backscatter AM TABS are well suited for simple yes/no type of event detection or coarse estimates in the parameter of interest. For instance, I successfully used backscatter AM TABS for temperature threshold sensing [30] [29] and to detect the presence or absence of fluid in a glass [56]. If the reader operating frequency was fixed, backscatter AM TABS could also be used to detect different beam displacement levels over a dynamic range of 17.5 mm [26].

In addition, backscatter power varies depending on the distance separation between the reader and the tag and measurements need to be made relative to a reference tag which is at a constant separation from the sensor tag. This in turn increases the sensor size and cost.

AM TABS using Threshold Transmitted Power

AM TABS using threshold power have two key advantages as well. First, they are prone to less measurement uncertainty because they are subject to multipath fading only in the forward power link and because the chip impedance is measured at a constant input power equal to the chip sensitivity. Therefore these sensors lend themselves well to applications that require better precision. Second, as with AM TABS based on backscatter power, this sensing strategy can be implemented with commercial RFID tags as seen from the case example of the displacement sensor in Chapter 2.

However, there is a time overhead associated with finding the threshold transmitted power. Most RFID readers allow the transmitted power to be set between some lower and upper bound. For instance, the Impinj reader used in our experiments has $N = 70$ discrete power levels between 15 dBm and 32.5 dBm [68]. Sweeping these

power levels searching for the threshold power takes a finite amount of time. Furthermore, as seen with AM TABS based on backscatter power, the absolute measurement of threshold power is dependent on the reader-tag separation and therefore measurements need to be made relative to a reference tag which is at a constant separation from the tag sensor. This increases the sensor cost and size.

FM TABS

Frequency domain-based measurements have the advantage of being relatively independent of reader-tag separation and changes in environment. Thus measurements relative to a reference tag are no longer necessary. This reduces sensor cost and size.

Akin to any research prototype, the FM TABS sensors developed in this thesis, over multiple iterations were all one-off production in small volumes. An observed 5-10 MHz variation in the optimal operating frequency band was observed during prototype development. The manufacturing challenges associated with taking these sensors to production scale is an open question which I do not address in this thesis.

In addition, smaller variations of 3-5 MHz are observed due to changes in reader-tag separation or environment. FM TABS are thus well suited for American UHF RFID frequency of operations where the 26 MHz bandwidth allows for sufficient separation between states to account for these sources of uncertainty.

Furthermore, in terms of speed of state inference, the FM TABS state detection technique is a two step process:

- For a given reader transmitted power setting, the reader sweeps the 26 MHz band looking for the channels on which the tag responds. This takes a finite amount of time.

- Of N possible transmitted power settings, the frequency response at the threshold transmitted power is considered for state detection. This involves an additional time overhead associated with sweeping N discrete power levels to determine the threshold transmitted power.

PM TABS

A PM TABS design is theoretically possible and, under ideal free-space conditions, state inferences are possible even without a priori knowledge of the reader-tag separation. For instance, in the case of the fluid level sensor design proposed in Chapter 5, the full vs. empty state of the glass can be inferred simply based on the linear vs. non-linear shape of the phase profile curves (*c.f* Fig 5-7) across different reader-tag separations. Thus, just like FM TABS, the PM TABS approach does not require measurements relative to a reference tag.

Furthermore, under ideal conditions, only one complete frequency sweep at any given transmitted power setting is sufficient to estimate the phase dependence on frequency. There is a time overhead associated with a single frequency sweep, however it is faster than the 2 step FM TABS state detection procedure. Thus phase-based sensing provides a compromise between the smaller size of FM TABS and the speed of AM TABS based on tag backscatter power.

However, PM TABS are extremely sensitive to the uncertainty associated with the following three extraneous factors that makes their practical implementation challenging:

- Real world propagation environments.
- Noise in the reader electronics.
- Tag antenna and RFID tag IC impedance matching.

In Chapter 5, I propose three open questions that if addressed would better identify the effect of these parameters on PM TABS performance. This would help better identify the scope of PM TABS application.

Table 6.1 presents a summary comparison of the the three classes of TABS along several different dimensions.

Table 6.1: Comparison of AM, FM and PM TABS

Dimension	**Backscatter AM TABS**	**Threshold AM TABS**	**FM TABS**	**PM TABS**
State Detection Speed	Fast - state inferred instantly	Medium - time overhead involved in sweeping N discrete power levels	Slow - involves sweeping N discrete power levels and a frequency sweep at each power level	Medium - inference takes one frequency sweep
Antenna Design	Can be implemented with commercial tags; use custom design for optimized performance	Can be implemented with commercial tags; use custom design for optimized performance	Requires custom narrow band design	Requires custom narrow band design
Practical Applicability	Coarse Precision: Ideal for applications needing fast inference	Finer Precision: Ideal for applications needing better precision	Coarse Precision: Ideal for binary state inferences exploiting two ends of the 26 MHz band	Challenging Implementation - highly sensitive to environment, reader and tag IC electronics and manufacturing variability
Area of operations	Worldwide	Worldwide	Americas	Americas
Sensor Form Factor	Large - requires reference tag	Large - requires reference tag	Small - no reference tag needed	Small - no reference tag needed

6.4 Other Potential Applications for Non-Electric Memory

The non-electric memory concept proposed in this thesis is a reliable way of recording that a critical threshold in the sensed parameter was exceeded. As observed in Chapter 3 and Chapter 4, for the temperature threshold sensor, a temperature threshold crossover triggers an abrupt change in the boundary conditions of an RFID tag. While this technique answers the question of *if* a threshold crossover occurred, it cannot predict *when* it occurred. Therefore a threshold TABS sensor enables those pervasive sensing applications which do not require immediate, real-time reporting of a threshold crossover, and where we can afford to wait for the next reader interrogation cycle to infer a threshold crossover. I attempt to highlight three scenarios which illustrate how the concept of non-electric memory can be used:

I first consider temperature threshold sensing in the cold chain using the design of the temperature threshold sensor proposed in Chapter 3 and Chapter 4. It may not be possible to monitor goods continually with a dedicated RFID reader during transit operations. However, products passing through RFID-enabled cold chains are inventoried at periodic nodes in the supply chain network to establish chain of custody. For example, products could be inventoried every time they pass through a distribution center. Therefore, it is possible to infer product health at least at every distribution center. Consider a batch of products passing from distribution center A to B. If an alarm is triggered at distribution center B, then this batch of produce can be discarded at B itself and transportation costs normally incurred in transporting these goods further down the supply chain can be avoided. Thus non-electric memory based threshold sensors can localize threshold crossovers to the nodes of the supply chain network. However, real time alarm updates — or recording a time history of data — cannot be accommodated by this technique unless a continuous reader monitoring strategy can be employed.

Strain monitoring in inhomogeneous materials like concrete would benefit from pervasive TABS-based strain threshold sensors that are triggered whenever design

strain levels are exceeded (see Section 6.5.3 for a prospective design concept). It would be ideal to trigger an alarm at the instant the threshold is exceeded — but this necessitates continuous reader monitoring of the structure which may not be possible. However, structural conditions remain fairly static over time and the time interval between the design strain threshold violation in a load bearing zone and systemic structural collapse is not instantaneous. Therefore even if the design strain crossover is conveyed to readers mounted on maintenance vans passing by once every day, it should be sufficient for health monitoring and remediation purposes.

We can conceive TABS sensors that are able to detect wood quality and termite damage in buildings (see Section 6.5.3 for a suggested design). Such threshold sensors can be embedded in the dry walls or sub floors of houses during construction and can be used to non-invasively convey termite ingress information to pest control inspectors during periodic house inspections using RFID readers. As long as the intervals between two monitoring cycles is not long enough for critical structural damage, appropriate remedial action can be taken while it is still cost effective to do so. While this sensor may not preclude detailed investigation into the event of termite ingress, it can help eliminate false negatives.

6.5 Scope for Future Work in Tag Antenna-Based Sensing

There are three distinct areas in which further contributions can be made to this field. The first highlights open research questions, the second outlines engineering implementation issues that merit consideration and the third motivates TABS development in two additional areas.

- Improvements in Sensing Fundamentals
- Techniques that facilitate Pervasive Sensor Deployment
- Expanding the Application Space

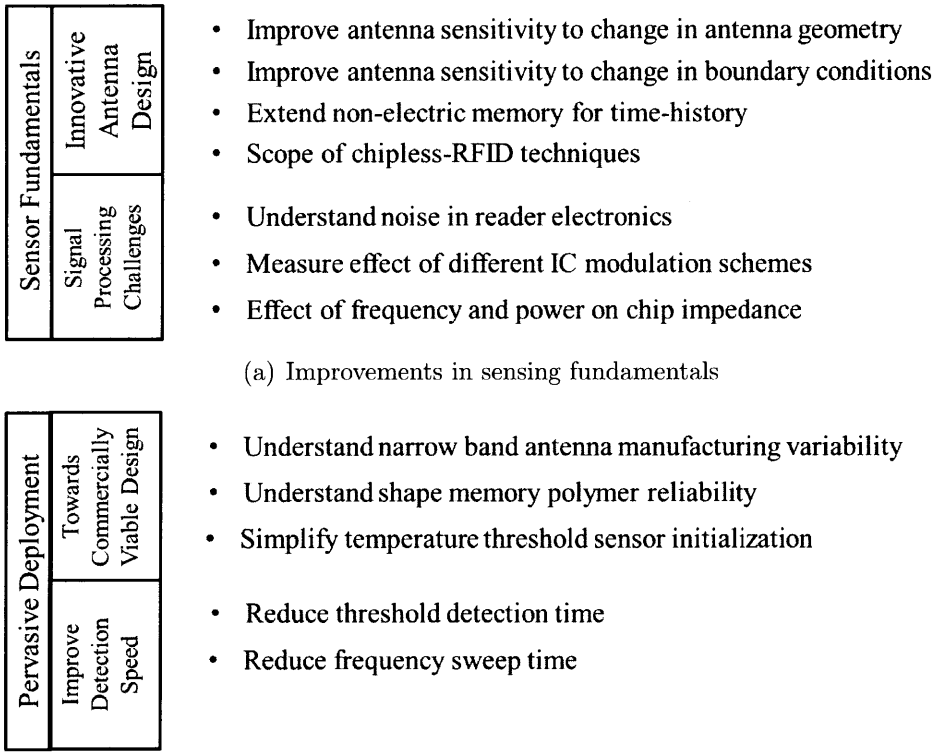

(a) Improvements in sensing fundamentals

(b) Techniques that facilitate pervasive deployment

Figure 6-1: Scope for future work in improving sensor design and facilitating commercial deployment

6.5.1 Improvements in Sensing Fundamentals

I define *Sensing Fundamentals* to include those open questions that would impact sensor precision and accuracy, robustness and efficiency (c.f Fig 6-1(a)). There are two primary areas in which advancements can be made:

Opportunities for Innovative Tag-Sensor Design

- **Improve tag sensitivity to changes in boundary condition**: Understanding the effect of antenna geometry — square, dipole, spiral or other shapes — on the sensitivity to changes in boundary conditions would help enhance the precision and dynamic range of TABS sensors. For example, in the case of the displacement sensor discussed in Chapter 2, it would be useful to know if the Impinj Banjo provides the best dynamic range or if there are other antenna shapes that would be better suited. An optimized antenna could then be designed to improve the dynamic range of measurements to more than 20 mm or improve the least count of the sensor to less than 2.5 mm.

- **Improve tag sensitivity to antenna constructs**: Understanding how tag sensitivity is influenced by changes in the antenna geometrical constructs themselves opens up the possibility for innovative sensing. For instance, antenna constructs such as a T-match [66], capacitive end loading [9] or meander lines [82] help control antenna size and impedance, but the opportunity to exploit these constructs for sensing presents itself. As an example, the meander line elements of a dipole antenna could be fabricated using a material, the resistivity of which is highly sensitive to strain. Section 6.5.3 introduces the concept for such a design. This would allow for the development of a planar TABS strain sensor since there would be no need to map the sensed parameter to a change in the background dielectric of the tag's antenna.

- **Improve versatility of non-electric memory**: The non-electric memory approach outlined in Chapter 3 detects whether or not a critical threshold in the parameter was exceeded, but not the question of when. There is scope for

multidisciplinary research in materials engineering and antenna design to design threshold sensors that preserve a time history of threshold crossovers. For example, recent work by Hasan *et.al* describe a polymer that records a time-temperature profile [65]. This polymer could be used as a dielectric boundary to an RFID tag or as part of the antenna's electrical circuit to build a TABS temperature-threshold sensor that records a time-temperature history of temperature threshold crossovers.

- **Chipless RFID based sensing techniques**: RFID tags terminating in printable microwave structures are gaining popularity in the literature [83]. These chipless RFID tags forgo the cumbersome manufacturing step of attaching the RFID IC to the antenna and can be produced at lower cost with an ink jet printer. Furthermore, with low-cost, printable inks, these tags can be manufactured at prices competitive with the bar code. The opportunity exists for integrating low-cost sensing with chipless RFID. For example, chipless RFID TABS techniques could be considered. Alternatively, the terminal microwave structure could be designed so as to be sensitive to a physical parameter of interest. Finally, a hybrid technique, where the chipless tag's antenna is affected by one parameter and the microwave structure is affected by another, could be designed for multi-modal chipless RFID-based sensing.

Towards better Signal Processing

- **Understand reader phase noise**: In Chapter 5, I assumed that the phase noise in the RFID reader electronics can be neglected. It is necessary to demonstrate whether or not this assumption is justified for commercial RFID readers such as the Impinj Revolution used in our experiments [68]. If not, it is necessary to examine if the phase noise's dependence on frequency can be determined so as to minimize its effect on the measured RF phase angle.

- **Effect of frequency and input power on chip impedance**: The RFID tag IC impedance varies with input power and reader operating frequency and there

have been several studies to quantify this for popular RFID tag ICs [84], [55]. However, to the best of my knowledge such a study has not been conducted on the Alien Higgs 3 IC used in most of my experiments [61]. For simplicity, in this thesis I assumed the tag IC impedance to be a fixed average value across all frequencies. This approximation affects frequency and reader-tag separation dependent impedance matching, especially the narrow band antenna designs considered for FM and PM TABS. It is necessary to quantify the effect these variations have on RF phase angle in the case of PM TABS and tag optimal operating frequency in the case of FM TABS.

- **Effect of different IC modulation schemes**: Amplitude Shift Keying is the most popular IC backscatter scheme implemented in RFID tag IC design. However other schemes such as Phase Shift Keying and other hybrids do exist [9] [44]. Each scheme features a trade-off between the forward link read range and the power scattered from the RFID tag antenna [9]. An interesting follow up question is to understand the effect of other possible IC modulation schemes on the performance of AM, FM and PM TABS.

6.5.2 Techniques that Facilitate Pervasive Sensor Deployment

This area of improvement highlights engineering implementation issues that would improve the speed of sensor interrogation and facilitate the large-scale commercial adoption of RFID TABS (c.f Fig 6-1(b)). There are two subcategories in which practical improvements can be made:

Towards Commercial Deployment

- **Understand manufacturing variability for FM TABS design**: As seen in Chapter 4, the narrow band RFID tag prototypes produced in small volumes were highly susceptible to performance variations. For instance, five of the six temperature threshold sensor prototypes demonstrated a 5-10 MHz variation in

the design optimal operating frequency band, while the sixth prototype showed a drastically different performance. The manufacturing challenges associated with taking these sensors to production scale is a potential area of investigation.

- **Implementation issues for the temperature threshold sensor**: Addressing the following would facilitate the commercial adoption of the SMP temperature threshold sensor:
  - *Understand reliability of SMP actuation*: An important component to the temperature threshold sensor concept is the shape memory polymer. At production scale, variations in the SMP must also be studied and controlled.
  - *Improve temperature threshold sensor initialization*: There is a need for automating the process of arming the sensor, i.e removing the constraining force once the SMP has hardened. The design requirement is two fold — First, the constraining force must be reliably removed once the SMP has hardened. Second, the mechanism for removing the constraining force on the SMP should not add significantly to the cost or size of the sensor.

Towards Large-Scale Implementation

- **Reduce threshold detection time**: Threshold power determination requires a finite amount of time. Many RFID readers allow the transmitted power to be set at N discrete levels. For instance, the Impinj reader used in this thesis has $N = 70$ discrete power settings. Reducing the threshold detection time involves sweeping these discrete power levels efficiently. One possibility is to use search algorithms to speed up the detection process — for example, a binary search would reduce the sweep from an O(N) process to an O(log(N)) process. Another possibility is to parallelize the threshold sweep. For instance, most RFID readers have the option to connect multiple antennas — the Impinj Revolution, used in our experiments, supports up to 4 antennas [68]. Distributing the threshold power sweep across 4 antennas in parallel would reduce the time taken for an

AM TABS threshold sweep by a factor of four. These are just two examples that motivate the scope for reducing the threshold detection time overhead.

- **Reduce the time for a frequency sweep**: In addition to sweeping N power settings to determine a threshold, FM TABS require a frequency sweep at each power level. On commercial RFID readers, this is implicitly done via FCC mandated frequency hopping — the readers are mandated to randomly hop on 500 kHz channels in the 902-928 MHz range at least every 400 ms [9]. The Impinj reader used in this thesis frequency hops every 400 ms which increases the time taken for a frequency sweep. In geographical regions mandating frequency hopping, there is scope for using custom RFID software radios that reduce the interval between frequency hops. This would reduce the time taken for the frequency sweep and for the FM TABS sensor interrogation process.

6.5.3 Expanding the Application Space

While the thesis introduces the application of TABS to three application areas in which there is a need for pervasive sensing, conceptual designs for two additional areas are mentioned in this section. The list presented is not meant to be exhaustive but rather illustrative. The TABS paradigm can be applied to any application that calls for cheap, pervasive sensing and where an appropriate transduction mechanism can be designed to monitor the parameter of interest.

- *Termite Control*: TABS are aptly suited for early detection of termite damage in wooden construction. Termite damage typically starts within a wall [85] and at the sub-floor before the hardwood floor [86]. Thus signs of visible damage occur once the damage has progressed. TABS-based termite detection sensors can be pervasively deployed on the plaster-boards which make up the dry wall or on the plywood that makes up the sub-floor of a wooden structure. Termite damage localization can then be automated by bringing an RFID reader into the room and scanning for those tag EPCs that register a change in backscatter signal or shift in operating frequency.

Researchers such as Peng *et.al* have developed conductive paper [87] — a form of cellulose. It would be interesting to see if this paper would be consumed by termites and if it could be used in the design of a TABS termite detector. Fig 6-2(a) illustrates a potential design. As the termites consume the conductive cellulose, the sensor's electrical circuit changes (c.f Fig 6-2(b)) which manifests itself as a change in AM or FM response. Fig 6-2(c) illustrates the pervasive deployment of the sensor on the plaster boards while Fig 6-2(d) illustrates the position of the plaster boards in the dry wall when monitored by an RFID reader.

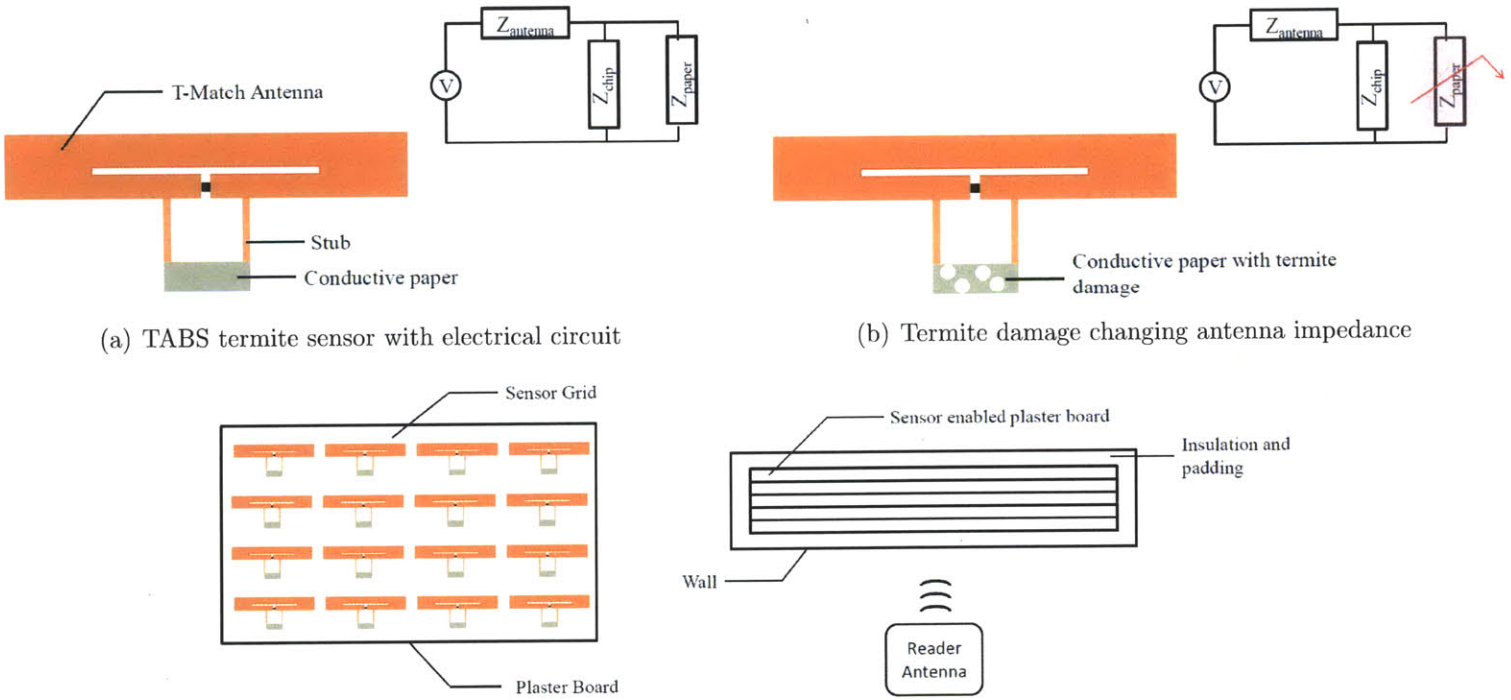

(a) TABS termite sensor with electrical circuit

(b) Termite damage changing antenna impedance

(c) TABS grid on plasterboard

(d) Sensor interrogation using reader antenna

Figure 6-2: Design and deployment of a TABS termite monitoring strategy

- *Strain Threshold Crossover Detection*: TABS find applications for monitoring crack development in structures. A good example of antenna-based strain sensing was proposed by Occhiuzzi *et.al* [88]. Their sensor design utilizes a meander line dipole antenna (MLA) where the spacing between the meander line elements changes with strain which manifests itself as a change in the tag backscatter power. The authors present the results of preliminary testing of the antenna and comment on its dynamic range and precision. The MLA is made of a copper alloy which has a yield point of 6% [88].

  Fig 6-3 illustrates a potential design of an antenna-based strain sensor that extends this concept to include non-electric memory. The antenna includes a bridge connection composed of a weaker, brittle material — for example, a type of carbon fiber that has a breaking strain of 3500 $\mu\epsilon$ [89] and a elastic modulus of 58.6 GPa. On being subjected to tensile force, this bridge connection will break off part of the antenna and this manifests itself as a change in the tag backscatter power or operating frequency. It would be interesting to see if this approach could be adapted to record impulse strain threshold crossovers in materials such as concrete which has a failure strain of 3500 $\mu\epsilon$.

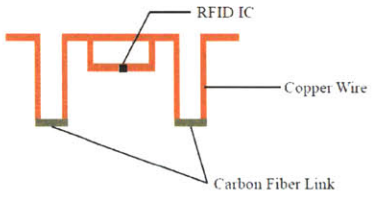

(a) TABS strain sensor design

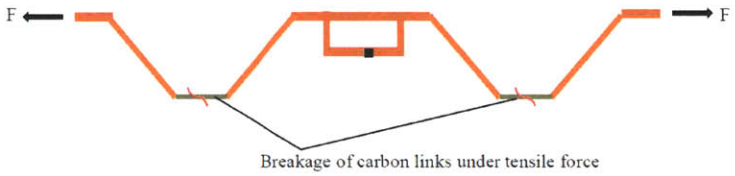

(b) Strain sensor working

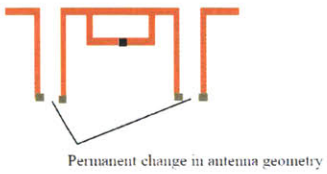

(c) Non-electric memory for strain sensing

Figure 6-3: Design and working concept of a TABS strain threshold sensor

Chapter 7

Conclusion

There are several applications that benefit from large-scale, highly integrated sensor deployment and most of today's wireless sensors are still too expensive to meet this need. I have considered the potential of using RFID tag-based sensors to enable pervasive sensing in these applications. This approach has the benefit of leveraging manufacturing practices for the mass production of low-cost RFID tag-sensors as well as the reliable, standardized RFID communication protocol. Furthermore, RFID has a proven track record of wide spread deployment for object identification in the supply chain and apparel industry and is thus well suited for pervasive sensing applications.

I have proposed the concept of *RFID Tag Antenna-Based Sensing (TABS)* and demonstrated how changes in the sensed parameter of interest can be encoded as changes to the electrical properties of an RFID tag's antenna. My thesis makes two contributions:

- I have proposed three classes of TABS. AM TABS relate changes in the sensed parameter to changes in RFID reader threshold power and tag backscatter power, FM TABS encode sensing information in a shift in the tag's optimal operating frequency while PM TABS relate sensed information to RFID tag backscatter phase. I have successfully implemented AM and FM TABS and highlighted three open questions that would better identify the scope of application for PM TABS. I have also drawn attention to the advantages and

shortcomings of each class of TABS.

- I have proposed the concept of low-cost non-electric memory and have demonstrated how permanent changes to the RFID tag geometry or boundary conditions could be effected once a critical threshold in the parameter of interest was crossed. Moreover, I have demonstrated how this technique could be implemented without adding significant cost to the sensor design. I have successfully implemented this technique by designing sensor prototypes and highlighted signature applications.

These contributions were conceptualized while considering low-cost sensor design techniques for the sensor prototypes considered in this thesis. Therefore the lessons learned while developing these sensors is a good way of illustrating the take away messages of this work.

Lessons learned from the Displacement Sensor

I proposed the class of *Amplitude Modifying (AM) TABS* using the displacement sensor as a case example and demonstrated how reader transmitted power and tag backscatter power could be used for sensing. The sensor design illustrated that a change in the sensed parameter of interest could be reliably detected by inducing a controlled change in the boundary condition of an RFID tag — in this case by using the relative motion between an RFID tag and a metal plate. It also illustrated that, with appropriate design, sensing functionality could be added to an RFID tag at very low cost. Furthermore, it showed that commercial off-the-shelf RFID tags could be used in the sensor design.

The displacement sensor design also gave me the opportunity to understand the sources of uncertainty and interrogation speed of amplitude-based measurements. I concluded that backscatter-power based AM TABS were best suited for applications demanding rapid response from the TABS sensor, however for situations requiring better precision threshold AM TABS were more appealing. The requirement of having an RFID tag at a fixed reference from a moving metal plate makes the commercial

deployment of the displacement sensor challenging. However, the successful implementation of AM TABS using this case example inspired the design of the temperature threshold sensor and fluid level sensor.

Lessons learned from the Temperature Threshold Sensor

I considered the application of TABS for temperature monitoring in the supply chain but was presented with two key challenges. First, like other passive sensors, TABS are limited to a read range of a few meters. Continuous monitoring with dedicated readers might not be possible during shipping operations and so impulse exposures to unacceptably high temperatures might be missed. There was a need to record the occurrence of such events without adding significant cost to the sensor design. Second, the form factor of the sensor needs to be small so as to enable deployment on packaging of diverse form factors.

To address the first challenge, I introduced the concept of low-cost *non-electric memory*. Exposure to unacceptably high thresholds in the sensed parameter of interest triggered a permanent change in the boundary condition of an RFID tag's antenna. I used the concept of non-electric memory to successfully implement an AM TABS temperature threshold sensor that made use of temperature-induced changes in the background dielectric of the RFID tag and the permanent actuation of a metal plate to record temperature threshold crossovers. I demonstrated that, just like the displacement sensor, this could be achieved using commercial RFID tags. While non-electric memory could address *if* a temperature threshold was violated it could not answer the question of *when* the threshold was violated — a cost-benefit tradeoff. Besides temperature thresholds, I also motivated two other case examples where non-electric memory was appealing.

To reduce the size of the sensor, I considered the use of shape memory polymers (SMP) as a one-way thermal switch to improve the design of the temperature threshold sensor. The use of SMPs reduced the sensor size, boosted the range and made the sensor independent of deployment orientation. Furthermore, I demonstrated how the use of a metallic isolator made the sensor performance independent of the material

on which the sensor was deployed. However, the requirement of a reference tag in the AM measurements still kept the sensor size large. The successful use of SMPs in this thesis, and the related work such as using chemically responsive films to sense volatile organics [64], served to highlight the potential collaborative research in materials engineering and RFID has for the development of TABS sensors.

In order to further reduce the size of the sensor, I considered exploiting the 902-928 MHz bandwidth available for RFID operations in the Americas and proposed the design of *Frequency Modifying (FM) TABS*. Exposure to temperature impulses triggered a permanent change in the optimal operating frequency of the RFID tag sensor. Frequency domain-based measurements no longer required the presence of a reference tag and reduced the size of the sensor even further. I successfully designed an FM TABS temperature threshold sensor that makes use of SMP actuation and shifts in the operating frequency of the RFID tag to implement non-electric memory. In doing so, I made two contributions. First, I outlined the methodology for designing a frequency selective antenna that related changes in boundary conditions of an RFID tag to a frequency shift in the 902-928 MHz band. Second, I outlined a set of design issues that need to be addressed before the temperature sensor is viable for commercial deployment.

Lessons learned from the Fluid Level Sensor

I illustrated that the frequency selective antenna design methodology proposed for FM TABS could be generalized to another application via the successful design of an FM TABS fluid level sensor used to detect whether or not a beverage glass was full of water. I then proposed the concept of *Phase Modifying (PM) TABS* by outlining the design of a PM TABS fluid level sensor that uses RFID tag backscatter phase to detect whether a beverage glass is full or empty. The PM TABS approach was a good compromise between the larger size of AM TABS and the slow interrogation speed of FM TABS. Using simulation and preliminary experimental results, I demonstrated that while the PM TABS approach was theoretically feasible, the sensitivity of phase to three extraneous factors makes its practical implementation challenging. I then

proposed what future work could be done to better quantify the effect of these factors on RF phase which would help better identify the scope of PM TABS in fluid level sensing and other applications.

In summary, my thesis introduced the concept of RFID TABS and demonstrated how three reader-tag signal parameters could be used for sensing. I also introduced the concept of low-cost, non-electric memory for recording critical threshold crossovers that may occur when the sensor is unpowered. I discussed a road map for future development work in three areas: The first are open questions that could improve sensor design. The second features engineering implementation issues that facilitate the commercial deployment of TABS. The third motivates two other application areas in which TABS deployment is appealing and proposes preliminary design ideas as to how this can be achieved.

Bibliography

[1] E. Welbourne, L. Battle, G. Cole, K. Gould, K. Rector, S. Raymer, M. Balazinska and G. Borriello. Building the Internet of Things Using RFID: The RFID Ecosystem Experience. *IEEE Internet Computing*, 13(3):48 –55, May 2009 ©2009 IEEE.

[2] EPC Global Standards and Specifications. EPC Tag Data Standard (TDS) . *http://www.gs1.org/gsmp/kc/epcglobal/tds/*, v. 1.6, 2011.

[3] D.A. Rodriguez-Silva, F.J. Gonzalez-Castano, S. Costas-Rodriguez, J.C. Burguillo-Rial, R. Gentile, S. Stanca, and R. Arona. Quantitative Assessment of the Benefits of RFID Technology for Libraries: a Trans-European Study. In *IEEE Workshop on Automatic Identification Advanced Technologies*, pages 128 –133, June 2007 ©2007 IEEE.

[4] May Tajima. Strategic value of RFID in supply chain management. *Journal of Purchasing and Supply Management*, 13(4):261 – 273, 2007.

[5] S. Sarma. Towards the 5c tag. *White Paper, MIT Auto ID Center*, 2001.

[6] V. Subramanian, P.C. Chang, B.J Lee, S.E Molesa and S.K Volkman. Printed organic transistors for ultra-low-cost RFID applications. *IEEE Transactions on Components and Packaging Technologies*, 28(4):742 – 747, December 2005 ©2005 IEEE.

[7] EPC Global. Class 1 Generation 2 UHF Air Interface Protocol Standard. *http://www.epcglobalinc.org/standards/uhfc1g2.*

[8] A. Juels. RFID Security and Privacy: A Research Survey. *IEEE Journal on Selected Areas in Communications*, 24(2):381 – 394, February 2006 ©2006 IEEE.

[9] Daniel M. Dobkin. *The RF in RFID: Passive UHF RFID in Practice.* Newnes, Newton, MA, USA, ©2007.

[10] The Oracle Corporation. http://www.sunspotworld.com/, 2012.

[11] A.P Sample, D.J Yeager, P.S Powledge, A.V Mamishev, J.R Smith. Design of an RFID-Based Battery-Free Programmable Sensing Platform. *IEEE Transactions on Instrumentation and Measurement*, 57(11):2608 –2615, November 2008 ©2008 IEEE.

[12] O. Kasten and K. Römer. Beyond Event Handlers: Programming Wireless Sensors with Attributed State Machines. In *Proceedings of the 4th International Symposium on Information Processing in Sensor Networks*, IPSN '05, Piscataway, NJ, USA, 2005. ©2005 IEEE Press.

[13] S. Cho, C. B. Yun, J. P. Lynch, A. Zimmerman, B. Spencer Jr, and T. Nagayama. Smart Wireless Sensor Technology for Structural Health Monitoring of Civil Structures. *International Journal of Steel Structures*, 8 No. 4:267–275, 2008.

[14] L. Ruiz-Garcia, L. Lunadei, P. Barreiro and L. Robla. A Review of Wireless Sensor Technologies and Applications in Agriculture and Food Industry: State of the Art and Current Trends. *Sensors*, 9:4728–4750, 2009.

[15] D. Puccinelli and M. Haenggi. Wireless Sensor Networks: Applications and Challenges of Ubiquitous Sensing. *IEEE Circuits and Systems Magazine*, 5(3):19 – 31, 2005 ©2005 IEEE.

[16] University of California at Berkeley WEBS: Wireless Embedded Systems. http://smote.cs.berkeley.edu:8000/tracenv/wiki.

[17] Research Projects: Networked and Embedded Systems Laboratory. http://nesl.ee.ucla.edu/research.

[18] G. Wang, G. Cao and T. La Porta. Proxy-Based Sensor Deployment for Mobile Sensor Networks. In *IEEE International Conference on Mobile Ad-hoc and Sensor Systems*, pages 493 – 502, October 2004 ©2004 IEEE.

[19] R. Jedermann and W. Lang. Semi-passive RFID and Beyond: Steps towards Automated Quality Tracing in the Food Chain. *International Journal of Radio Frequency Identification Technology and Applications*, 1 No. 3:247–259, 2007.

[20] PowerTMP: Gen 2 Temperature Sensor RFID Tags. http://www.power-id.com/Products/Sensors.aspx.

[21] P.D Mitcheson, E.M Yeatman, G.K Rao, A.S Holmes, and T.C Green. Energy Harvesting From Human and Machine Motion for Wireless Electronic Devices. *Proceedings of the IEEE*, 96(9):1457 –1486, September 2008 ©2008 IEEE.

[22] M. Ferrari,V. Ferrari, D. Marioli and A. Taroni. Autonomous Sensor Module with Piezoelectric Power Harvesting and RF Transmission of Measurement Signals. In *Proceedings of the IEEE Instrumentation and Measurement Technology Conference*, pages 1663 –1667, April 2006 ©2006 IEEE.

[23] G. Scholl, C. Korden, E. Riha, C.C.W Ruppel,U. Wolff, G. Riha, L. Reindl, and R. Weigel. SAW-based radio sensor systems for short-range applications. *IEEE Microwave Magazine*, 4(4):68 – 76, December 2003 ©2003 IEEE.

[24] A.P Sample, D.J Yeager and J.R Smith. A Capacitive Touch Interface for Passive RFID Tags. In *IEEE International Conference on RFID*, pages 103 –109, April 2009 ©2009 IEEE.

[25] G. Anastasi, M. Conti and M. Di Francesco. Data Collection in Sensor Networks with Data Mules: An Integrated Simulation Analysis. In *IEEE Symposium on Computers and Communications*, pages 1096 –1102, July 2008 ©2008 IEEE.

[26] R. Bhattacharyya, C. Floerkemeier and S. Sarma. Towards Tag Antenna-Based Sensing - An RFID Displacement Sensor. In *IEEE International Conference on RFID*, pages 95 –102, April 2009 ©2009 IEEE.

[27] J. Siden, X. Zeng, T. Unander, A. Koptyug and H.E Nilsson. Remote Moisture Sensing Utilizing Ordinary RFID Tags. In *IEEE Sensors*, pages 308 –311, October 2007 ©2007 IEEE.

[28] G. Marrocco, L. Mattioni, and C. Calabrese. Multiport Sensor RFIDs for Wireless Passive Sensing of Objects - Basic Theory and Early Results. *IEEE Transactions on Antennas and Propagation*, 56(8):2691 –2702, August 2008 ©2008 IEEE.

[29] R. Bhattacharyya, C. Floerkemeier and S. Sarma. RFID Tag Antenna-Based Temperature Sensing. In *IEEE International Conference on RFID*, pages 8 –15, April 2010 ©2010 IEEE.

[30] R. Bhattacharyya, C. Di Leo, C. Floerkemeier, S. Sarma and L. Anand. RFID Tag Antenna-Based Temperature Sensing using Shape Memory Polymer Actuation. In *IEEE Sensors*, pages 2363 –2368, November 2010 ©2010 IEEE.

[31] S. Caizzone, C. Occhiuzzi and G. Marrocco. Multi-chip RFID antenna integrating shape-memory alloys for temperature sensing. In *Proceedings of the 5th European Conference on Antennas and Propagation (EUCAP)*, pages 2810 –2813, April 2011.

[32] R.A Potyrailo, C. Surman, W.G Morris, S. Go, Y. Lee, J. Cella and K.S Chichak. Selective Quantitation of Vapors and their Mixtures using Individual Passive Multivariable RFID Sensors. In *IEEE International Conference on RFID*, pages 22 –28, April 2010 ©2010 IEEE.

[33] R. Bhattacharyya, D. Deavours, C. Floerkemeier and S. Sarma, S. RFID Tag Antenna-Based Temperature Sensing in the Frequency Domain. In *IEEE International Conference on RFID*, pages 70 –77, April 2011 ©2011 IEEE.

[34] Y. Gu, Q. Wu, X. Cai and J. Bond. On Efficient Deployment of High-End Sensors in Large-Scale Heterogeneous WSNs. In *IEEE 6th International Conference on Mobile Adhoc and Sensor Systems*, pages 912 –917, October 2009 ©2009 IEEE.

[35] I. Chatti, A. Delahaye, L. Fournaison and J-P Petitet. Benefits and drawbacks of clathrate hydrates: a review of their areas of interest. *Energy Conversion and Management*, 46(910):1333 – 1343, 2005.

[36] P.V Nikitin and K.V.S Rao. Antennas and Propagation in UHF RFID Systems. In *IEEE International Conference on RFID*, pages 277 –288, April 2008 ©2008 IEEE.

[37] X. Liu, M. D. Corner and P. Shenoy. Ferret: RFID Localization for Pervasive Multimedia. In *Proceedings of the 8th International Conference on Ubiquitous Computing*, pages 422–440, 2006.

[38] L.M Ni, Y. Liu, Y.C Lau and A.P Patil. LANDMARC: indoor location sensing using active RFID. In *Proceedings of the First IEEE International Conference on Pervasive Computing and Communications*, pages 407 – 415, March 2003 ©2003 IEEE.

[39] S.R Aroor and D.D Deavours. Evaluation of the State of Passive UHF RFID: An Experimental Approach. *IEEE Systems Journal*, 1(2):168–176, 2007 ©2007 IEEE.

[40] Constantine A. Balanis. *Antenna Theory: Analysis and Design.* Wiley-Interscience, 2005 ©2005 John Wiley and Sons.

[41] P.V Nikitin, K.V.S Rao, S.F Lam, V. Pillai, R. Martinez and H. Heinrich. Power Reflection Coefficient Analysis for Complex Impedances in RFID Tag Design. *IEEE Transactions on Microwave Theory and Techniques*, 53(9):2721 – 2725, September 2005 ©2005 IEEE.

[42] P.V Nikitin, K.V.S Rao, R. Martinez and S.F Lam. Sensitivity and Impedance Measurements of UHF RFID Chips. *IEEE Transactions on Microwave Theory and Techniques*, 57(5):1297 –1302, May 2009 ©2009 IEEE.

[43] P.V Nikitin, K.V.S Rao and R.D Martinez. Differential RCS of RFID tag. *Electronics Letters*, 43(8):431 –432, 12 2007 ©2007 IEEE.

[44] U. Karthaus and M. Fischer. Fully integrated passive UHF RFID transponder IC with 16.7 μW minimum RF input power. *IEEE Journal of Solid-State Circuits*, 38(10):1602 – 1608, October 2003 ©2003 IEEE.

[45] D.D Deavours. Improving the near-metal performance of UHF RFID tags. In *IEEE International Conference on RFID*, pages 187 –194, April 2010 ©2010 IEEE.

[46] N.A Mohammed, M. Sivakumar and D.D Deavours. An RFID tag capable of free-space and on-metal operation. In *IEEE Radio and Wireless Symposium*, pages 63 –66, January 2009 ©2009 IEEE.

[47] I. Ehrenberg, S. Sarma and B.I Wu. 3D metamaterial for ultra compact artificial Magnetic Conductor . *to appear IEEE International Conference on Microwaves, Communications, Antennas and Electronic Systems*, 2011 ©2011 IEEE.

[48] X. Hou, X. Yang and Q. Huang. Using Inclinometers to Measure Bridge Deflections. *Journal of Bridge Engineering*, 10:564–569, 2005.

[49] Impinj RFID Products: Typical form factors of Impinj manufactured tags. www.impinj.com/WorkArea/downloadasset.aspx?id=2553.

[50] Impinj RFID Products: The Monza 3 RFID tag IC Specification Page. http://www.impinj.com/products/tag-chips.aspx.

[51] Voyantic Tagformance Lite Equipment for RFID Tag Measurements. http://www.voyantic.com/.

[52] L.H Hemming. *Electromagnetic Anechoic Chambers: A Fundamental Design and Specification Guide.* IEEE Press, 2002 ©2002 IEEE.

[53] The Impinj Speedway Gen 2 UHF RFID Reader. http://www.impinj.com/products/rfid-reader.aspx.

[54] T.H Cormen, C. Stein, R.L Rivest and C.E Leiserson. *Introduction to Algorithms.* McGraw-Hill Higher Education, 2nd edition, 2001.

[55] C.H. Loo, K. Elmahgoub, F. Yang, A. Z. Elsherbeni, D. Kajfez, A. A. Kishk, T. Elsherbeni, L. Ukkonen, L. Sydanheimo, M. Kivikoski, S. Merilampi, and P. Ruuskanen. Chip impedance matching for UHF RFID tag antenna design. *Progress in Electromagnetics Research*, 81:359–370, ©PIERS 2008.

[56] R. Bhattacharyya, C. Floerkemeier and S. Sarma. RFID tag antenna based sensing: Does your beverage glass need a refill? In *IEEE International Conference on RFID*, pages 126 –133, April 2010 ©2010 IEEE.

[57] M.C. O'Connor. Cold-chain project reveals temperature inconsistencies. *RFID Journal*, 2006.

[58] S. Estrada-Flores. Acoustic measurement of avocado firmness during low temperature storage : Effect of storage temperature. *International Conference on Quality in Chains. An Integrated View on Fruit and Vegetable Quality*, pages 323–329, 2003.

[59] A. Dada and F. Thiesse. Sensor Applications in the Supply Chain: The Example of Quality-Based Issuing of Perishables. In C. Floerkemeier, M. Langheinrich, E. Fleisch, F. Mattern and S. Sarma, editor, *The Internet of Things*, volume 4952 of *Lecture Notes in Computer Science*, pages 140–154. Springer Berlin / Heidelberg, 2008 ©2008 Springer Berlin / Heidelberg.

[60] Alexander Ilic, Thorsten Staake, and Elgar Fleisch. Using sensor information to reduce the carbon footprint of perishable goods. *IEEE Pervasive Computing*, 8(1):22–29, 2009 ©2009 IEEE.

[61] Alien RFID Products: The Squiggle UHF RFID Tag with Higgs^{TM}- 3 IC. http://www.alientechnology.com/tags/index.php.

[62] D.L. Safranski and K. Gall. Effect of chemical structure and crosslinking density on the thermo-mechanical properties and toughness of (meth)acrylate shape memory polymer networks. *Polymer*, 49(20):4446 – 4455, 2008 ©Elsevier 2008.

[63] E. Bobelyn, A. Schenk, B. Verlinden, M.L.A.T.M. Hertog and B. Nicolai. Time Temperature Integrators (TTI) to Control the Distribution Chain of Horticultural Products. *Proceedings of the 5th International Postharvest Symposium*, pages 893–900, ©2005 International Society of Horticultural Science.

[64] R.A Potyrailo, C. Surman, W.G Morris, S. Go, Y. Lee, J. Cella and K.S Chichak. Selective quantitation of vapors and their mixtures using individual passive multivariable RFID sensors. In *IEEE International Conference on RFID*, pages 22 –28, April 2010 ©2010 IEEE.

[65] A. Hasan, A.F Peterson and G.D Durgin. Reflected electro-material signatures for self-sensing passive RFID sensors. In *IEEE International Conference on RFID*, pages 62 –69, April 2011 ©2011 IEEE.

[66] N.A Mohammed, K.R Demarest and D.D Deavours. Analysis and synthesis of UHF RFID antennas using the embedded T-match. In *IEEE International Conference on RFID*, pages 230 –236, April 2010 ©2010 IEEE.

[67] ANSYS HFSS: 3D Full Wave Electromagnetic Field Simulation. http://www.ansoft.com/products/hf/hfss/.

[68] Impinj Speedway®Revolution RFID Reader with AutoPilot Features. http://www.impinj.com/Speedway_Revolution_UHF_RFID_Reader.aspx.

[69] Fosstrak: Open Source RFID Software Platform. http://fosstrak.org/.

[70] Klaus Finkenzeller. *RFID Handbook: Fundamentals and Applications in Contactless Smart Cards and Identification.* John Wiley & Sons, Inc., New York, NY, USA, 2 edition, 2003.

[71] J.P Lynch. An overview of wireless structural health monitoring for civil structures. *Philosophical Transactions of the Royal Society*, 365:345–372, 2007.

[72] D. Garcus, T. Gogolla, K. Krebber and F. Schliep. Brillouin optical-fiber frequency-domain analysis for distributed temperature and strain measurements. *Journal of Lightwave Technology*, 15(4):654 –662, April 1997 ©1997 IEEE.

[73] R. Fletcher and N. Gershenfeld. Remotely Interrogated Temperature Sensors Using Magnetic Materials. *IEEE Transactions on Magnetics*, 36 No. 5 Part 1:1569–1575, 2000 ©2000 IEEE.

[74] R. Fletcher, J. Levitan, J. Rosenberg and N. Gershenfeld. Applications of Smart Materials to ID Tags and Remote Sensing. *Proceedings of Materials Research Society Fall Meeting*, 360, 1996.

[75] P.V Nikitin, R. Martinez, S. Ramamurthy, H. Leland, G. Spiess and K.V.S. Rao. Phase based spatial identification of UHF RFID tags. In *IEEE International Conference on RFID*, pages 102 –109, April 2010 ©2010 IEEE.

[76] L.M Ni, L. Yunhao, Cho Lau Yiu and A.P Patil. LANDMARC: indoor location sensing using active RFID. In *Proceedings of the First IEEE International Conference on Pervasive Computing and Communications*, pages 407 – 415, March 2003 ©2003 IEEE.

[77] D. Hahnel, W. Burgard, D. Fox, K. Fishkin, and M. Philipose. Mapping and localization with RFID technology. In *Proceedings of the IEEE International Conference on Robotics and Automation*, volume 1, pages 1015 – 1020 Vol.1, April 2004 ©2004 IEEE.

[78] R. Mittra, and U. Pujare. Real time estimation of motion and range of RFID tags. In *Proceedings of the 5th European Conference on Antennas and Propagation*, pages 3804 –3808, April 2011.

[79] C. Hekimian-Williams, B. Grant, Xiuwen Liu, Z. Zhang and P. Kumar. Accurate localization of RFID tags using phase difference. In *IEEE International Conference on RFID*, pages 89 –96, April 2010 ©2010 IEEE.

[80] W.K Tam and V.N Tran. Multi-ray propagation model for indoor wireless communications. *Electronics Letters*, 32(2):135 –137, January 1996 ©1996 IEEE.

[81] Laird Technologies: Circular Polarity RFID Panel Antenna. http://disti-assets.s3.amazonaws.com/arcadianinc/files/datasheets/4123.pdf.

[82] T. Endo, Y. Sunahara, S. Satoh and T. Katagi. Resonant frequency and radiation efficiency of meander line antennas. *Electronics and Communications in Japan (Part II: Electronics)*, 83(1):52–58, 2000.

[83] S. Preradovic and N.C Karmakar. Chipless RFID: Bar Code of the Future. *IEEE Microwave Magazine*, 11(7):87 –97, December 2010 ©2010 IEEE.

[84] P.V Nikitin, K.V.S Rao, R. Martinez and S.F Lam. Sensitivity and Impedance Measurements of UHF RFID Chips. *IEEE Transactions on Microwave Theory and Techniques*, 57 No. 5:1297–1302, 2009 ©2009 IEEE.

[85] Termites.com: Structural Termite Damage in Homes. Termites in Drywall Damage. *http://www.termites.com/damage/structural-damage/termites-in-drywall-damage/*, 2011.

[86] Termites.com: Structural Termite Damage in Homes. Termite Damage in Sub Floor. *http://www.termites.com/damage/structural-damage/termite-damage-in-sub-floor/*, 2011.

[87] C. Q Peng, Y. S Thio and R. A Gerhardt. Conductive paper fabricated by layer-by-layer assembly of polyelectrolytes and ITO nanoparticles. *Nanotechnology*, 19 No. 50, 2008 ©2008 IOP Publishing Ltd.

[88] C. Occhiuzzi, C. Paggi, and G. Marrocco. Passive RFID Strain-Sensor Based on Meander-Line Antennas. *IEEE Transactions on Antennas and Propagation*, 59 No. 12:4836–4840, 2011 ©2011 IEEE.

[89] Matweb: Material Property Data. RTP Company RTP 1391 HM Polyphenylene Sulfide (PPS), High Modulus - Carbon Fiber. *http://www.matweb.com/*.